AD- A123 701

NAVAL OCEAN SYSTEMS CENTER, SAN DIEGO, CA
SHIPBOARD VISIBILITY MEASUREMENT SYSTEM DEFINITION
STUDY BY: JA DOWLING, TJ ROGNE OPTIMETRICS, INC.,
LAS CRUCES, NM

1 OF 2
CR 131
JAN 1982

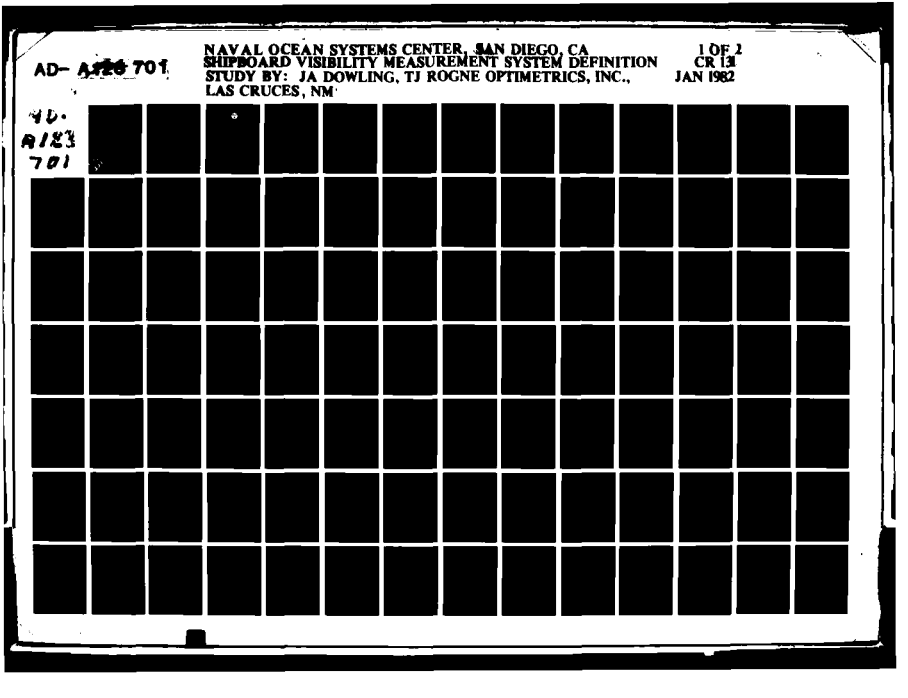

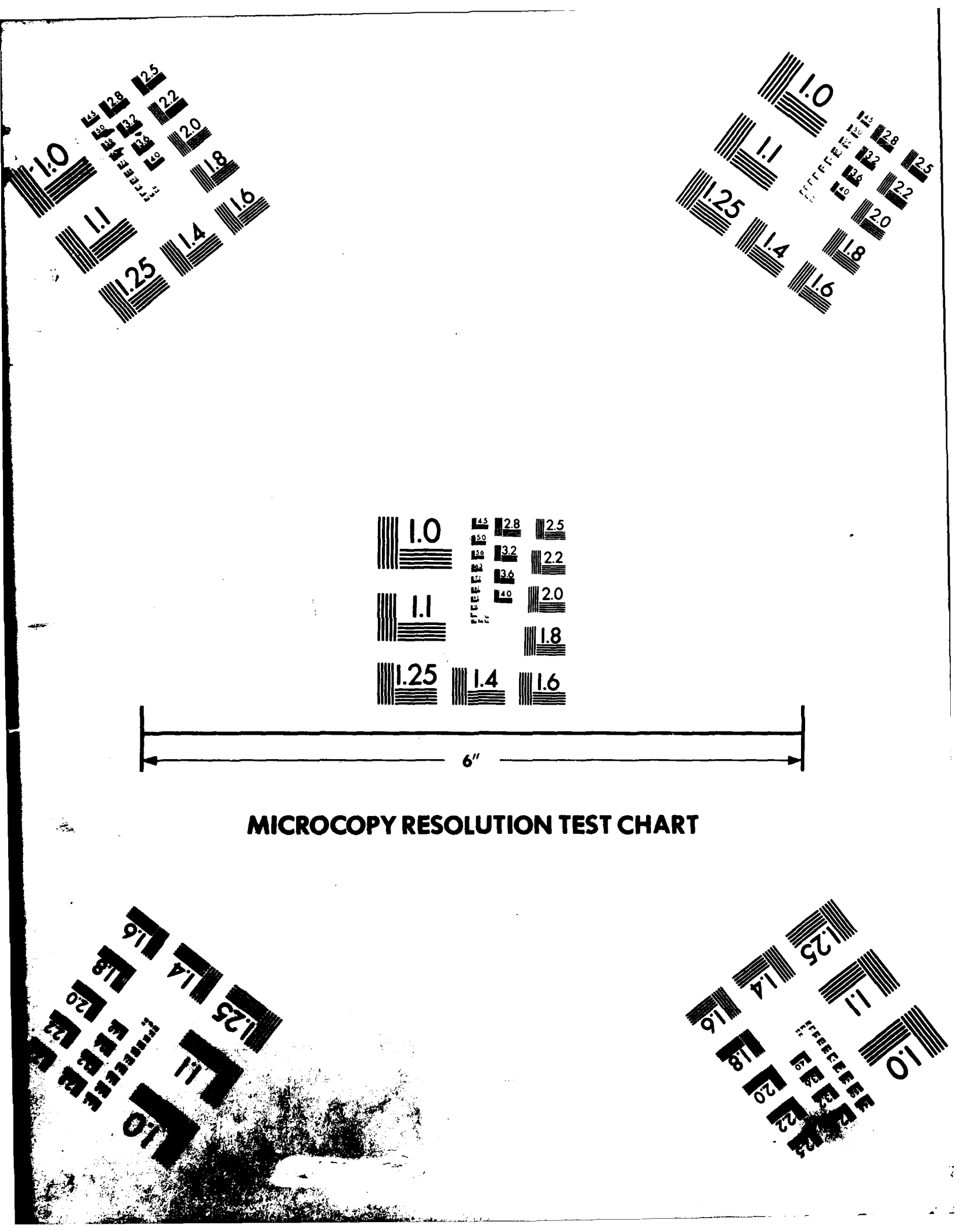

MICROCOPY RESOLUTION TEST CHART

NOSC CR 131

NOSC CR 131

Contractor Report 131

SHIPBOARD VISIBILITY MEASUREMENT SYSTEM DEFINITION STUDY

JA Dowling, TJ Rogne
Optimetrics Inc
Las Cruces, NM

January 1982

Prepared for
NOSC EM Propagation Division (Code 532)

Sponsored by
Naval Sea Systems Command

NAVAL OCEAN SYSTEMS CENTER
San Diego, California 92152

NAVAL OCEAN SYSTEMS CENTER, SAN DIEGO, CA 92152

AN ACTIVITY OF THE NAVAL MATERIAL COMMAND

JM PATTON, CAPT, USN
Commander

HL BLOOD
Technical Director

ADMINISTRATIVE INFORMATION

Work was done by Optimetrics Inc, Las Cruces, NM, for NOSC EM Propagation Division (Code 532).

Released by
JH Richter, Head
EM Propagation Division

Under authority of
JD Hightower, Head
Environmental Sciences
Department

Unclassified

SECURITY CLASSIFICATION OF THIS PAGE (When Data Entered)

REPORT DOCUMENTATION PAGE		READ INSTRUCTIONS BEFORE COMPLETING FORM
1 REPORT NUMBER NOSC Contractor Report 131 (CR 131)	2 GOVT ACCESSION NO	3 RECIPIENT'S CATALOG NUMBER
4 TITLE (and Subtitle) SHIPBOARD VISIBILITY MEASUREMENT SYSTEM DEFINITION STUDY		5 TYPE OF REPORT & PERIOD COVERED Final Report 6 PERFORMING ORG REPORT NUMBER OMI-82-003
7 AUTHOR(s) James A. Dowling, Timothy J. Rogne		8 CONTRACT OR GRANT NUMBER(s) N66001-81-C-0217
9 PERFORMING ORGANIZATION NAME AND ADDRESS OptiMetrics, Inc. 106 E. Idaho Ave., Suite G Las Cruces, NM 88001		10 PROGRAM ELEMENT PROJECT TASK AREA & WORK UNIT NUMBERS 62759N SF59-551-697
11 CONTROLLING OFFICE NAME AND ADDRESS Naval Sea Systems Command Washington, DC 20362		12 REPORT DATE January 1982 13 NUMBER OF PAGES 150
14 MONITORING AGENCY NAME AND ADDRESS (if different from Controlling Office) Naval Ocean Systems Center San Diego, CA 92152		15 SECURITY CLASS (of this report) Unclassified 15a DECLASSIFICATION/DOWNGRADING SCHEDULE

16 DISTRIBUTION STATEMENT (of this Report)

Approved for public release; distribution unlimited

17 DISTRIBUTION STATEMENT (of the abstract entered in Block 20, if different from Report)

18 SUPPLEMENTARY NOTES

19 KEY WORDS (Continue on reverse side if necessary and identify by block number)

Maritime Visibility
Marine Aerosol Models
Marine Aerosol Data
LIDAR
Infrared Aerosol Extinction
Eye-Safe LIDAR

20 ABSTRACT (Continue on reverse side if necessary and identify by block number)

A study has been performed to define the required characteristics of a shipboard Light-Detection-and-Ranging (LIDAR) system to be used for shipboard aerosol extinction measurements at visible and infrared wavelengths.

The study is based on an evaluation of several elements including a characterization of maritime aerosol scattering and

DD FORM 1 JAN 73 1473 EDITION OF 1 NOV 65 IS OBSOLETE

Unclassified

SECURITY CLASSIFICATION OF THIS PAGE (When Data Entered)

extinction, an evaluation of various LIDAR system configurations and the practical considerations involved in the use of a shipboard LIDAR measurement system. Performance of an existing hand-held LIDAR system and a suggested "upgraded" version of this system have been performed and compared. Eye safety considerations and system operating parameters including laser source pulse energy and operating wavelength as well as optical system size have been considered.

Recommendations for the development and use of a prototype shipboard LIDAR system have been developed and are included.

ACKNOWLEDGEMENT

The authors wish to thank Dr. Juergen H. Richter of the Naval Ocean Systems Center for his interest in and support of this work. The assistance of Joseph L. Manning of the OMI Ann Arbor, Michigan office in obtaining the calculated transmission spectra shown in Figures 30 and 31 is greatly appreciated. The assistance of Mr. Douglas Poer, U.S. Army Missle Command and Dr. W.A. Shand, U.K. Royal Signals and Radar Establishment in obtaining information and specifications concerning MIL-SPEC 1.06 μm and 10.6 μm laser hardware was very helpful in carrying out this effort. The authors would like to acknowledge helpful discussions concerning stimulated Raman scattering techniques with Professor Robert Byer of Stanford University and Dr. David Rockwell of Hughes Research Laboratories. The authors would like to thank especially Ms. Deborah Burton for her dedicated typing and assistance in preparing this report.

TABLE OF CONTENTS

LIST OF ILLUSTRATIONS

LIST OF TABLES

1
INTRODUCTION AND SUMMARY

1.1 PURPOSE AND OBJECTIVES OF THE STUDY

The Navy-wide component of the current DOD Plan for Atmospheric Transmission Research and Development is encompassed in the E-O MET Program managed by the Naval Ocean Systems Center (NOSC). The Navy's broad area of responsibility within E-O MET is measurement and modeling of atmospheric propagation conditions as affected by the marine environment. Specific E-O MET goals include:

- Establishment of a marine aerosol measurements data base including vertical distributions.
- Development of relationships between meteorological measurements and aerosol models.
- Performance of meteorological and propagation measurements in concert with systems tests.
- Development and validation of systems performance models based on weather climatology.

A key element of the E-O MET plan is an E-O systems performance assessment system which goes under the name Prediction of Performance Range for E-O Systems (PREOS). When implemented on a desktop Programmable Calculator (PROCAL) the system is known as PROCAL-PREOS [1]. The primary function of PROCAL-PREOS is to provide real time shipboard assessment of airborn FLIR performance. As a requirement of the development process, PROCAL-PREOS must be designed and validated against the expected range of the operational marine environments. It is to this broad objective that the work described in this report responds. Herein, the development and implementation of a LIDAR specifically for the E-O MET requirements is evaluated.

This evaluation has taken the form of a study in which several distinct but nevertheless key areas pertaining to the development and deployment of a shipboard LIDAR system have been analyzed. It is intended that the use of such a LIDAR will provide a real-time or near real-time measurement of infrared aerosol extinction coefficient profiles, which information can in turn be used as input into a real-time FLIR performance prediction such as PROCAL-PREOS operating aboard ship. Such a LIDAR measurement system is intended to replace the use of meteorological visual range (visibility) measurements performed by human observers, coupled with models for wavelength scaling of these data, and/or the sole reliance upon predictive models which use measured wind and relative humidity values to estimate infrared aerosol extinction.

Included among the major areas of investigation in this work are a review of marine aerosol modeling techiques and comparisons to recently measured optical and aerosol counter data collected in marine environments. The objective of this portion of the study is a realistic characterization of the marine environment in which a shipboard LIDAR will operate so that meaningful estimates of performance can be made and that system design trade-offs can be analyzed. These include selection of operating wavelengths, laser source operating mode and cw output power or pulse energy and transmitter and receiver optical system size.

Various approaches to the use of LIDAR systems for the measurement of atmospheric aerosol attentuation have been proposed and tested. Several approaches using cw laser sources which somewhat relax the eye safety considerations associated with the use of high-peak-power pulsed lasers were reviewed in this study. Some of the more important considerations concerned with the extraction of

atmospheric extinction coefficients from pulsed LIDAR return data have been considered and the implications for use of data collected at shorter wavelengths for the estimation of aerosol extinction coefficients at longer wavelengths have been considered to determine the optimum choice of system operating wavelength and the inherent limitations associated with this choice.

The important area of diverse approaches to LIDAR data signal processing was also reviewed in this study in order to best satisfy the somewhat conflicting requirements for rapid data reduction and the generation of near-real-time information versus a requirement to collect and efficiently process and manipulate LIDAR data in a more nearly "raw-data" condition, so that important but lacking information on inversion method validity and suitability can be further investigated.

The major factors involved in the implementation of a LIDAR measurement system in a shipboard context were considered to take into account some of the many practical considerations which will ultimately have a major impact on the degree of success with which such a system can be designed, constructed and operated reliably.

Performance estimates for an exsisting, prototype, hand-held LIDAR system (the US Army Atmospheric Sciences Laboratory Model-1 visioceilometer) have been performed and compared to ones performed for an upgraded system which would use a more energetic laser source together with a larger optical system. Performance comparisons of systems operating at 1.06 μm to ones operating in the 3-5 μm and 8-12 μm bands were performed to provide guidance for future system development.

1.2 STATEMENT OF TASKS

The several wide-ranging topics included in the present study were divided into four major tasks which are:

(1) A definition of the marine shipboard environment,

(2) A review of LIDAR measurement system approaches and data processing techniques,

(3) A survey of exsisting MIL-SPEC and ruggedized laser and E-O hardware which might be incorporated into a shipboard LIDAR system as critical, key building blocks, and

(4) Preparation of a summary of findings and the development of recommendations relating to the design, construction and use of a proposed shipboard LIDAR system.

The organization and content of this report closely follow the division of the study into the above four tasks.

1.3 INTERIM PROGRESS

1.3.1 INTERIM REPORT #1

An interim progress report [2] on the present study was prepared and supplied to NOSC in September 1981. The contents of that report have been substantially incorporated into this final report.

1.3.2 OPTICAL SOCIETY OF AMERICA PRESENTATION

A verbal presentation describing results and tentative conclusions reached in the study and available at the time of the presentation (October, 1981) was made by one of the authors (JAD) at the 1981 Optical Society of America National Conference held in Orlando, Florida. Copies of the viewgraphs used in that presentation are included as an Appendix to this report.

1.4 ORGANIZATION OF THE REPORT

This final report is organized into five major sections, the first of which is this Introduction. Features of several marine aerosol models currently in use and several examples of recent experimental, infrared aerosol extinction data are discussed and compared in Section 2 entitled Characterization of the Marine Environment. Measurement approaches and techniques for both pulsed and cw LIDAR systems are presented and discussed in Section 3. Several important factors involved in the application of a LIDAR measurement system to a shipboard installation, including eye safety considerations and the utilization of MIL-SPEC E-O hardware components are discussed in Section 4. Section 5 contains a statement of specific recommendations which have resulted from the review and analysis performed during this study.

1.5 SUMMARY

A study has been performed for the NOSC to review and evaluate several factors pertaining to the Definition of a Shipboard Visibility Measurement System. This study was divided into four major tasks which include a characterization of the marine environment, a review of LIDAR measurement system approaches and techniques, a survey of exsisting MIL-SPEC and ruggedized E-O hardware, and the preparation of summary findings and the generation of recommendations for the development of a shipboard LIDAR system.

The major conclusions reached in this study are as follows:

1. <u>Regarding Aerosol Models</u>

   - The models predict a very wide range of visible and infrared aerosol extinction as a function of windspeed and relative humidity.

- Infrared aerosol extinction predictions of the Katz-Ruhnke (K/R) aerosol model are lower than LOWTRAN 5 for 5 m/s windspeeds and higher than LOWTRAN 5 for windspeeds $\gtrsim$ 15 m/s.

- Values of the backscatter coefficient β for 1.06 μm wavelengths range over a factor of 300 for a 2 km visibility fog compared to a 5 km visibility oceanic aerosol.

- The ratio of β to the aerosol extinction coefficient, σ decreases with increasing wavelength by a factor of 30 for wavelengths from 4 μm to 10 μm.

2. Regarding Aerosol Measurements

- Aerosol data show:
  - no clear choice of model
  - moderate correlation of visible, 1.06 μm and 3-5 μm scattering
  - relative independence of visible/near IR and 10.6 μm scattering

- Data for the ratio of infrared to visible aerosol extinction coefficients, $\sigma_{IR}/\sigma_{.55}$, show large amounts of scatter and usually fall below predicted values.

3. Regarding LIDAR System Performance Evaluations

- The ASL Model-1 visioceilometer system appears limited to operation for ranges of about 1-2 km.

- An upgraded 1.06 μm system with a pulse energy of 10^{-1} J/pulse and a receiver aperture diameter of 30.5 cm (12 inches) promises good performance for ranges $\gtrsim$ 5 km.

- Large optics, higher pulse energy ($\gtrsim 10^{-1}$ J/pulse) and heterodyne detection will be required for 10.6 μm systems due to decreased values of β and β/σ at this wavelength.

- The condition required for use of the "Klett method" for LIDAR data inversion, namely that $\beta = A\sigma^k$ where A and k are constants and not wavelength dependent is not borne out by calculations of the ratio of scattering to extinction

at 10.6 μm, rendering the use of this approach at 10.6 μm questionable.

- A reliable method for estimation of σ_{8-12} from analysis of 1.06 μm LIDAR returns has not been established.

4. Regarding LIDAR Shipboard Implementation

- Wavelengths longer than 1.4 μm provide a reduction of over 500 in eye safety hazards for the same laser pulse energy.

- Increasing the transmitted beam diameter to 30.5 cm (12 inches) from 0.8 cm (ASL Model-1 visioceilometer) reduces the transmitted beam energy density at the transmitter by a factor of 1450.

- Army AN/TVQ-2 (GLLD) and Navy A-6 TRAM laser designator systems are promising candidates as sources for reliable, high performance, MIL-SPEC hardware modules.

- A prototype system using a wavelength shifted 1.06 μm laser (shifted to 1.54 μm using a stimulated Raman scattering cell in tandem with the 1.06 μm source) and a transmit/receive optics diameter of 30.5 cm should provide good performance for ranges in excess of 5 km while remaining eye-safe.

- A two-color LIDAR system should be developed. Simultaneous near IR (1.54 μm) and 10.6 μm shipboard measurements will be required to:
  - generate needed information to supplement the inadequate exsisting marine aerosol data base
  - evaluate and develop a system required for reliable routine shipboard measurement of aerosol extinction in the 3-5 μm and 8-12 μm FLIR operating bands.

2
CHARACTERIZATION OF THE MARINE ENVIRONMENT

2.1 MARINE AEROSOL MODELS

In this section we will be interested in the relationship of aerosol attenuation at infrared wavelengths to that in the visible or photopic region which can be derived from a simple visibility measurement.

Aerosol attenuation at optical wavelengths (visible light) can be directly related to the meteorological visibility or visual range through Koschmeider's law:

$$\sigma_A = \frac{3.91}{R_V}$$

where σ_A is the aerosol extinction coefficient and R_V is the visual range or visibility. This range corresponds to the distance over which an observer can barely discern a distant object. The contrast between the object and the surrounding background in the observer's field-of-view is taken to be 0.02 by convention. When R_V is expressed in km then σ_A has units of km^{-1}.

The simplest relationship or model between visible and infrared aerosol extinction which has been used in the past has the form:

$$\sigma_{IR} = \sigma_{VIS} \lambda^{-n}$$

where σ_{IR} and σ_{VIS} are aerosol extinction coefficients for infrared and visible wavelengths, respectively, λ is wavelength and n is an exponent slightly greater than unity.

This type of scaling between visible and infrared aerosol extinction has been shown to be better suited for describing extinction by continental rather than marine aerosols where a larger variation in the ratio of visible to infrared extinction is seen than for the continental case. In an effort to better quantify the variations both in magnitude of visible aerosol extinction, i.e., visibility, and also the ratio of infrared to visible extinction, models have been developed for marine aerosol scattering which relate the large variations in observed extinction directly to changes in the shape of the marine aerosol distribution. The modeled marine aerosol distribution is then used in a Mie scattering calculation to predict the magnitude of aerosol extinction at the wavelength of interest. Not only does the density of aerosol particles per unit volume scale with visibility (visible extinction), which is predominately determined by particle sizes with radii of a few tenths of a micron, but the shape of the distribution also changes, depending upon additional input parameters such as windspeed and relative humidity. Since particles with radii comparable to the wavelength under consideration are most effective in scattering that wavelength, the decreased fall-off of particle number density with increasing particle size in the marine aerosol model results in infrared scattering more nearly comparable with that in the visible. In this regard recent marine aerosol models are more consistent with both maritime optical and infrared transmission measurements as well as aerosol distribution measurements performed in maritime locations.

The development of marine aerosol models has been the subject of much interest in recent years and has been discussed recently in detail by Richter and Hughes [4] and by Katz [5]. Only the essential features of the models will

be described here since we are primarily interested in the predicted ranges of infrared and visible aerosol scattering values obtained using these models and not in the development or detailed validation of the models themselves. We will also summarize some recent infrared and visible aerosol scattering measurements so that together with the range of predicted scattering values obtained with the models, we are likely to bracket a range of values representative of the marine environment.

The comparisons of measured and predicted aerosol scattering for the marine environment to be discussed later should by no means be taken to be exhaustive or conclusive. Within the scope of the effort presented here such comparisons are rather intended to contrast certain features of recent modeling developments and to review a few selected examples of marine aerosol scattering measurements to provide a reasonable assessment of the environment in which a shipboard LIDAR system will operate.

Aerosol models for the marine environment are characterized by an admixture of two components (continental and maritime). The work of Barnhardt and Streete [6], the earlier version of LOWTRAN 3B [7] and the recent LOWTRAN 5[8] model are all based on this combination of two components, but various descriptions are used for each in the different models. See reference 4 for a discussion of these differences.

The LOWTRAN models use a mixture of oceanic and continental components in a fixed ratio with the total number density normalized by visibility. The relative contributions of each component and their mathematical form differ in the two versions.

The model of Wells, Gal and Munn (WGM) [9] and the Katz/Ruhnke (K/R) model [10] both contain continental and oceanic components as in the LOWTRAN models but not in fixed proportions to each other. In the WGM and K/R models the relative contribution of the oceanic component depends on windspeed and relative humidity. The major distinction between the WGM and K/R models has to do with a difference in altitude dependency, which is an exponential particle density decrease in the WGM model and a particle size dependent form in the K/R model that provides a more uniform height distribution of larger particles during high wind conditions.

In the K/R model the continental to maritime mixing ratio is determined by the saturation ratio (relative humidity divided by 100) whereas it is an adjustable input parameter in the WGM model. The particle growth factor with relative humidity was changed in the K/R model from that of Barnhardt and Streete (also used in the WGM model) to that devised by Fitzgerald [11]. In the WGM model the calculated aerosol size distribution is normalized by the observed visual range but this feature was removed in the K/R model due to the questionable precision and utility of shipboard meteorological observer visibility measurements. Results obtained with the K/R model will be compared to those obtained with the two versions of LOWTRAN in the subsections that follow.

The recently developed K/R model is an outgrowth of the WGM approach and in addition to the differences cited above it incorporates changes in the values of some of the constants used in the WGM particle size distribution formulae. Consequently the more recent K/R model rather than the earlier WGM approach will be considered in comparisons to the LOWTRAN models and to experimental data.

A comparison of the aerosol particulate distributions calculated separately with the oceanic and continental components of the LOWTRAN 3B model and their sum (the LOWTRAN 3B maritime distribution) is shown in Figure 1. As one can see in the figure the continental component dominates the LOWTRAN maritime distribution for particle sizes below about 0.5 μm while the oceanic component is larger for sizes greater than this value. The K/R model on the other hand, predicts a decreased concentration of larger particles and consequently a smaller ratio of σ_{IR}/σ_{VIS} (ratio of infrared to visible aerosol extinction), than does LOWTRAN for 3.5 m/s windspeed, growing to an increased value compared to LOWTRAN for a 20 m/s windspeed. The two model distributions are seen to coincide for an intermediate windspeed value around 10 m/s.

2.1.1 WINDSPEED DEPENDENCE

The impact of the similarities and distinctions between the LOWTRAN models and the K/R approach can be readily seen by examining the ratio of infrared aerosol extinction to visible extinction predicted by each model for different values of relative humidity and windspeed. Figure 2 shows data taken from reference 5 plotted as the ratio of infrared to visible aerosol scattering coefficient, σ_{IR}/σ_{VIS} versus wind speed in m/s.

Figure 2(A) shows a comparison of the ratio $\sigma_{3-5}/\sigma_{VIS}$ for the 3-5 μm IR band for the three models previously discussed, namely LOWTRAN 3B, LOWTRAN 5 and the Katz/Rhunke (K/R) model. The LOWTRAN 3B calculation is independent of variations in windspeed and relative humidity and predicts a constant value for σ_{IR}/σ_{VIS} for the 3-5 μm band (Figure 2(A)) and a smaller constant value for the 8-12 μm band (Figure 2(B)).

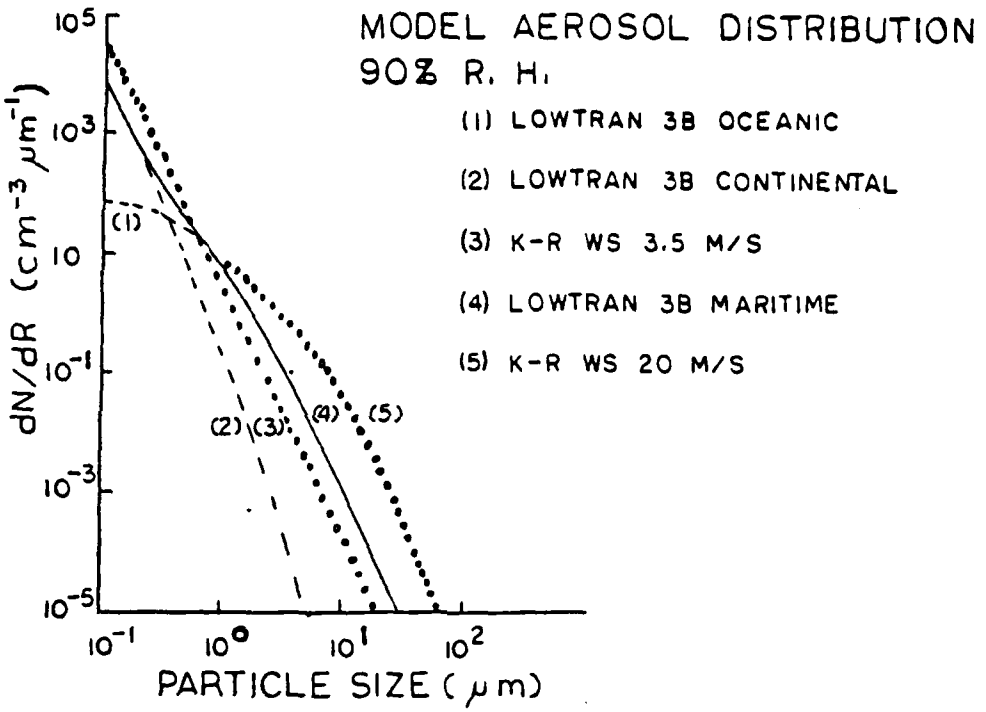

FIGURE 1. AEROSOL DISTRIBUTION FOR LOWTRAN AND KATZ-RUHNKE MODELS.

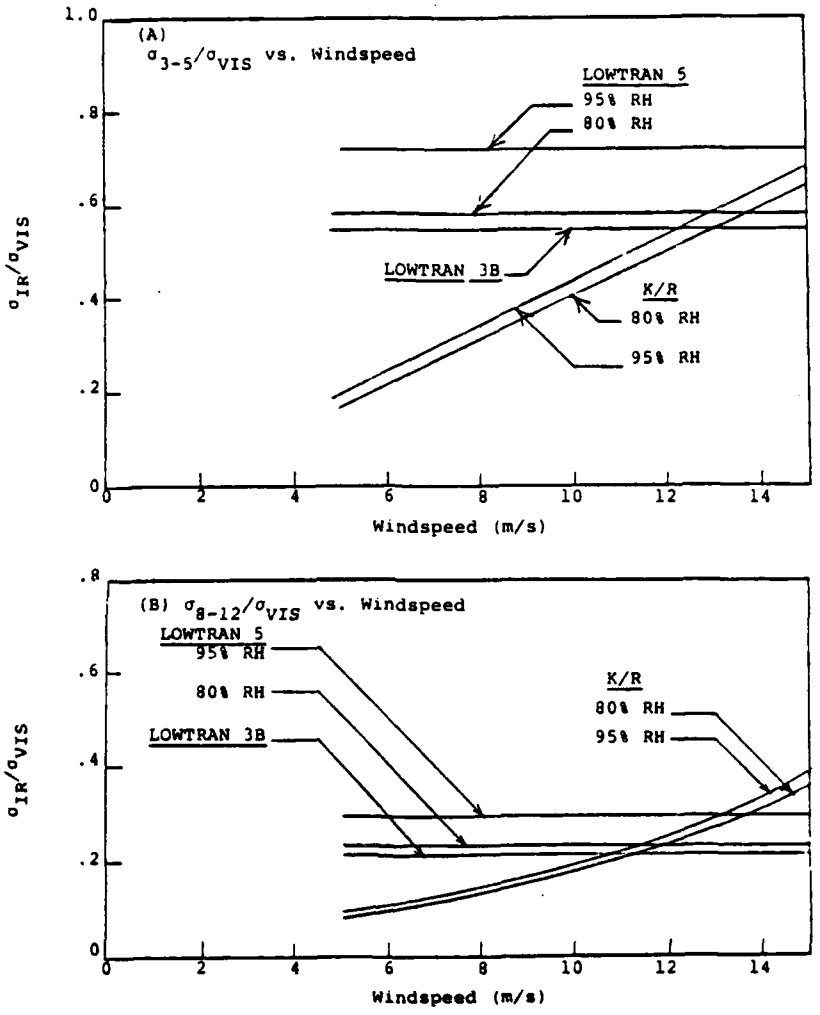

FIGURE 2. RATIO OF INFRARED TO VISIBLE AEROSOL EXTINCTION VERSUS WINDSPEED FOR LOWTRAN AND K/R MARITIME AEROSOL MODELS: (A) 3-5 μm REGION; (B) 8-12 μm REGION.

The LOWTRAN 5 model predicts a significant variation of 25% in σ_{IR}/σ_{VIS} for a change of RH from 80% to 95% for the 3-5 μm band and about the same relative change for the 8-12 μm band although the actual values of σ_{IR}/σ_{VIS} for 8-12 μm are only about a third of those for the 3-5 μm band.

The K/R model by contrast exhibits a smaller variation in σ_{IR}/σ_{VIS} with RH than LOWTRAN 5 (only 5% to 12% over the range of wind speeds from 5 m/s to 15 m/s for the 3-5 μm band). The absolute values of σ_{IR}/σ_{VIS} predicted by the K/R model only approach the LOWTRAN 5 predictions for windspeeds in excess of 11 to 12 m/s and always fall below the 95% RH LOWTRAN 5 calculation for the 3-5 μm band while matching the 8-12 μm value for 13 m/s windspeed and exceeding it for higher values. The region of overlap of predictions for the two models is seen to be confined to higher windspeeds > 11 m/s and the K/R model predictions for σ_{IR}/σ_{VIS} are always lower for windspeeds less than this value.

2.1.2 RELATIVE HUMIDITY DEPENDENCE

The sensitivity of infrared aerosol scattering to changes in relative humidity for the three marine aerosol models can be examined by again plotting the ratio σ_{IR}/σ_{VIS}, but in this case versus relative humidity (RH). The values of σ_{IR}/σ_{VIS} predicted by each model overlap for the range of RH values between 70% and 90% and for the range of windspeeds between 10 m/s and 15 m/s. As shown in Figure 3, the predictions obtained with LOWTRAN 3B are independent of changes in RH. LOWTRAN 5 predictions on the other hand bracket the LOWTRAN 3B values, predicting lower values below about 78% RH for the 3-5 μm case and below 85% RH for 8-12 μm, and higher values of σ_{IR}/σ_{VIS} in each case for higher values of RH. The K/R model predictions by comparison span the range of LOWTRAN 5 predictions for each wavelength

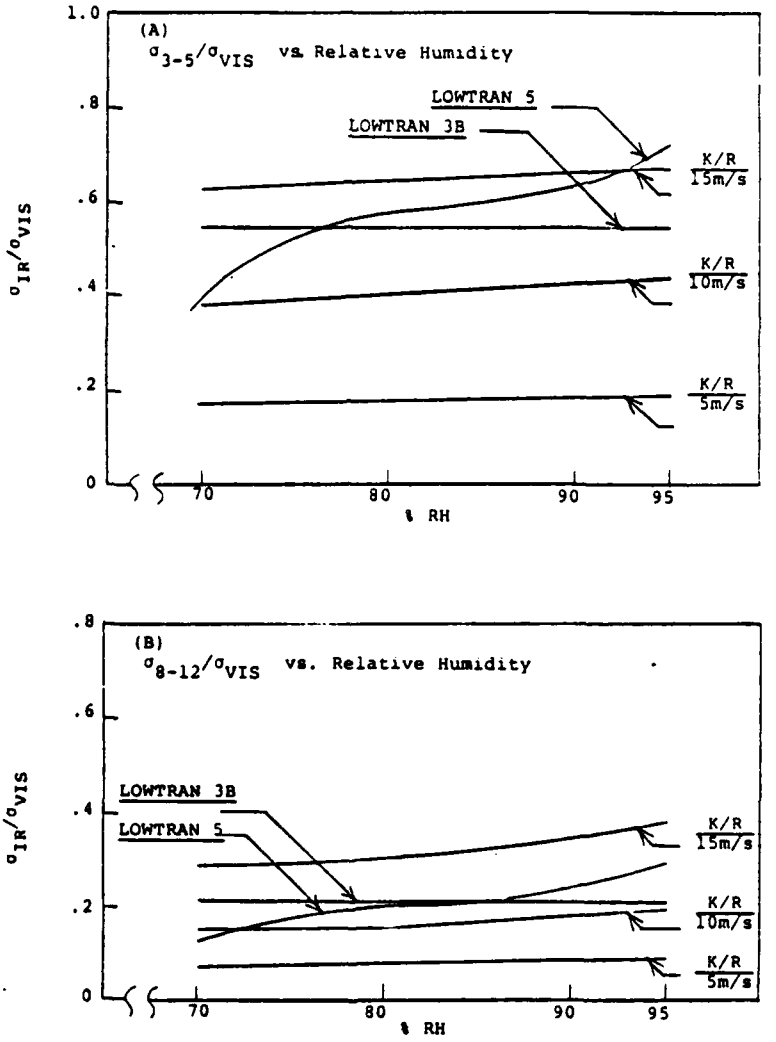

FIGURE 3. RATIO OF INFRARED TO VISIBLE AEROSOL EXTINCTION VERSUS RELATIVE HUMIDITY FOR LOWTRAN AND K/R MARITIME AEROSOL MODELS: (A) 3-5 μm REGION; (B) 8-12 μm REGION.

region (3-5 μm shown in Figure 3(A) and 8-12 μm shown in Figure 3(B)) for windspeed values between 10 m/s and 15 m/s. In both wavelength regions the K/R model predictions for 5 m/s windspeeds are substantially lower than either LOWTRAN model prediction.

Within the combined range of 10 m/s to 15 m/s windspeed and 70% to 95% RH the models are thus seen to predict comparable results. Values of σ_{IR}/σ_{VIS} predicted by LOWTRAN 3B are constant, independent of both windspeed and RH. LOWTRAN 5 is one step more sophisticated by incorporating the RH dependence seen in Figure 3, but does not include a component representing a windspeed dependent sea-spray contribution as does the K/R model. As is evident in Figures 2 and 3, the K/R model incorporates both a windspeed and RH dependence and therefore should be more representative of observations by allowing for independent variations in both of these parameters. The values of σ_{VIS}/σ_{IR} predicted by the K/R model as always lower than the LOWTRAN models for windspeeds less than 11 to 12 m/s due to the predominance of the continental aerosol component in the model for low windspeeds.

2.1.3 WAVELENGTH DEPENDENCE

Based on the discussions presented in the previous two sections the region of comparability of results obtained with the three aerosol models under consideration is confined to the combined ranges of 10-15 m/s windspeeds and 70%-90% RH. Within this region, the values of σ_{IR}/σ_{VIS} for the 3-5 μm predicted by the three models vary by a little more than a factor of 2 from 0.38 to 0.78. The same type of comparison shows about a factor of 3 variation for the 8-12 μm region, but lower overall values of the ratio $\sigma_{8-12}/\sigma_{VIS}$ between 0.12 and 0.38. The values of σ_{IR}/σ_{VIS} predicted

by LOWTRAN 3B are fixed at 0.55 and 0.21 for 3-5 μm and 8-12 μm respectively, independent of both windspeed and RH. LOWTRAN 5 shows the variation with RH seen in Figure 3 but is independent of windspeed while the K/R model contains both dependencies as previously noted.

The wavelength dependence of the K/R model and its' dependence upon windspeed is demonstrated in Figure 4. For low windspeeds of 5 m/s the extinction ratio σ_{IR}/σ_{VIS} is 40% at 4 μm of its' value at 1.06 μm and only 15% of this value at 10 μm. For increased windspeeds the magnitude of σ_{IR}/σ_{VIS} increases and the decrease in this ratio for longer wavelengths becomes weaker. This behavior reflects the relative growth of the wind-driven sea spray component in the K/R aerosol model, causing aerosol extinction in the infrared to increase relative to visible scattering as greater numbers of larger sea-spray-derived particles are generated. The graph of σ_{IR}/σ_{VIS} tends to flatten out with increasing wavelengths just as the actual particle distributions shown in Figure 1 show a slower fall-off of dN/dR for larger particle sizes.

The aerosol model predictions discussed in this section will be compared to experimental data in Section 2.2.

2.1.4 CLIMATOLOGIES

For our purposes it is useful to consider results obtained from statistical analyses of maritime meteorological data collected during periods of several years which have been used in developing E-O systems performance estimates. Exsisting weather ship data have been used by Davis et al [12], Katz et al [13] and recently by Katz and Goroch [14] to produce climatological statistics. These have been combined with atmospheric effects models to generate statistical performance estimates for E-O systems. Typically

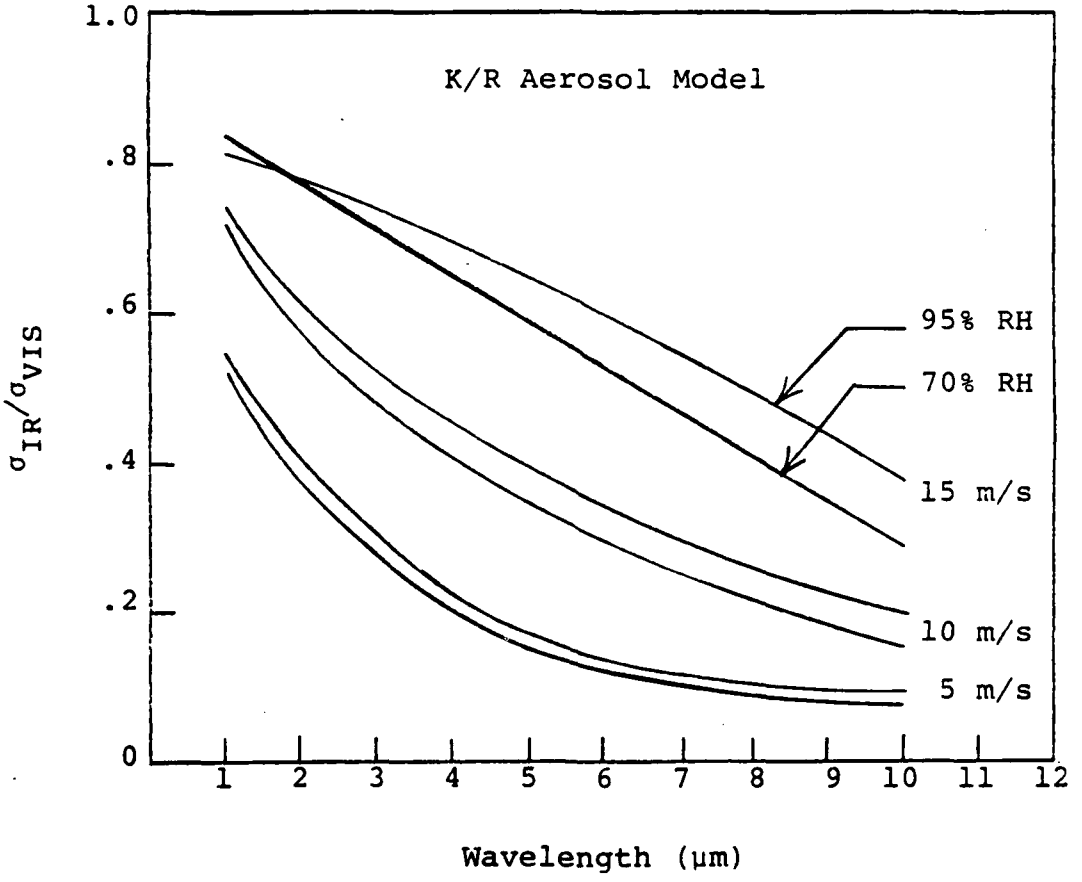

FIGURE 4. RATIO OF INFRARED TO VISIBLE AEROSOL EXTINCTION VERSUS WAVELENGTH FOR THE K/R MARITIME AEROSOL MODEL FOR DIFFERENT WINDSPEEDS.

studies such as these have concentrated on performance estimates for Forward Looking Infrared (FLIR) systems operating in the 3-5 μm and 8-12 μm regions. Aerosol extinction models such as those in LOWTRAN and the K/R model as well as molecular absorption calculations are used in relating system performance to the weather data.

To the extent that "climatological-like" statistics of aerosol extinction at infrared wavelengths are available as published intermediate results in studies such as references 12-14, they can be used to assess the range of aerosol scattering values to be expected at different wavelengths and for different maritime locations.

Such "climatological" results are only as valid as the specific aerosol extinction model used. There is evidence that factors related to air mass character and length of long-term averaging time for windspeed, which are not explicitly contained in the aerosol models are correlated with observed extinction values and/or measured maritime aerosol distributions.

2.2 MARINE AEROSOL MEASUREMENTS

2.2.1 LONG-PATH OPTICAL TRANSMISSION MEASUREMENTS

Several measurement programs have been undertaken at various maritime locations throughout the world during recent years. Extended over-water measurement programs were begun around 1975 by Physical Laboratory TNO in Holland [15], more recently by the Electronics Research Laboratory, Defense Science and Technology Organization, South Australia [16-18] and by the Pacific Missile Test

Center (PMTC) at San Nicolas Island (SNI), California [19]. Representative results obtained from these measurement programs were recently compared in the context of a Workshop on Atmospheric Water Vapor [20]. In many of the cases examined in reference 20 comparisons of the optical measurements to models such as LOWTRAN pointed out probable deficiencies in the atmospheric molecular absorption (water vapor) modeling rather than the aerosol scattering components of the model. Most of the data considered were measured under relatively high visibility conditions, consequently the aerosol attenuations were correspondingly low.

Not considered in reference 20 but relevant to the present considerations are selected data collected under the OPAQUE program [21]. In particular, data collected at the Netherlands OPAQUE site near the North Sea are often strongly subjected to the influence of maritime conditions arising during on-shore wind conditions. These data have been used in the development of the Electro-Optical Systems Atmospheric Effects Library (EOSAEL) [22]. Selected examples from this analysis will be discussed below.

Long-Path infrared transmission measurements have also been performed by the Naval Research Laboratory at a variety of locations which have included coastal sites at Cape Canaveral Air Force Station, Florida and San Nicolas Island, California [23-24]. Representative results from these experiments taken during on-shore wind conditions providing maritime air along the transmission measurement path will also be reviewed.

Recent Marine Aerosol Distribution Measurements will be discussed in Section 2.2.2.

2.2.1.1 Physical Laboratory TNO (Holland) Long-Path Infrared Transmission Measurements

The Physical Laboratory TNO, Netherlands, has been conducting maritime atmospheric transmission measurements at two locations on the North Sea coast [15]. One is across an estuary of the Scheldt near Flushing, along a 6 km path. More recently, an 18.2 km path between a shore site and an artificial island in the North Sea has been used. Two bands were studied in the first set of measurements conducted during 1974 and 1975, namely, 3.4 μm to 4.1 μm and 8.2 μm to 13.8 μm. Uncooled pyroelectric detectors were used. More recently in the longer path measurements, cooled detectors were employed and several individual filter bands in each of the two regions were studied.

Figures 5 and 6 show transmission data for these experiments plotted against atmospheric water vapor density along with LOWTRAN calculations for the 18.2 km path. The data for the mid-IR region between 3.4 μm and 4.1 μm shown in Figure 5 display a substantially smaller decrease in transmission with increasing water vapor density than do corresponding data for 8 μm and 13 μm shown in Figure 6. It is interesting to note that the ranges of transmission values are not significantly different for the two bands although the slopes of the lines fitted to the data are.

The measured data for the long wavelength band shown in Figure 6 show greater transmission than the LOWTRAN model predicts for the 18.2 km path. The data for the mid-IR band shown in Figure 5 show greater scatter but appear to be in better agreement with the LOWTRAN model for the band between 3.4 μm and 4.1 μm.

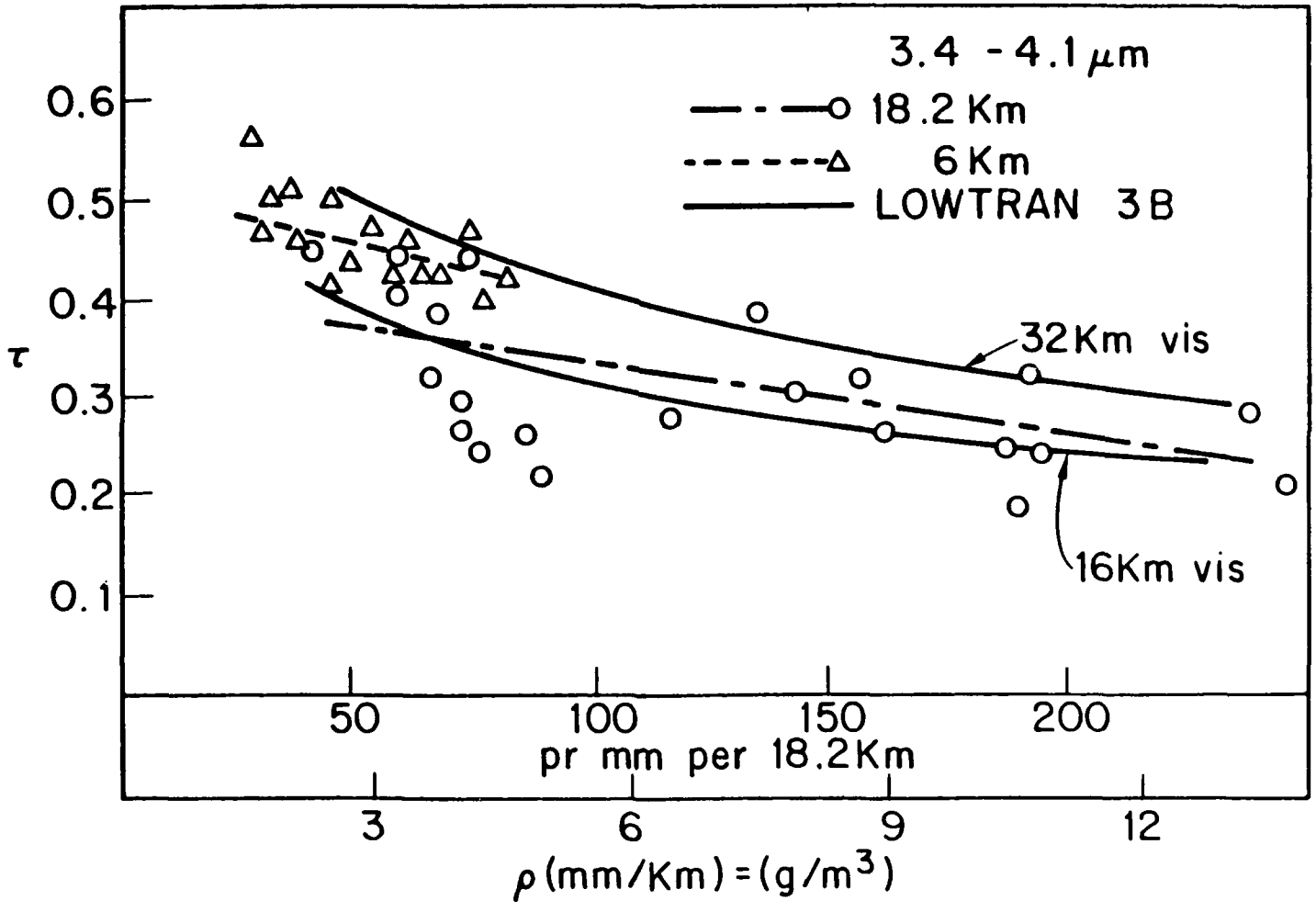

FIGURE 5. ATMOSPHERIC TRANSMISSION IN THE 3.4 μm TO 4.1 μm BAND MEASURED OVER 18.2 km AND 6 km PATHS (TNO-NETHERLANDS).

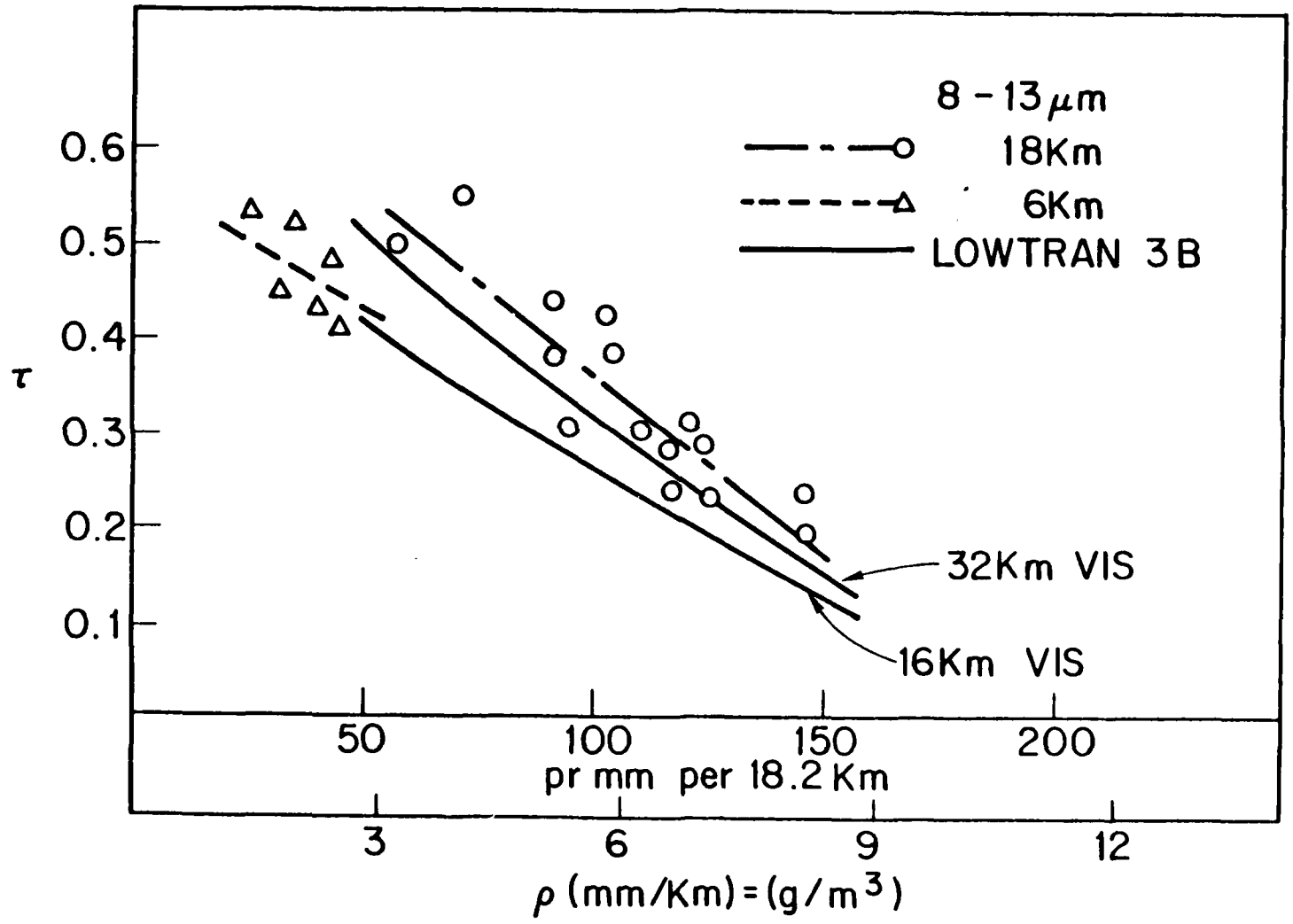

FIGURE 6. ATMOSPHERIC TRANSMISSION IN THE 8 μm TO 13 μm BAND MEASURED OVER 18.2 km AND 6 km PATHS (TNO-NETHERLANDS).

These data were taken for conditions of moderate visibility, i.e. R_V > 15 km (σ_{VIS} < 0.26 km^{-1}). The reasonably good agreement of the data with the LOWTRAN 3B calculations for R_V = 16 km shown for comparison in Figure 5 indicates that the sum of contributions due to molecular absorption and aerosol extinction are being accurately predicted by the model. The variability of the data for the 18.2 km path measurements for the range of atmospheric water vapor density around 75-80 precipitable mm per 18.2 km may well be accounted for by variability in the actual aerosol scattering not modeled by LOWTRAN 3B but due to wind and relative humidity variations which are taken into account in the WGM and K/R models. For the low values of absolute humidity corresponding to these measurements (i.e. 3 to 6 gm/m^3 of water vapor) the coefficient for molecular absorption should be only about 10% of that for aerosol extinction. Accordingly the general agreement between the data shown in Figure 5 and the LOWTRAN 3B prediction is primarily determined by agreement between the measurements and the LOWTRAN 3B aerosol model predictions.

The TNO data shown in Figure 6 for the 8-13 μm are not as useful as the mid-infrared-band data in verifying the LOWTRAN aerosol model predictions. Here the relative contributions of molecular absorption and aerosol scattering are more nearly comparable, the former being about a factor of six larger than for the data shown in Figure 5 while aerosol scattering in the 8-13 μm band should be less than 30% of that in the shorter wavelength band for the atmospheric conditions corresponding to most of the data shown in Figures 5 and 6, (i.e. 15-18 km visibilities, 60% to 80% relative humidities and wind speeds > 10 m/s) [25].

For the conditions corresponding to most of the TNO measurements, the LOWTRAN 3B, LOWTRAN 5 and K/R aerosol

models will give roughly comparable predictions. Differences in predictions by the various models only become apparent for windspeeds below 12 m/s (see Figure 2) where the K/R model predicts smaller values of σ_{IR}/σ_{VIS} than does either version of LOWTRAN, and/or for relative humidities < 70% or > 90%.

2.2.1.2 Australian Defense Science Establishment Long-Path Infrared Transmission Measurements

The Electronics Research Laboratory of the Australian Defense Scientific Technical Office carried out a measurement program using maritime paths located at Victor Harbor, 80 km south of Adelaide in 1977 and 1978. The path lengths used were 5.03 km and 9.05 km. A large reentrant blackbody cavity at a temperature of 980 K was used as a source and combined with an all-reflective receiver by using three detectors (PbS, InSb, and HgCdTe) and various filters to cover selected spectral bands between 1 μm and 13 μm [18].

Figures 7 and 8 show samples of data collected for each of the two paths during this program. Here transmission in the band between 4.41 μm and 5.4 μm is plotted against water vapor concentration in gm/m^3. The data were collected during very high visibility conditions for which the visual range exceeded 96 km. The figures show comparisons of LOWTRAN model calculations with the measured transmission values. The experimental data are at variance with the LOWTRAN calculation for water vapor densities greater than about 9 gm/m^3. Figures 9 and 10 show comparable data for the 8.2 μm to 11.8 μm band for the same two paths, again compared with the LOWTRAN model. Here the agreement between measurement and calculation for the shorter path is better than that for the shorter wavelength band shown in

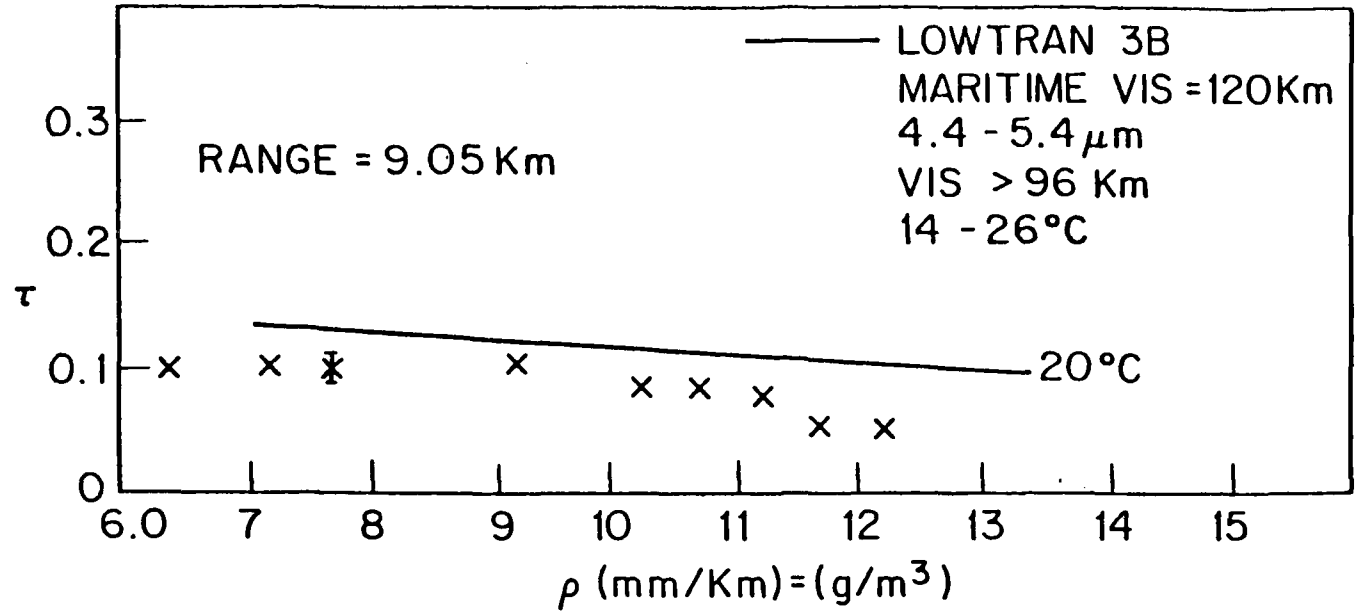

FIGURE 7. ATMOSPHERIC TRANSMISSION IN THE 4.4 μm TO 5.4 μm BAND MEASURED OVER A 9.05 km PATH (DSTO-AUSTRALIA).

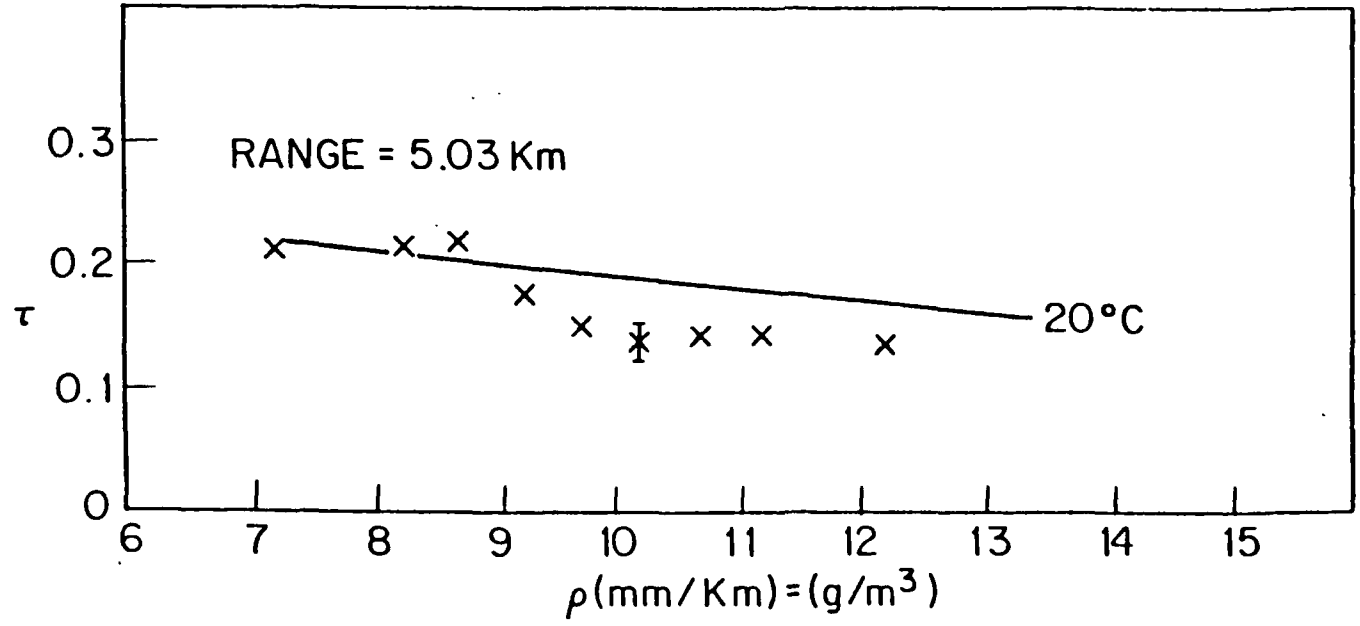

FIGURE 8. ATMOSPHERIC TRANSMISSION IN THE 4.4 μm TO 5.4 μm BAND MEASURED OVER A 5.03 km PATH (DSTO-AUSTRALIA).

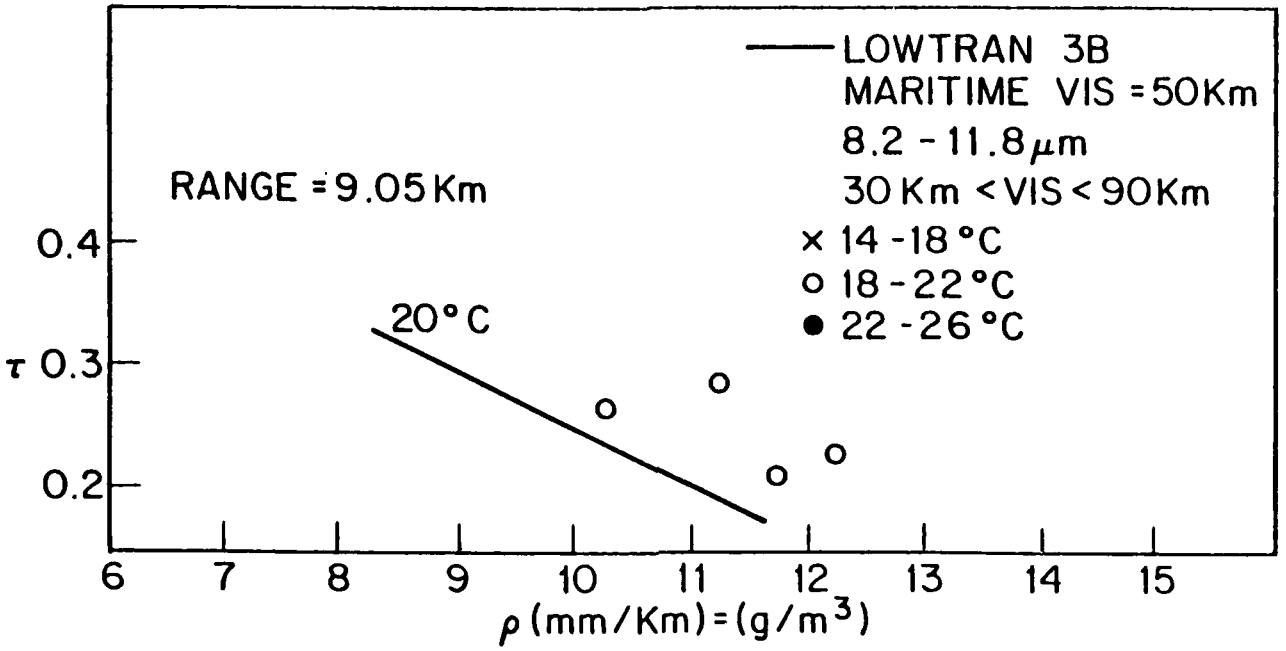

FIGURE 9. ATMOSPHERIC TRANSMISSION IN THE 8.2 μm TO 11.8 μm BAND MEASURED OVER A 9.05 km PATH (DSTO-AUSTRALIA).

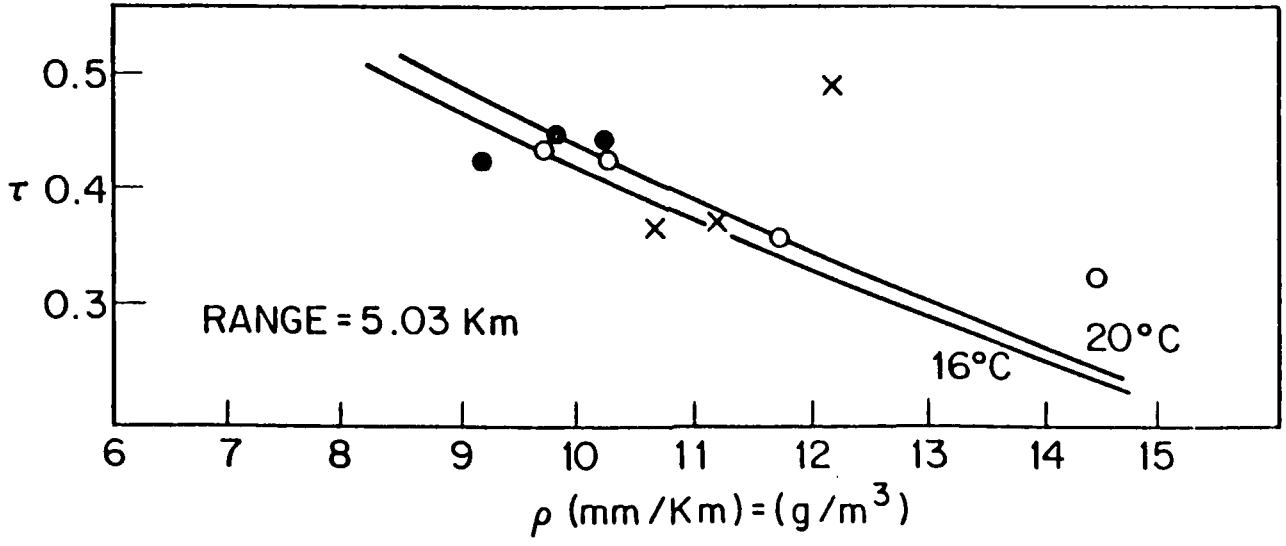

FIGURE 10. ATMOSPHERIC TRANSMISSION IN THE 8.2 μm TO 11.8 μm BAND MEASURED OVER A 5.03 km PATH (DSTO-AUSTRALIA).

Figures 7 and 8. However, for the 9.05 km path LOWTRAN significantly underestimates the transmission.

The data shown in Figures 7 through 10 are of interest in testing the validity of the molecular absorption components of LOWTRAN but are not particularly useful in verifying aerosol models since the actual aerosol extinction component of the measurements is vanishingly small (R_V > 96 km in all cases). All outdoor transmission measurements will contain contributions from each source of attenuation. Hopefully, selection of certain sub-sets of data can be made depending upon which components of a transmission model are of interest. The Australian DSTO data are useful for molecular absorption model validation but not for the topic of present concern in this work, i.e., aerosol model comparisons. The TNO data on the other hand which are shown in Figures 5 and 6 were collected under moderate visibility ($R_V \sim$ 15 km) and low water vapor (3-6 torr H_2O) conditions and are therefore more useful in aerosol model comparisons, particularly the data for the 3-5 μm region. Data in which the relative contribution of molecular absorption and aerosol extinction are comparable, are typically less useful for model comparison purposes, except in cases where the molecular absorption coefficients are very well known. The residual attenuation is then a reliable measure of the aerosol contribution to total attenuation.

2.2.1.3 OPAQUE Measurement Program Long-Path Infrared Transmission Measurements

An extensive measurement program at several sites in Western Europe was begun under the OPAQUE program in 1976 and continued into 1980 [21]. Selected data from the Netherlands measurement site located at the Hague near the North Sea coast were analyzed in reference 22. The data

available for that study were collected during the period from 1 March 1977 to 31 May 1977. At this time of year the Netherlands is subject to a wide range of weather conditions varying from cold temperatures and dry conditions resulting from polar airmasses to mild, moist conditions associated with maritime air masses.

Examples of the OPAQUE data analyzed in reference 22 are shown in Figures 11 and 12 where they are compared to LOWTRAN predictions and to a water haze model whose development is described in reference 22. Supporting meteorological data for the optical measurements shown here are not readily available without recourse to magnetic data tapes obtainable from the OPAQUE program. Detailed analysis of these data and comparison to LOWTRAN 5 and K/R model predictions is beyond the scope of the present effort, however the trends apparent in the data shown in Figures 11 and 12 and the comparisons to the maritime and rural components of LOWTRAN 3B are instructive to note. The data for the ratio $\sigma_{3-5}/\sigma_{VIS}$ lie between the LOWTRAN calculations for the two types of atmospheres and are in fair agreement with the water haze model described in Reference 22. A large amount of scatter is evident in the data however. The data for the 8-12 μm region shown in Figure 12 show quite a different trend indicating that $\sigma_{8-12}/\sigma_{VIS}$ is generally larger than the predictions obtained with either version of LOWTRAN or the SAI water haze model. The ranges of values for σ_{3-5} and σ_{8-12} shown in the figures are still useful in assessing the range of scattering values at these wavelengths to be expected for maritime conditions.

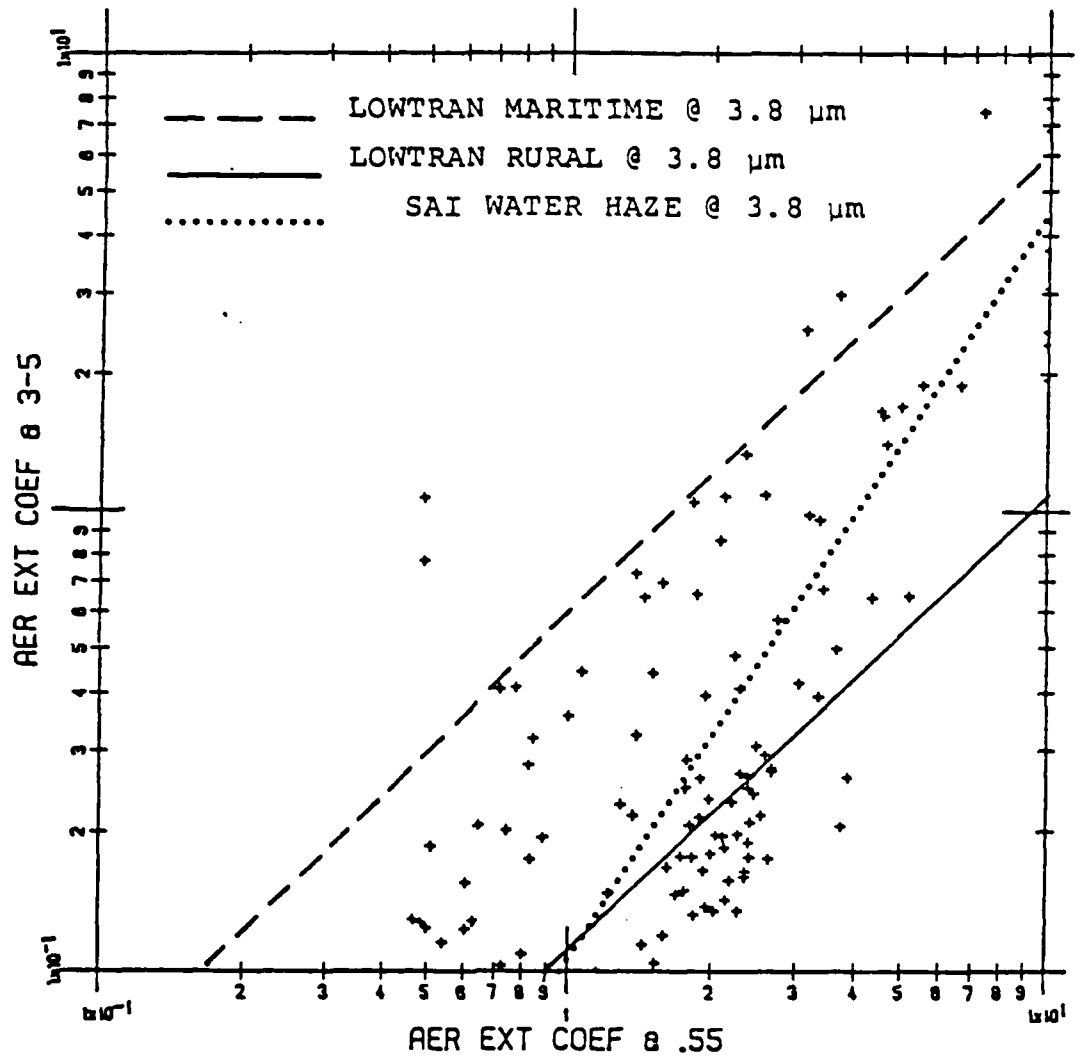

FIGURE 11. COMPARISON OF VARIOUS AEROSOL MODELS WITH OPAQUE DATA AEROSOL EXTINCTION COEFFICIENT @ 0.55 μm VERSUS AEROSOL EXTINCTION COEFFICIENT @ 3-5 μm DERIVED FROM OPAQUE NETHERLANDS 3/77-5/77 DATA.

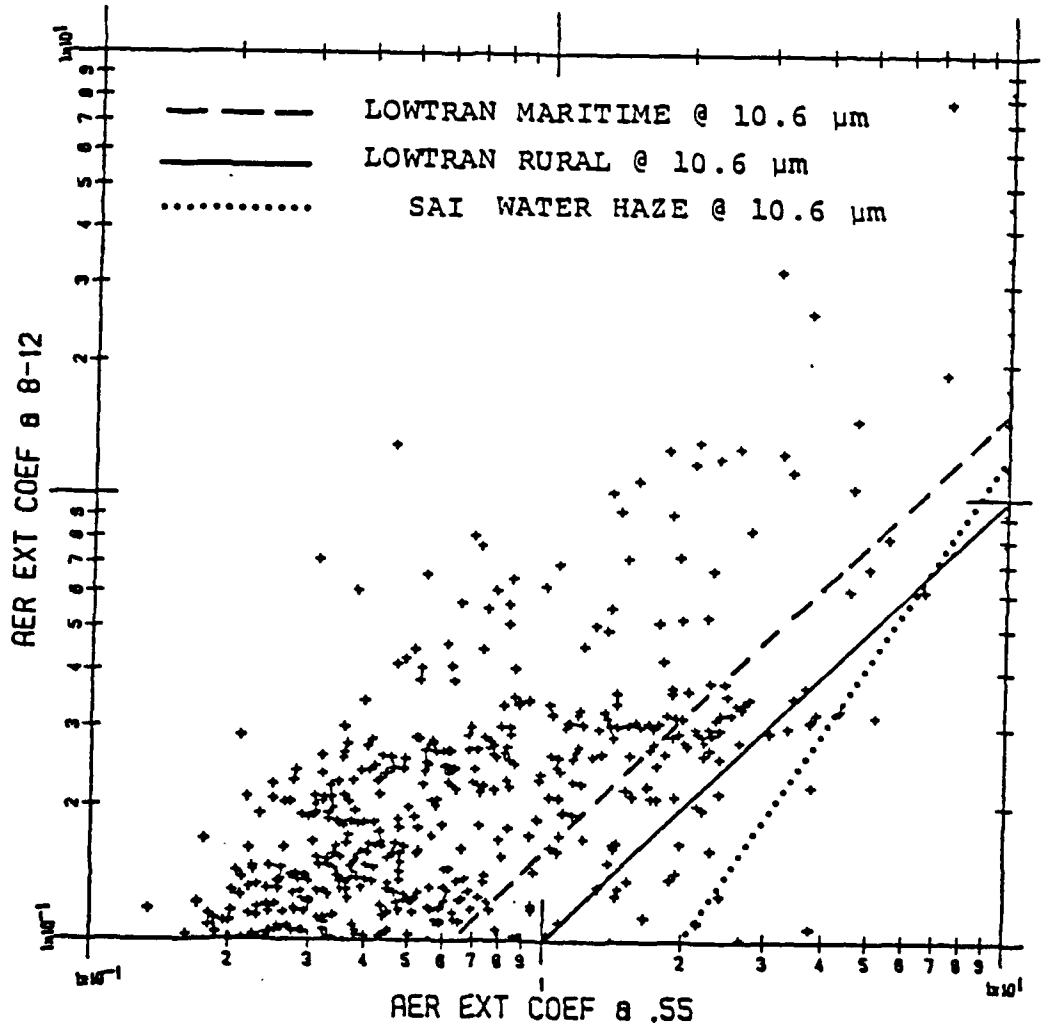

FIGURE 12. COMPARISON OF VARIOUS AEROSOL MODELS WITH OPAQUE DATA AEROSOL EXTINCTION COEFFICIENT @ 0.55 μm VERSUS AEROSOL EXTINCTION COEFFICIENT @ 8-12 μm DERIVED FROM OPAQUE NETHERLANDS 3/77-5/77 DATA.

2.2.1.4 Pacific Missile Test Center (PMTC)/Naval Weapons Center Optical Signatures Program (NWC-OSP) Long-Path Infrared Transmission Measurements

Overwater long-path infrared transmission measurements using 2.4 km and 4.07 km paths have been performed at San Nicolas Island, California starting in 1978 [26]. A small quantity of preliminary data generated by this program was analyzed and described in reference 22. Examples of volume extinction coefficients at 1.06 μm, 3.7 - 3.9 μm and 4.8 - 5.0 μm plotted versus 0.55 μm extinction coefficients from this limited set of data are shown in Figures 13, 14 and 15 respectively. The reasonably good linear curve fits to the σ_{IR}/σ_{VIS} ratios shown in these figures indicate that a simple approximate relationship of the form $\sigma_{IR} \sim \sigma_{VIS}^{n}$ might be used to relate infrared to visible aerosol attenuation. When much larger samples of data are considered greater scatter is typically observed and a power law relationship no longer fits the data very well. It is likely that this observation corresponds to the super-position of data sets corresponding to different values of n in a power law relationship which may be related to different air masses. That is, a given value of n may provide a good fit to data such as shown in Figures 13-15 under the influence of a constant air mass, whereas a different value of n may be appropriate for different air masses. When the data for several air masses are superimposed on a single plot of σ_{IR} versus σ_{VIS}, no single value of n fits the data and the more sophisticated aerosol models (e.g. K/R model dependence on windspeed and RH) are required. Recently a more comprehensive statistical analysis of data generated under the PMTC/OSP measurement program between 1978 and 1979 has been performed by Katz and DeBold [27]. In this analysis data were compared to the K/R,

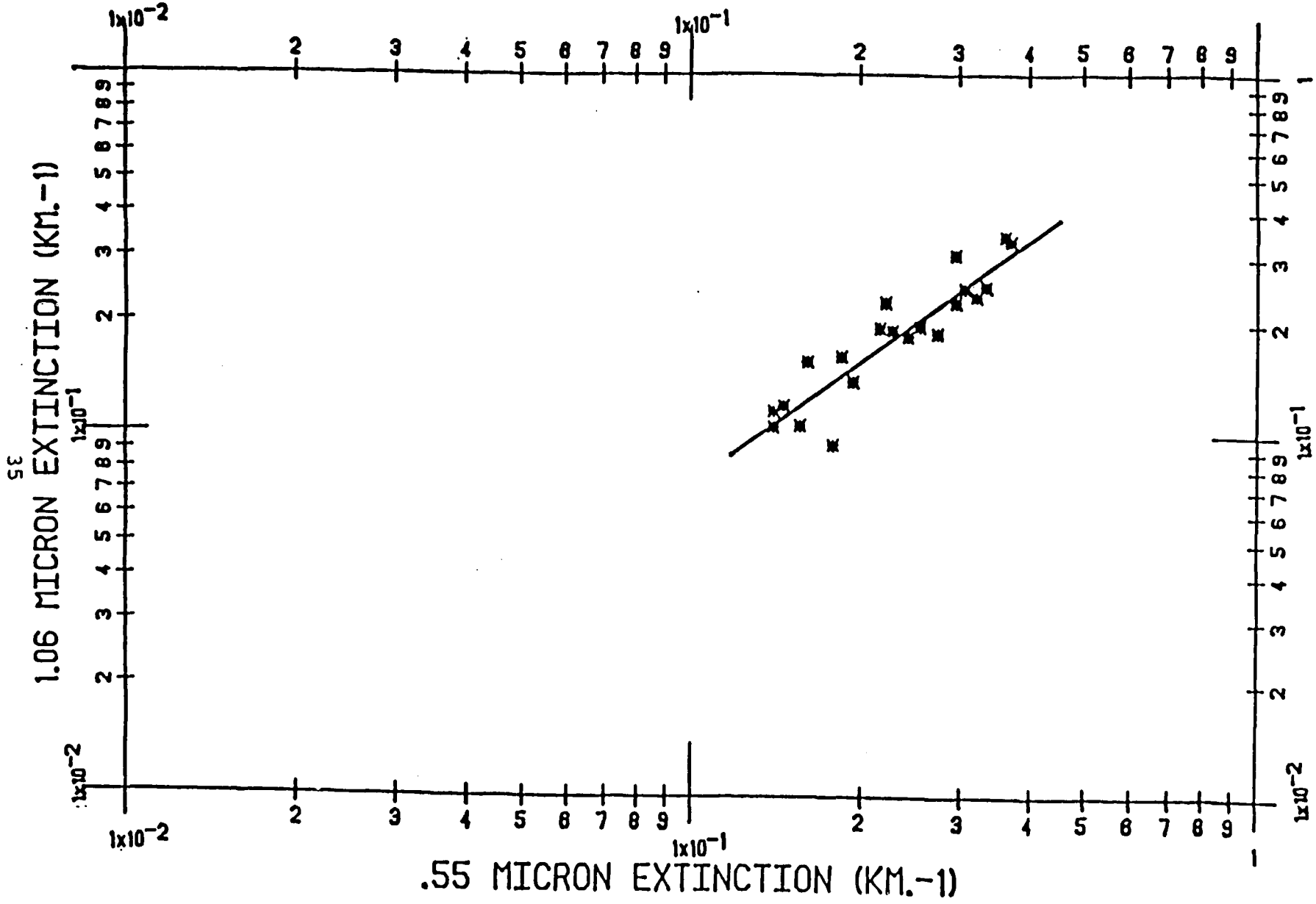

FIGURE 13. VOLUME EXTINCTION COEFFICIENTS AT 1.06 μm AND 0.55 μm FOR OSP DATA TAKEN AT SAN NICOLAS ISLAND BETWEEN 4/27/78 AND 5/18/78.

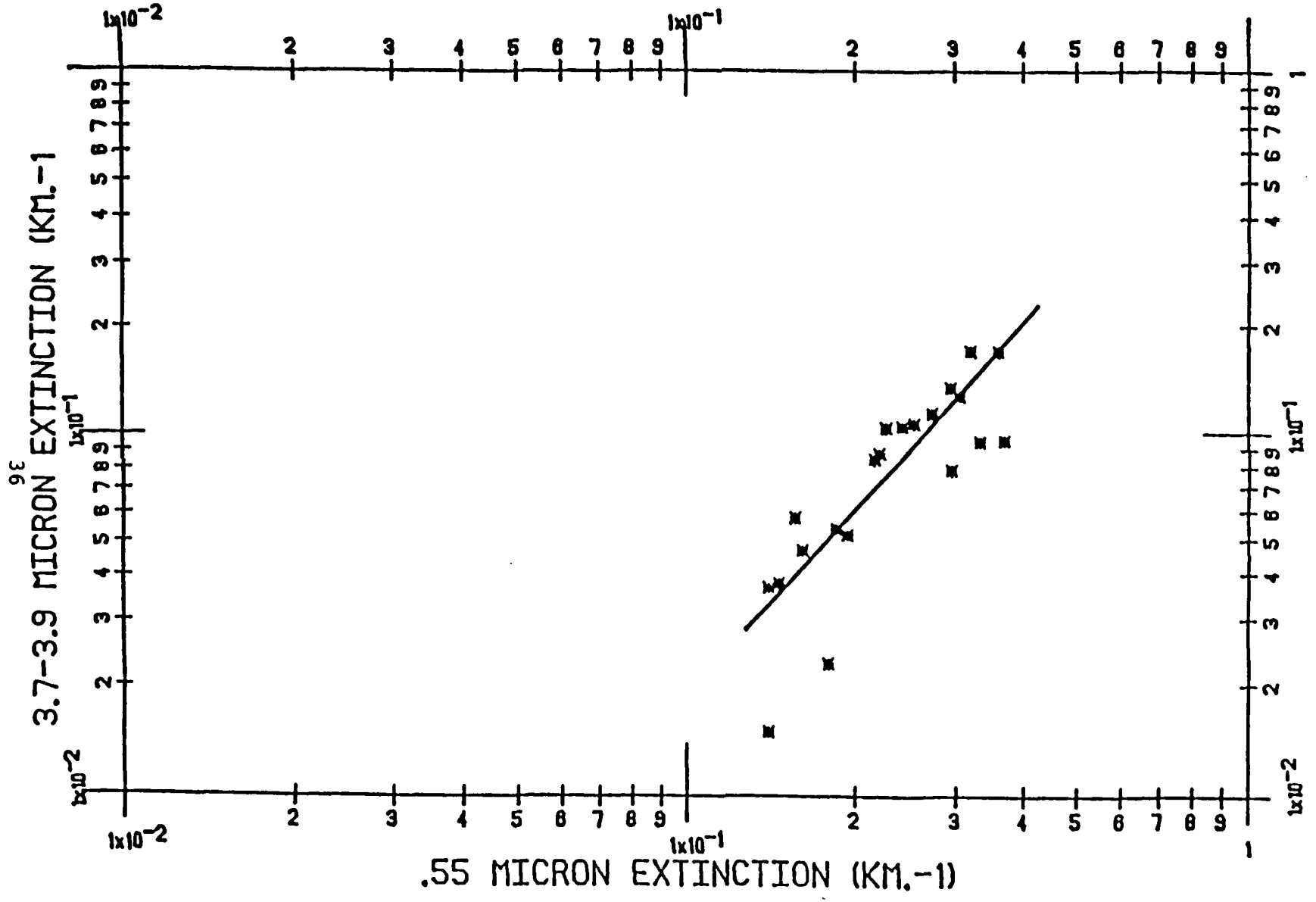

FIGURE 14. VOLUME EXTINCTION COEFFICIENTS AT 3.7-3.9 μm AND 0.55 μm FOR OSP DATA TAKEN AT SAN NICOLAS ISLAND BETWEEN 4/27/78 AND 5/18/78.

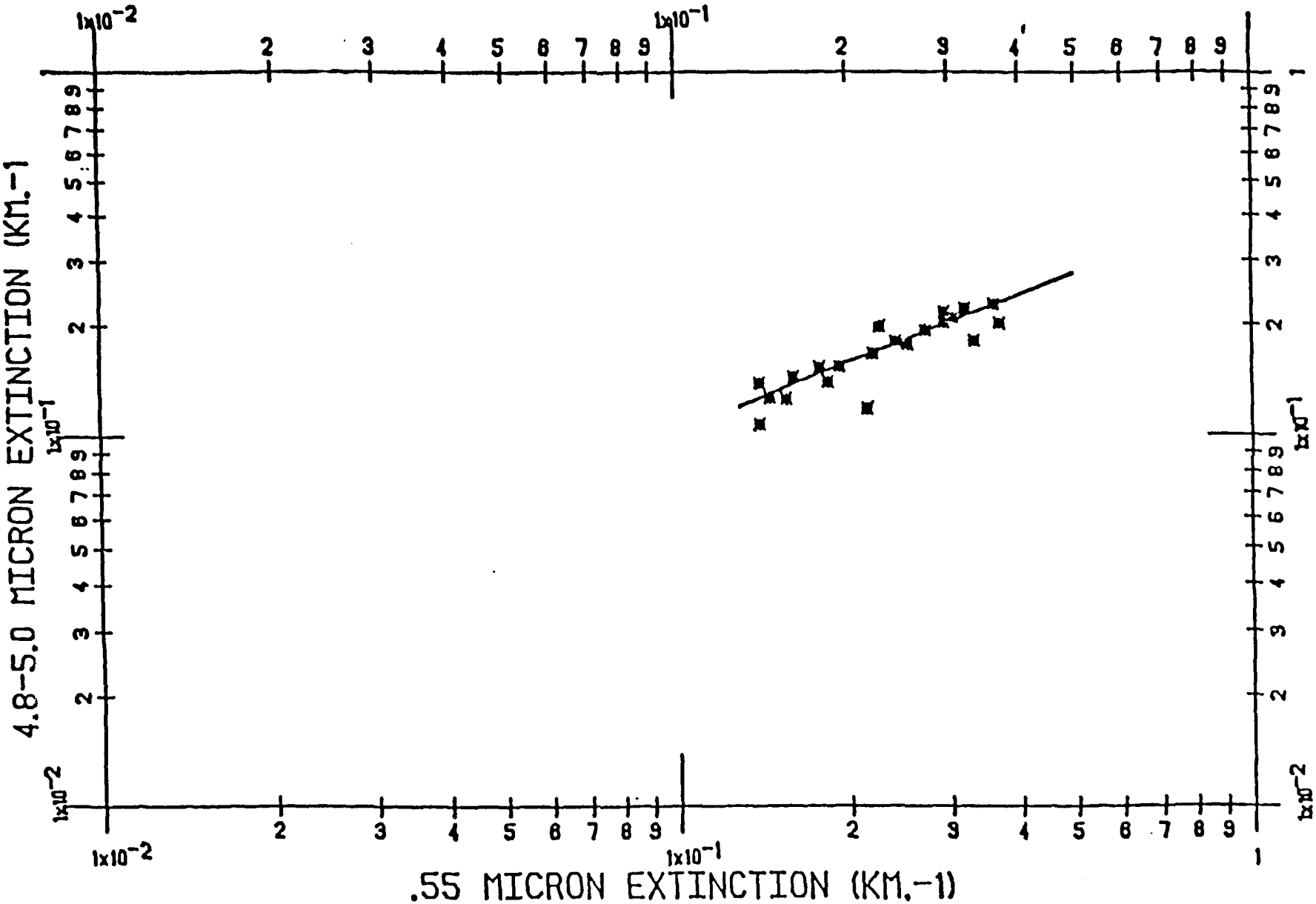

FIGURE 15. VOLUME EXTINCTION COEFFICIENTS AT 4.5-5.0 μm AND 0.55 μm FOR OSP DATA TAKEN AT SAN NICOLAS ISLAND BETWEEN 4/27/78 AND 5/18/78.

LOWTRAN 3B Maritime and GAP (low visibility) [22] models. Figure 16 shows an example of comparisons of the OSP-SNI data for the ratios σ_{IR}/σ_{VIS} for different wavelength bands plotted versus windspeed. The extinction data were divided into windspeed intervals of 2 m/s. The error bars indicate the standard deviations about the mean value for each windspeed group. The LOWTRAN 3B model predictions are in agreement with the experimental data (solid lines) for windspeeds near 10 m/s. The broken lines show calculations performed with the K/R model which are seen to be in reasonable agreement with the experimental data. The LOWTRAN calculations can be seen to significantly overestimate the ratio σ_{IR}/σ_{VIS} for windspeeds < 10 m/s.

2.2.1.5 Naval Research Laboratory (NRL) Long-Path Infrared Transmission Measurements

Long-path atmospheric transmission measurements were performed by NRL during the period 1974-1979 using laser-transmissometer-calibrated high-resolution Fourier transform spectroscopy [28,29]. During this measurement program overwater experiments were conducted at Cape Canaveral Air Force Station (CCAFS), Florida and also at SNI using the same optical path as the PMTC-OSP measurements. A compendium report containing a tabulation of data acquired at CCAFS was published in 1977 [30] and an analysis of these measurements will be presented in a forthcoming report [23]. A report describing the NRL long-path transmission measurements at SNI in 1979 will be available in the near future [24]. Selected examples of analysis drawn from these reports are available and will be considered since they contain relevant maritime aerosol infrared extinction data.

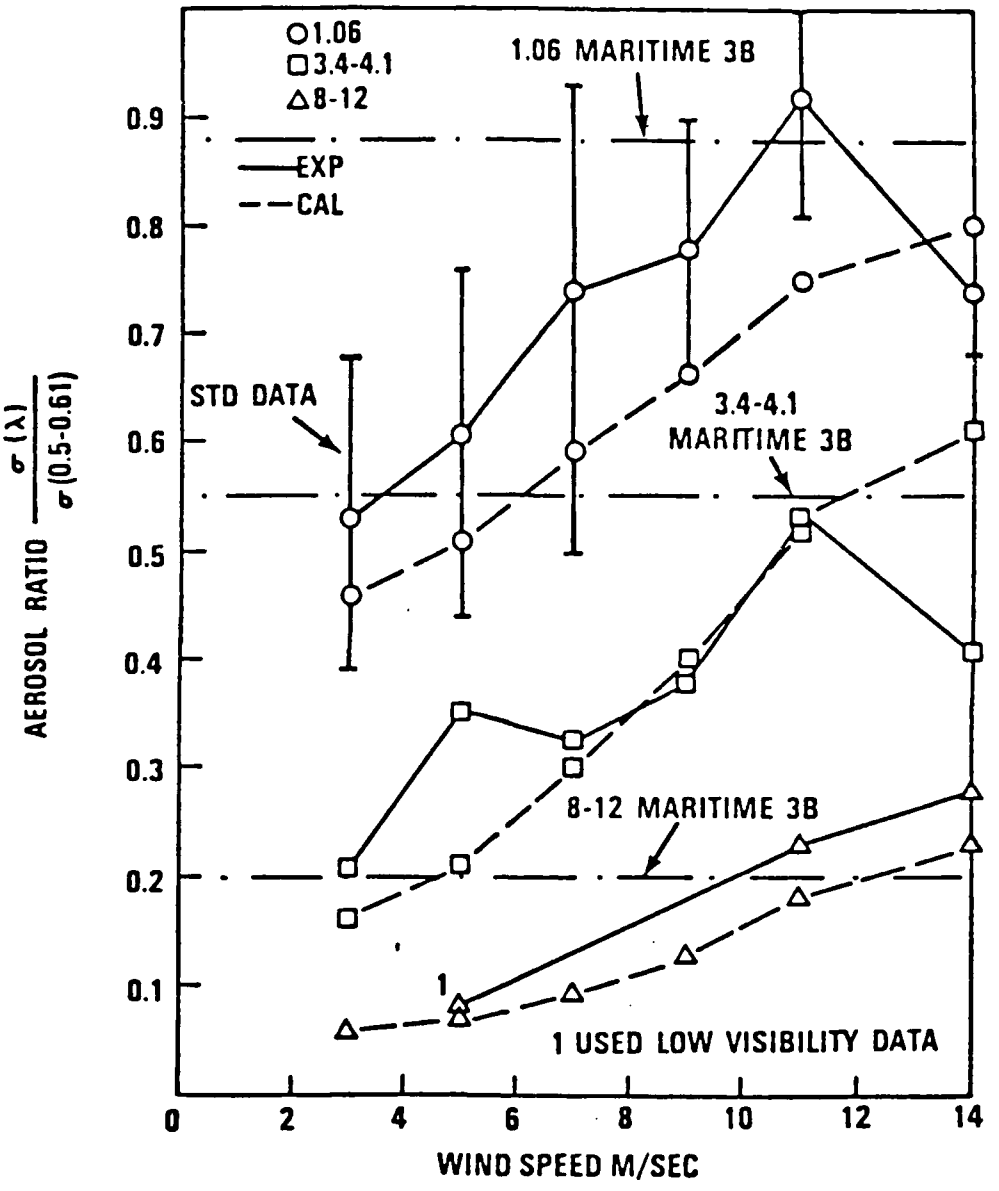

FIGURE 16. AEROSOL IR TO VISIBLE EXTINCTION RATIOS VERSUS 12 HOURLY AVERAGE WINDSPEED. A COMPARISON BETWEEN SNI EXPERIMENTAL DATA, NPGS NORTH ATLANTIC AEROSOL DISTRIBUTION DATA AND SUBSEQUENT EXTINCTION RATIO CALCULATIONS, AND THE K/R AND LOWTRAN 3B MARITIME MODEL RESULTS.

Table 1 which is based on reference 23 contains a summary of the daily observations of wind speed and direction, visibility, absolute humidity, air temperature and apparent aerosol extinction (AAE) values determined for the different laser wavelengths measured in the 1977 NRL-CCAFS experiment. The AAE values correspond to measured extinction coefficients for HeNe and Nd-YAG laser wavelengths and to the quantity EXT-CMA for DF and CO_2 laser wavelengths, where EXT are measured total extinction coefficients and CMA are calculated molecular absorption values corresponding to the atmospheric conditions and laser wavelengths studied during a particular set of measurements. When several laser frequencies were measured during a particular experimental run (on a particular day) an average value of AAE for the several measurements was determined. Occasionally long-path extinction measurements for many laser lines were collected (as many as 80 CO_2 laser lines on some days and repeated measurements of a manifold of several DF laser lines). A representative value for AAE appropriate to the spectral interval covered by the several laser lines was then determined and used as the value appearing in Table 1. The measurements performed for overwater wind conditions (designated by OW in column 3 of the table) are considered to be most representative of maritime conditions.

Ratios of selected AAE values appearing in Table 1 were formed and are compared to K/R model predictions in Table 2. The ratio of the experimental data for the different laser wavelengths are designated by the symbol Re and the laser identification in appropriate columns of the table. Data were selected for overwater wind conditions of at least 2 m/s and for relative humidities > 65%. One can see from an examination of the entries in the table that the K/R model predictions for Re are generally lower

TABLE 1

Daily Record of Wind Character, Meteorological Parameters and Apparent Aerosol Extinction (AAE) Values from NRL 1977 CCAFS Data Base

Date	Wind Direction (DEG)	OL/OW†	Wind Speed (m/s)	Visibility (km)	ppH_2O (torr)	AT (°C)	AAE HeNe (km^{-1})	AAE Nd-YAG (km^{-1})	AAE DF (km^{-1})	AAE CO_2 (km^{-1})	Date/ Time	AAE HeNe (km^{-1})	AAE Nd-YAG (km^{-1})
3-2-77	30	OL	4.0	33	5.5	18.0	.065			.011			
3-3-77	100	OW	3.7	18	13.4	18.6			.140				
3-7-77	245	OL	0.1	11	17.0	27.3	.091		.060				
3-8-77	27	OL	3.3	20	10.0	19.8	.104		.070	.005	3-14-77		
3-9-77	67	OW	3.3	12	11.0	19.5	.134		.080	.020	1006	.099	
3-10-77	70	OW	2.3	8	14.5	20.0	.347			.030	1603	.099	
3-11-77	115	OW	0.1	14	16.0	22.0	.214		.120	-.015			
3-12-77	145	OW	2.0	16	17.0	22.0	.140		.085		4-2-77		
3-14-77	40	OL	2.5	23	7.0	24.2	.099		.050	.050	1151	.127	.074
3-15-77	310	OL	1.8	30	11.0	22.8	.103		.030	.015	1237	.126	.080
											1315	.116	.075
3-31-77	150	OW	4.5	24	18.2	25.0			.055		1422	.110	.077
4-1-77	130	OW	4.0	14	18.4	24.1	.196		.040	-.030	1503	.104	.087
4-2-77	137	OW	5.0	~30	18.7	25.0	.115	.083	.030	-.055	1545		.089
4-4-77	157	OW	8.7	20	18.3	24.2	.160	.148	.080	-.030			
4-5-77	270	OL	6.3	48	9.8	24.9	.063	.050	.020	.007	4-4-77		
											1053	.127	.105
5-16-77	100	OW	5.5	24	15.0	25.0	.117	.049		-.020	1133	.113	.107
5-17-77	62	OW	6.1	14	15.3	26.0	.138	.038		-.020	1709		.106
5-20-77	78	OW	3.3	25	14.7	26.2	.101	.049	.080		1452	.172	.160
5-21-77	~85	OW	5.0	16	16.4	26.3	.164	.062	.040		1533	.183	.171
5-23-77	~90	OW	~3.0	46	18.2	25.8	.048	.055	.030	-.055	1617	.207	.195
5-24-77	115	OW	~4.9	33	20.8	26.5	.057	.056	.045	-.055			
5-25-77	220	OW	2.9	22	20.4	28.6	.100	.068	.040	-.065			

† OL = overland; OW = overwater

* ~ = approximately or variable with average value indicated; // = parallel; ⊥ = perpendicular

TABLE 2

Comparison of σ_{IR}/σ_{VIS} Values from NRL 1977 CCAFS Data Base to Aerosol Model Predictions

DATE	RH %	VIS (KM)	WS m/s	Re Nd-YAG	K/R	LW 3B	LW 5	Re DF	K/R	LW 3B	LW 5
3-12-77	86	16	2.0					.607	.07		
4-2-77	79	30	5.0	.722	.53	.72	.87	.261	.170	.55	.60
4-4-77	82	20	8.7	.925	.62	.72	.87	.500	.300	.55	.60
5-21-77	65	16	5.0	.378	.51	.72	.76	.244	.16	.55	.36
5-23-77	73	46	3.0	1.146	.50	.72	.77	.625	.16	.55	.39
5-24-77	80	33	4.9	.983	.53	.72	.77	.789	.17	.55	.60
5-25-77	70	22	2.9	.680	.50	.72	.87	.400	.16	.55	.38

than those observed for the Nd-YAG laser transmission data. On the average, the K/R predictions are about 74% of the measured values for Re = σ_{IR}/σ_{VIS} for the Nd-YAG laser data and about 47% of the values measured for the DF laser data. The windspeed values corresponding to these data are generally in the 3 to 5 m/s range and under these conditions, as shown in Figure 2, the K/R model predicts significantly lower values for σ_{IR}/σ_{VIS} than does either version of LOWTRAN.

The variability in the data for both wavelengths does not appear to be particularly well represented by the K/R model. The LOWTRAN 3B and LOWTRAN 5 models show better agreement in magnitude of Re with the experimental data than does the K/R model but the scatter in Re values in this limited set of comparisons is too large for this small sample set to provide any conclusive results.

Figures 17-21 shows plots of DF laser extinction data collected during the NRL-SNI measurements. Measured extinction coefficients (α) minus calculated molecular absorption values (CMA) are plotted versus wavenumber for the set of 7 DF laser lines used in the experiment. The quantity α - CMA is then a direct measure of aerosol attenuation over the 4.07 km path provided the CMA values are correct. Based on extensive comparisons of similar measurements to molecular absorption models [31,32], the CMA values are known quite well. The largest remaining uncertainty in the molecular absorption values concerns the magnitude of the weak absorption due to the water vapor continuum in the DF laser region.

The consistent trends showing a decrease of the α - CMA values versus wavenumber in Figures 17-21 are probably due to minor discrepancies in the spectral shape of the

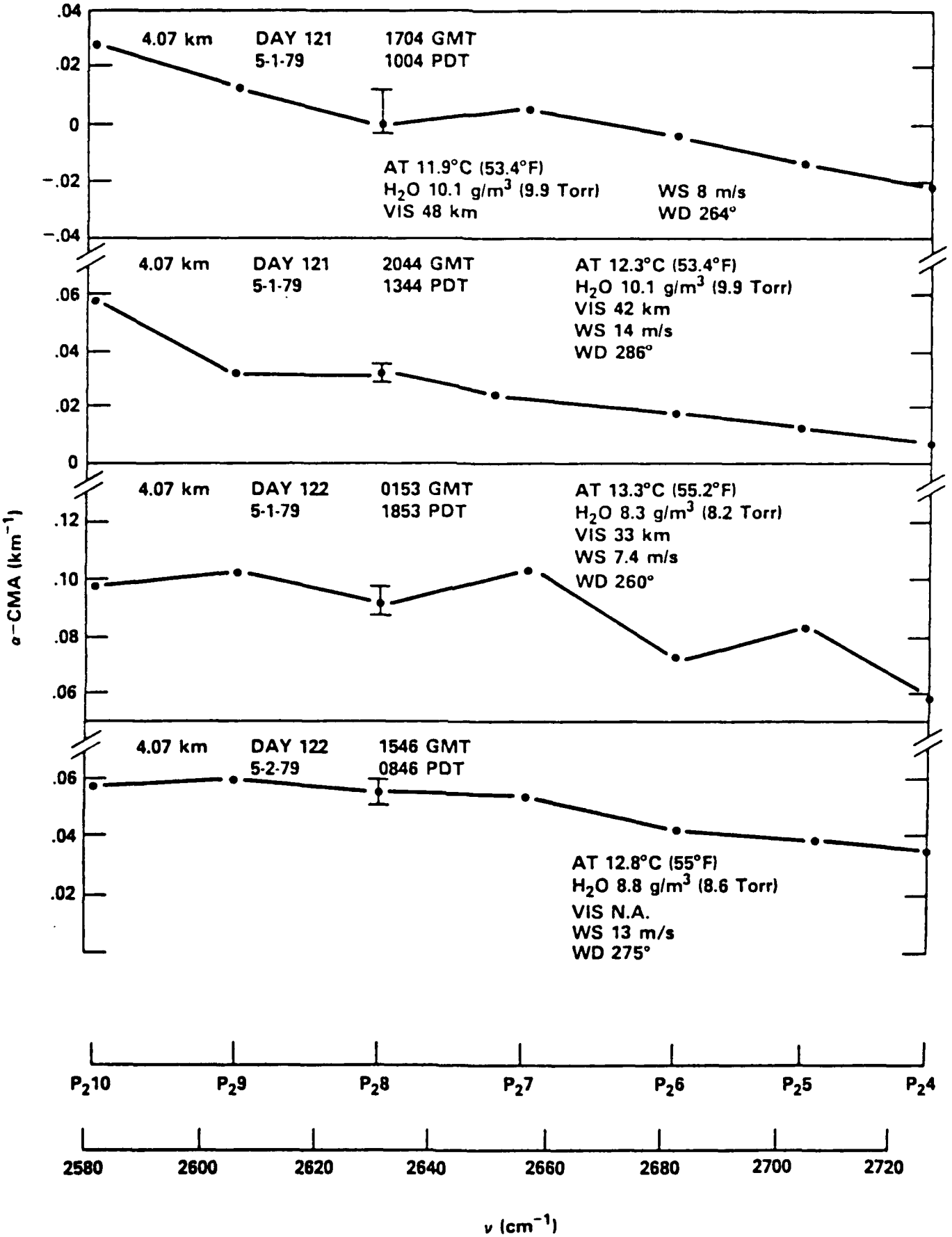

FIGURE 17. MEASURED EXTINCTION COEFFICIENTS MINUS CALCULATED MOLECULAR ABSORPTION COEFFICIENTS VERSUS WAVE-NUMBER FOR NRL MEASUREMENTS AT SNI OF SEVERAL DF LASER LINES. FROM TOP TO BOTTOM: DATA FOR 5/1/79 AND 5/2/79 RESPECTIVELY.

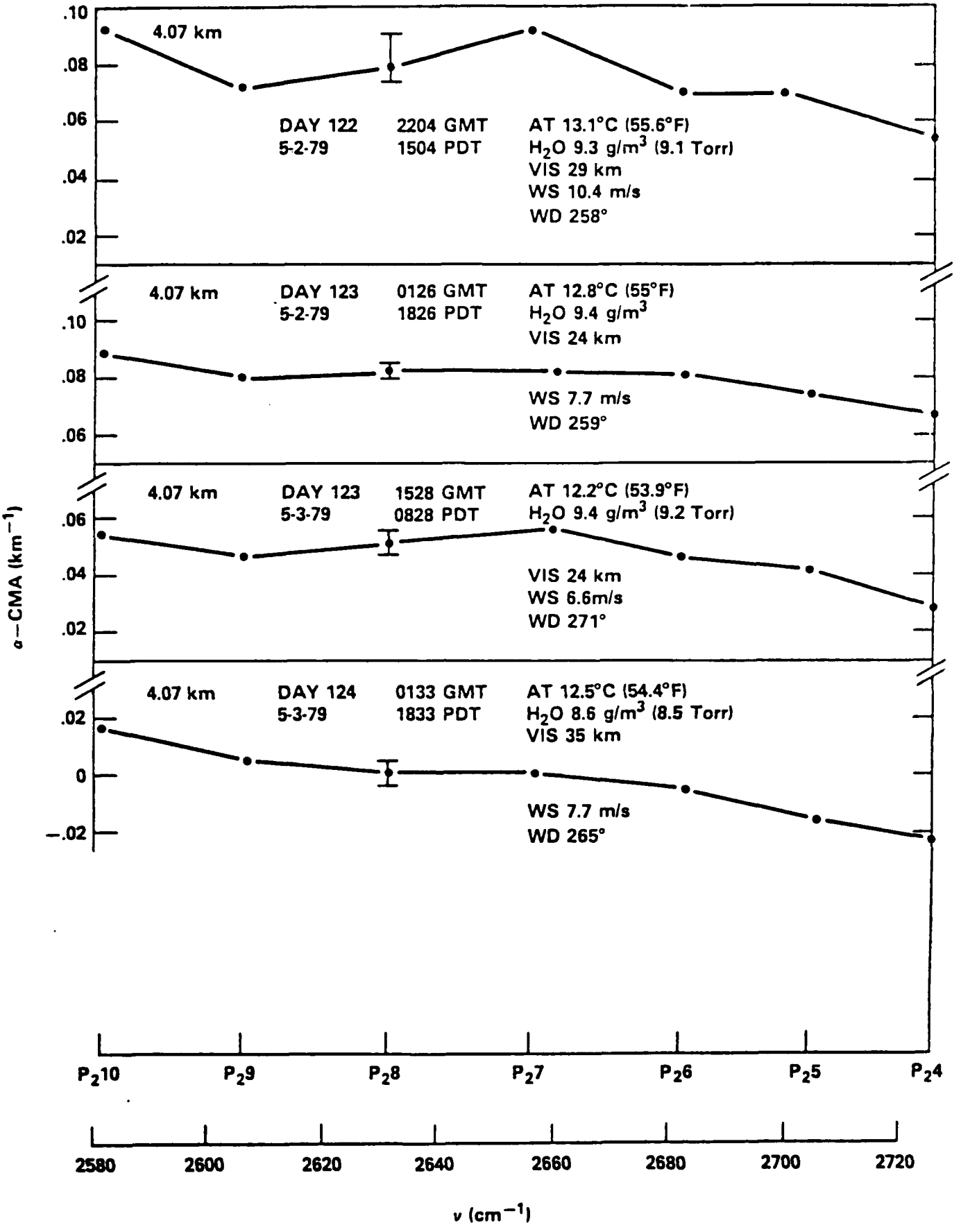

FIGURE 18. MEASURED EXTINCTION COEFFICIENTS MINUS CALCULATED MOLECULAR ABSORPTION COEFFICIENTS VERSUS WAVE-NUMBER FOR NRL MEASUREMENTS AT SNI OF SEVERAL DF LASER LINES. FROM TOP TO BOTTOM: DATA FOR 5/2/79 AND 5/3/79 RESPECTIVELY.

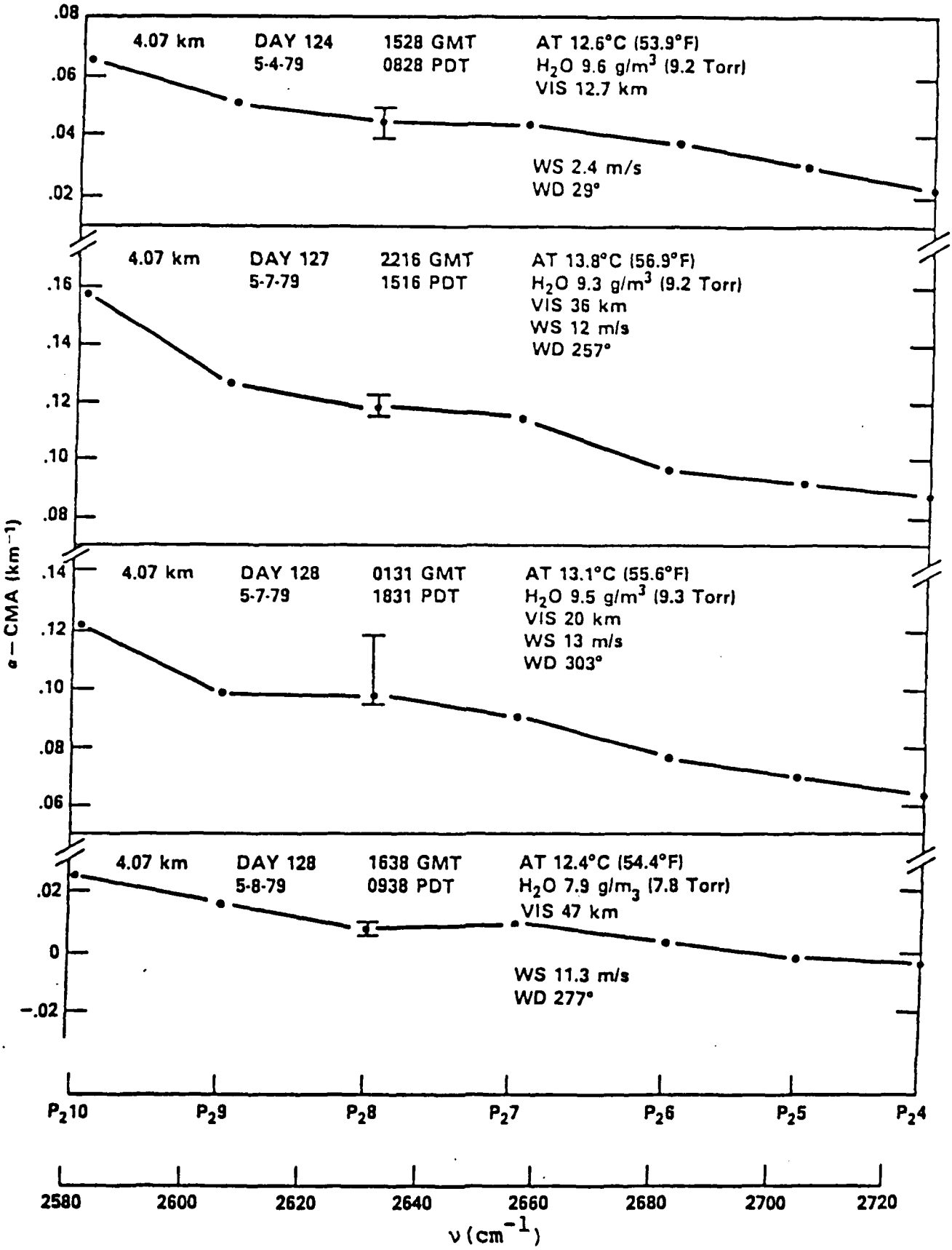

FIGURE 19. MEASURED EXTINCTION COEFFICIENTS MINUS CALCULATED MOLECULAR ABSORPTION COEFFICIENTS VERSUS WAVE-NUMBER FOR NRL MEASUREMENTS AT SNI OF SEVERAL DF LASER LINES. FROM TOP TO BOTTOM: DATA FOR 5/4/79 THROUGH 5/8/79 RESPECTIVELY.

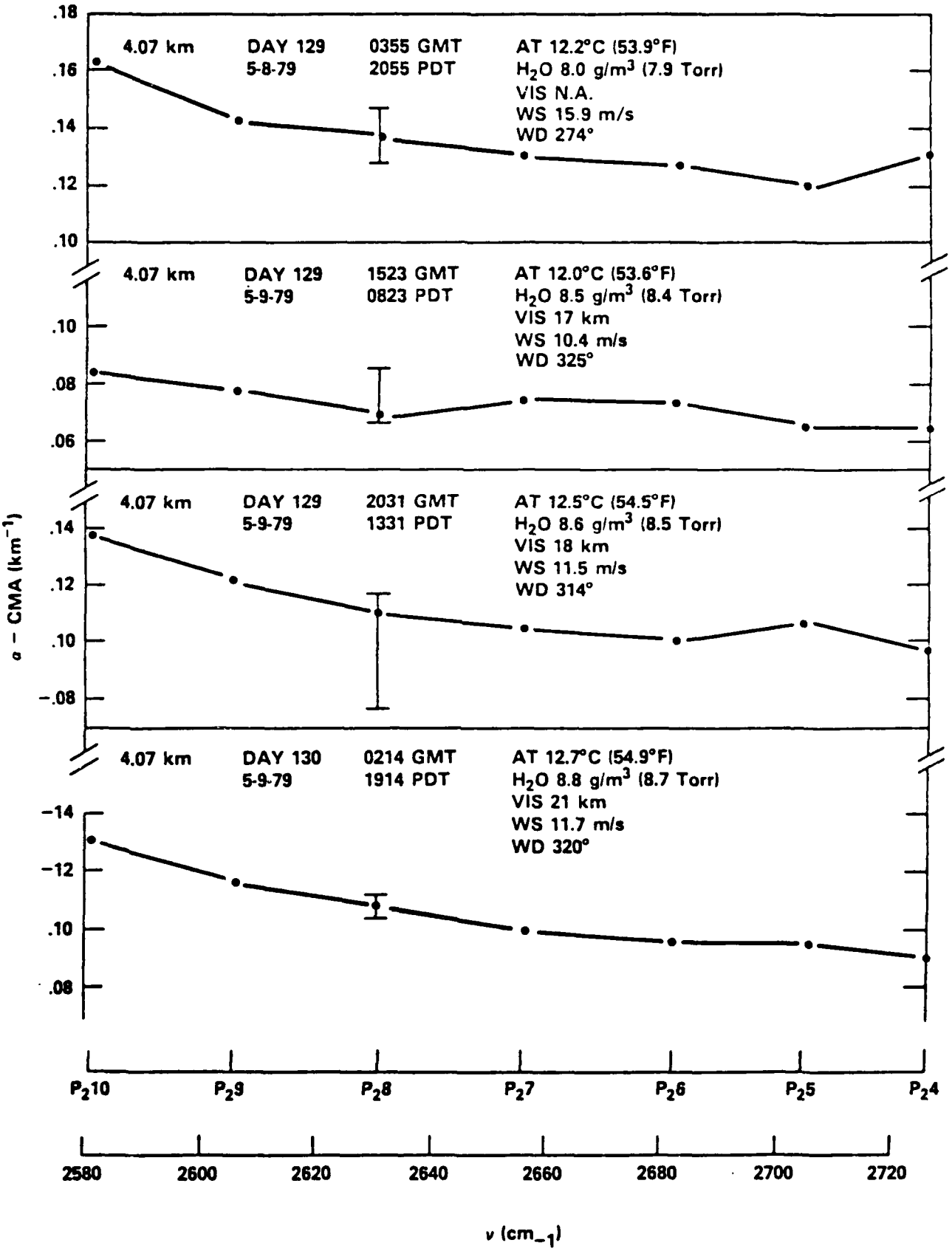

FIGURE 20. MEASURED EXTINCTION COEFFICIENTS MINUS CALCULATED MOLECULAR ABSORPTION COEFFICIENTS VERSUS WAVE-NUMBER FOR NRL MEASUREMENTS AT SNI OF SEVERAL DF LASER LINES. FROM TOP TO BOTTOM: DATA FOR 5/8/79 AND 5/9/79 RESPECTIVELY.

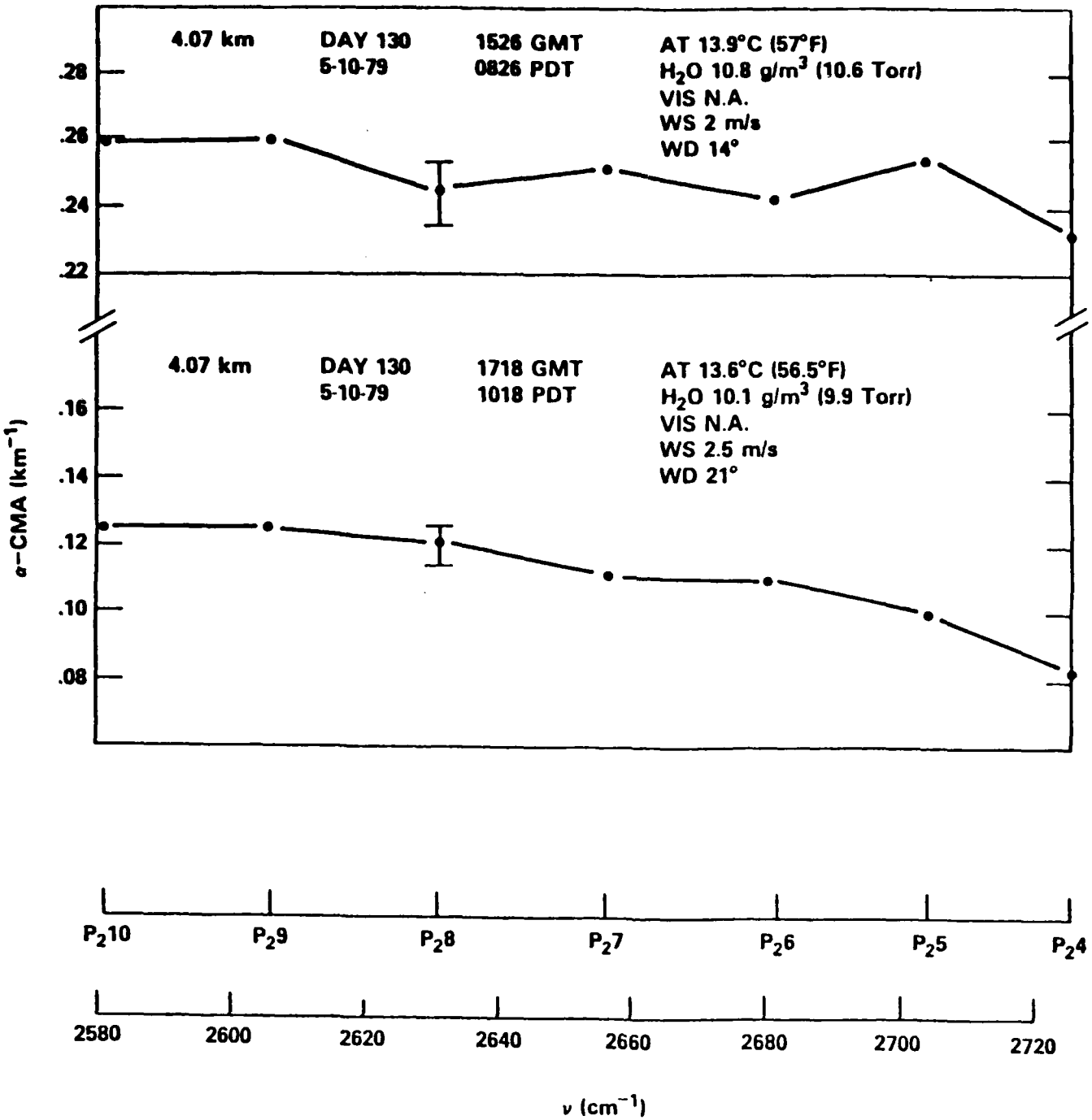

FIGURE 21. MEASURED EXTINCTION COEFFICIENTS MINUS CALCULATED MOLECULAR ABSORPTION COEFFICIENTS VERSUS WAVENUMBER FOR NRL MEASUREMENTS AT SNI OF SEVERAL DF LASER LINES. TOP-0826 PDT: BOTTOM-1018 PDT.

H_2O continuum absorption model used in generating the CMA values. Average values of α - CMA were determined from several of the curves plotted in Figures 17-21 and are tabulated in column 7 of Table 3. The ratios $\overline{\sigma_{DF}}/\sigma_{VIS}$ for the experimental data are tabulated in column 9. Comparable ratios determined from the K/R and LOWTRAN 5 models are tabulated in columns 10 and 11 respectively. A comparison of the entries in the last three columns of the table shows that the experimental values ($\overline{\sigma_{DF}}/\sigma_{VIS}$) are lower than either model prediction for the high visibility conditions encountered on 5-1-77. The K/R model, although predicting a somewhat lower magnitude than experimentally observed, reproduces the trends as a function of windspeed shown by the data better than the LOWTRAN 5 model. The advantage of the windspeed dependence incorporated into the K/R model can be seen from this comparison.

2.2.2 MARINE AEROSOL DISTRIBUTION MEASUREMENTS

Comparisons of infrared aerosol extinction values derived from aerosol spectrometer measurements in maritime conditions have been recently performed using aircraft measurements by the Naval Ocean Systems Center (NOSC) [4] and in conjunction with British weather ship operations in the North Atlantic by the Naval Research Laboratory (NRL) [33]. Certain NRL measurements performed at CCAFS [30] were supported by shore-based aerosol spectrometer measurements. During analysis of the NRL-CCAFS data [23] it became apparent that for overwater wind directions aerosol extinction values derived from aerosol spectrometer data would significantly overestimate the actual aerosol extinction.

Figure 22 is a plot of differences between apparent aerosol extinction (AAE) values from the 77 CCAFS experiment

TABLE 3

Comparison of Values for $\sigma_{3.8}/\sigma_{VIS}$ to K/R and LOWTRAN 5 Calculations Based on NRL-SNI Data

DATE	VIS (km)	PPH_2O (torr)	AT (°C)	WS (m/s)	RH %	$\overline{\sigma_{DF}}$	σ_{VIS}	$\overline{\sigma_{DF}}/\sigma_{VIS}$	K/R	LW 5
5-1-79	48	9.9	11.9	8	94	.010	.081	.123	.34	.72
5-1-79	42	9.9	12.3	14	93	.030	.093	.323	.63	.72
5-1-79	33	8.2	13.3	7.4	73	.090	.118	.763	.33	.55
5-2-79	29	9.1	13.1	10.4	81	.080	.135	.593	.43	.58
5-2-79	24	9.2	12.8	7.7	83	.090	.163	.552	.38	.58
5-2-79	24	9.2	12.2	6.6	87	.053	.163	.325	.25	.67
5-3-79	35	8.5	12.5	7.7	79	.010	.112	.090	.29	.58
5-7-79	36	9.2	13.8	12	79	.115	.109	1.05	.54	
5-7-79	20	9.3	13.1	13	83	.095	.196	.485	.58	.59
5-8-79	47	7.8	12.4	11.3	72	.010	.083	.121	.44	.50
5-9-79	17	8.4	12.0	10.4	80	.073	.230	.317	.42	.58
5-9-79	18	8.5	12.5	11.5	78	.110	.217	.507	.46	.56
5-9-79	21	8.7	12.7	11.7	80	.105	.186	.565	.48	.58

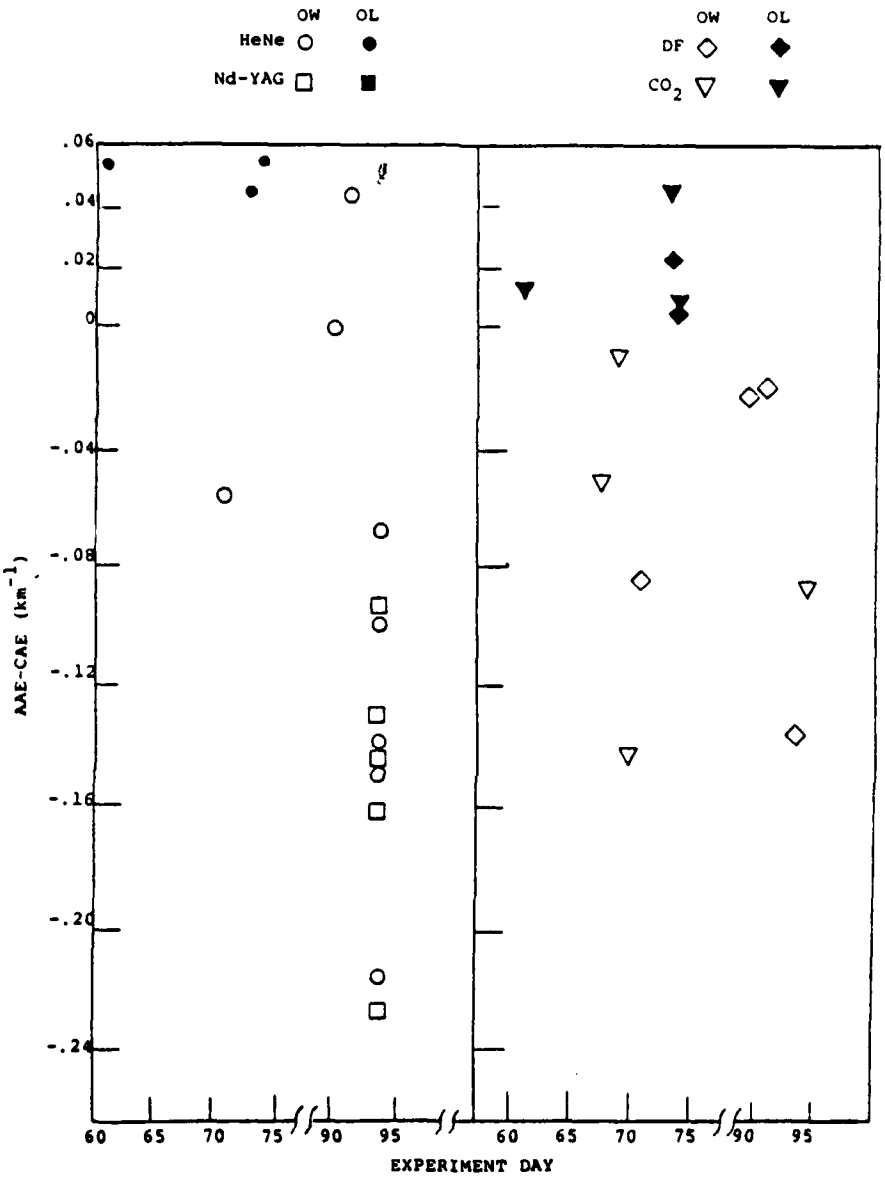

FIGURE 22. PLOT OF APPARENT AEROSOL EXTINCTION (AAE) COEFFICIENTS DERIVED FROM NRL LONG-PATH TRANSMISSION MEASUREMENTS AT CCAFS MINUS CALCULATED AEROSOL EXTINCTION COEFFICIENTS FOR EACH DAY OF THE EXPERIMENT.

and values calculated from shore-based aerosol spectrometer measurements (calculated aerosol extinctions - CAE). Data for the HeNe and Nd-YAG wavelengths are shown in the left-hand portion of the figure and data for DF and CO_2 laser wavelengths are shown on the right. The solid symbols correspond to measurements during conditions of overland wind directions (blowing from land toward the ocean) while the open symbols represent overwater wind conditions. The fact that most of the overwater wind differences are negative indicates that the CAE values are unrealistically large on account of surf generated particles. In these cases the conditions sampled by the aerosol spectrometer were not representative of the overwater optical path. This problem has also been observed in more recent measurements at SNI when extinction coefficients derived from shore-based aerosol spectrometer measurements were compared to the PMTC-OSP transmissometer data.

2.2.2.1 Naval Ocean Systems Center (NOSC) Aerosol Spectrometer Measurements

NOSC has developed an airborne aerosol spectrometer measurement capability which has been used in several locations during recent years and notably at SNI during recent experiments. Comparisons of vertical profiles of extinction coefficients at 3.75 μm to predictions of WGM, K/R and LOWTRAN 3B models were recently published [4]. Figures presented in reference 4 show that the WGM model generally predicts higher extinctions and consequently shows better agreement with the measured data than does the K/R model. The LOWTRAN 3B model does not compare favorably with the experimental data since it shows much less resemblence to the vertical profile of σ than does either of the other two models. Direct comparisons of measured and calculated aerosol distributions shown in reference 4 show that the

K/R predictions more closely resemble the measured distributions for larger values of RH than measured, possibly indicating that the particle growth factor in the K/R model should be increased. Other comparisons in this same report support earlier observations that the K/R model underestimates particle concentration and consequently aerosol extinction at lower windspeeds.

2.2.2.2 Naval Research Laboratory (NRL) Aerosol Spectrometer Measurements

The NRL open-ocean aerosol spectrometer data were collected during a 28-day station-keeping session aboard the British weather ship Fitzroy in late June 1978. As discussed in reference 32, measurements were limited to fair-weather conditions.

The conditions occurring during most of the measurement periods were windspeeds between 3 and 6 m/s and RH values between 80% and 100%. The measurement results are presented as frequency of occurance plots in reference 32 and show that the most frequently occurring value of σ_{VIS} (0.55 μm) calculated from the measured aerosol distribution data was $\sim$ 0.03 km^{-1}. Corresponding values for 3.8 μm and 10.0 μm were about 0.008 km^{-1} and 0.003 km^{-1} respectively. A preliminary tabulation of the data contained in reference 32 was available prior to publication [34] and was used in an effort to derive ratios of aerosol scattering in marine air at 3.75 and 10 μm as part of the analysis contained in reference 23.

Figure 23 is a plot of the ratios σ_{IR}/σ_{VIS} derived from the NRL marine aerosol spectrometer data. As evident from the distributions of data points seen in the figure, a large amount of scatter is present in the data. Least squares fits to the groups of data points were performed

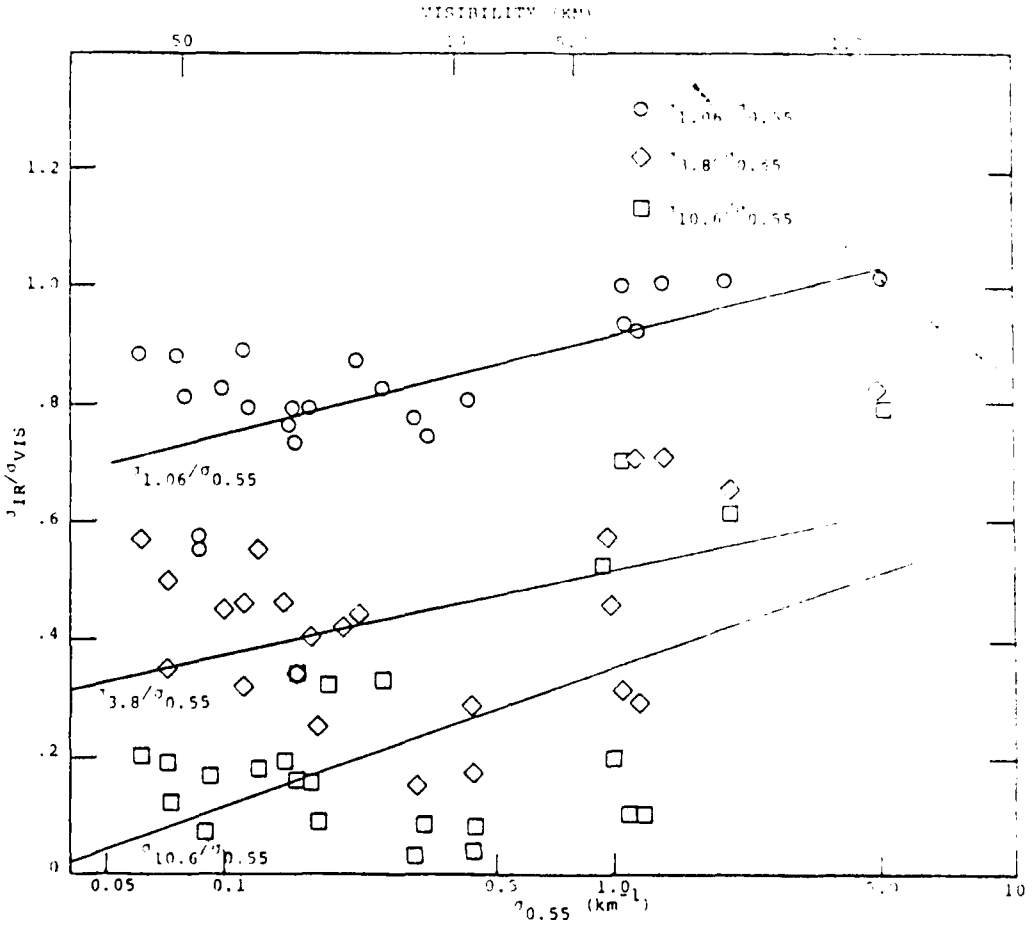

FIGURE 23. RATIO OF INFRARED TO VISIBLE AEROSOL EXTINCTION COEFFICIENTS VERSUS VISIBLE AEROSOL EXTINCTION COEFFICIENTS DERIVED FROM NRL NORTH ATLANTIC AEROSOL SPECTROMETER DATA. O: FITTED EQUATION IS σ1.06/σVIS=0.574 + 0.281 (σ0.55), CORR. COEFF.=0.714; ◇ :FITTED EQUATION IS σ3.8/σ0.55=0.234 + 0.208 (σ0.55), CORR. COEFF.=0.420; □ : FITTED EQUATION IS σ10.6/σ0.55= -0.121 + 0.360 (σ0.55), CORR. COEFF.=0.597.

and the fitted equations are given in the figure legend. The poor correlation coefficients for the curve fits reflect the fact that the data exhibit a large amount of scatter.

2.3 SUMMARY COMPARISON OF MODEL AND MEASURED MARITIME EXTINCTION VALUES

A detailed comparison of the features of the marine aerosol extinction models has been discussed in Section 2.2. In summary, the K/R model predicts much lower values of σ_{IR}/σ_{VIS} for low windspeeds than do either the LOWTRAN 3B or LOWTRAN 5 models. The three models predict comparable results in the range of windspeeds around 10 m/s and for RH values between 70% and 90%. The relative humidity dependence of LOWTRAN 5 is more severe than the K/R model above and below these values.

Comparisons of experimental long-path aerosol extinction values show that the seemingly unsophisticated LOWTRAN 3B model represents measured values reasonably well (see Figure 5). The TNO Laboratory data which were collected under moderate visibility conditions were seen to be more useful for aerosol model comparison purposes than the Australian DSTO measurements performed under very high visibility conditions.

All of the examples of σ_{IR}/σ_{VIS} values obtained from optical transmission data that were shown in Section 2.2 exhibit large amounts of scatter which are probably attributable to the influence of different air masses (variations in the relative concentrations of continental and maritime air).

The OPAQUE data (Figures 11 and 12) show typically large amounts of scatter and coarse agreement with the SAI water haze model for 3-5 μm but not for 8-12 μm where the ratio σ_{IR}/σ_{VIS} is nearly always lower than the LOWTRAN

model predictions. The limited examples of OSP data shown in Figures 13-15 are intriguing in that they indicate that a simple power-law dependence of σ_{IR} on σ_{VIS} agrees with the data. Presumably the data relate to a nearly constant air mass and we might expect to see different slopes on graphs of this same type for different air masses.

The importance of long averaging times for wind speed values used in modeling aerosol extinction ratios is demonstrated by the comparisons shown in Figure 16 of the PMTC-SNI data to the K/R model. Reasonably good agreement is seen to be obtained by the use of extended time average windspeeds.

The NRL long-path optical data contained in Tables 1-2 and Figures 17-21 and Table 3 show no obvious agreement with any of the three aerosol models considered although the K/R model shows better agreement at low values of windspeed with the NRL-CCAFS data (Table 2) than does either version of LOWTRAN.

The NRL-SNI data were collected during conditions that conform more nearly to the region of greatest overlap in the model predictions, i.e., $\sim$ 10 m/s windspeeds and 80% RH. On the average the K/R model seems to predict σ_{IR}/σ_{VIS} values closer to observations than does the LOWTRAN 5 model.

The aerosol spectrometer measurements performed by NOSC [4] indicate that the K/R model RH dependence may be too weak and, as seen in other comparisons, that better agreement with measured values of the ratio of infrared to visible scattering occurs for windspeeds around 10 m/s.

The NRL weather ship aerosol spectrometer data are seen to exhibit large amounts of scatter in the ratios σ_{IR}/σ_{VIS}, emphasizing the ambiguity inherent in comparisons of infrared aerosol extinction data and models.

2.4 ANTICIPATED RANGES OF MARINE ATMOSPHERIC EXTINCTION AND BACKSCATTER

A summary of the ranges of aerosol scattering values for the various measurements described in Section 2.3 is listed in Table 4. Corresponding ratios of σ_{IR}/σ_{VIS} for 1.06 μm, 3.8 μm and 10.6 μm derived from the extremes of these data are also included. As expected, the median values of the ratio σ_{IR}/σ_{VIS} decrease with increasing wavelength. The very low visibility OPAQUE data exhibit quite large values for $\sigma_{.55}$ and $\sigma_{3.8}$ which are not seen in the other data. The range of values of σ_{IR}/σ_{VIS} for 1.06 μm is about a factor of 2, increasing to a factor of about 4 for 3.8 μm and as much as a factor of 7 for the SNI-K/R data at 10.6 μm.

Such an increase in the range of values of σ_{IR}/σ_{VIS} is in keeping the increased variability of particle density for large sizes relative to the concentrations of smaller particles effective in scattering shorter wavelengths.

We have discussed the variations of model-predicted ratios of infrared to visible aerosol extinction and compared measured values to model predictions in Sections 2.2 and 2.3 and found no obvious "best overall representation" by any one of the models. It thus seems reasonable to exercise one or two of the models for a typical set of maritime conditions for the purposes of estimating a LIDAR system performance at sea, and then to evaluate the excursions from this "nominal case" based on the model and data review presented in the previous sections.

Table 5 contains the results of calculations performed with the maritime component of the LOWTRAN 5 model. Aerosol extinction, absorption, scattering and backscattering were calculated for the four laser wavelengths shown and for 2 km and 5 km visibilities and for 70% and 95% RH.

TABLE 4

Summary of Observed Aerosol Extinction Values and Ratios of σ_{IR}/σ_{VIS}

DATA SOURCE	$\sigma_{.55}$ (km^{-1})	$\sigma_{1.06}$ (km^{-1})	$\sigma_{3.8}$ (km^{-1})	$\sigma_{10.6}$ (km^{-1})	$\frac{\sigma_{1.06}}{\sigma_{.55}}$	$\frac{\sigma_{3.8}}{\sigma_{.55}}$	$\frac{\sigma_{10.6}}{\sigma_{.55}}$
OPAQUE (3-5)	.5-8		.1-2			.2-.25	
OPAQUE (8-12)	.15-7			.1-1			.14-.67
OSP	.15-.4	1-.3	.02-.2		.65-.75	.13-.5	
SNI-K/R*					.53-.92	.2-.6	.08-.28
NRL-CCAFS	.082-.49	.038-.148	.02-.14		.30-.46	.24-.29	
NRL-SNI	.081-.23		.01-.115			.12-.50	

* Data from reference 26 presented in Figure 16.

TABLE 5

Calculations of Aerosol Extinction, Absorption, Scattering and Backscatter for Different Wavelengths, Visibilities and Relative Humidities Using The LOWTRAN 5 Maritime Model (Oceanic Component)

λ (μm)	Extinction (km^{-1})	Absorption (km^{-1})	Scattering (km^{-1})	Scatt/Ext	Backscatter (km^{-1} $sterad^{-1}$)
	70% Relative Humidity		2 km Visibility		
.55	1.956	.000	1.956	1.000	2.391E-02
1.06	5.127E-01	4.394E-04	5.123E-01	.9992	9.023E-03
3.8	1.197E-02	2.168E-03	9.798E-03	.8185	9.153E-04
10.6	1.249E-02	1.238E-02	1.094E-04	8.759E-03	1.266E-05
	70% Relative Humidity		5 km Visibility		
.55	7.824E-01	.000	7.824E-01	1.000	9.963E-03
1.06	2.051E-01	1.883E-04	2.049E-01	.9990	3.609E-03
3.8	4.786E-03	8.675E-04	3.919E-03	.8188	3.661E-04
10.6	4.995E-03	4.951E-03	4.376E-05	8.761E-03	5.066E-06
	95% Relative Humidity		2 km Visibility		
.55	1.956	.000	1.956	1.000	1.878E-02
1.06	1.275	1.085E-04	1.274	.9992	1.166E-02
3.8	9.895E-02	5.944E-03	9.301E-02	.9400	3.818E-03
10.6	3.508E-02	3.436E-02	7.244E-04	2.065E-02	7.481E-05
	95% Relative Humidity		5 km Visibility		
.55	7.824E-01	.000	7.824E-01	1.000	7.513E-03
1.06	5.098E-01	4.338E-05	5.098E-01	.9999	4.664E-03
3.8	3.958E-02	2.381E-03	3.720E-02	.9399	1.527E-03
10.6	1.403E-02	1.374E-02	2.898E-04	2.066E-02	2.993E-05

We are interested in how the ratio of scattering to extinction behaves as a function of wavelength since it is required that this ratio remain constant if we wish to implement the "Klett method" [35,36] for processing LIDAR return signals. The Klett method will be discussed in greater detail in Section 3.2.

One sees that the ratio of scattering to extinction does not change drastically between 0.55 μm and 3.8 μm wavelengths but that it is appreciably smaller at 10.6 μm due to increased absorption by the water droplet aerosols at the longer wavelength. The 70% RH cases for 2 km and 5 km visibilities are seen to be somewhat worse than the 95% RH case. The ratio of scattering to extinction changes by about 20% between 0.55 μm and 3.8 μm in the former case and only by about 6% in the latter case.

The calculated backscatter ratio (km^{-1} $sterad^{-1}$) listed in the sixth column of Table 5 is required to estimate the LIDAR return signal strength. One can see that both the scattering magnitude σ and the backscatter coefficient β decrease with increasing wavelength.

The backscatter coefficient β is determined by performing a Mie angular scattering calculation based on the marine aerosol distribution generated by the particular model being used, e.g. LOWTRAN, K/R or WGM. The product of the angular scattering phase function for a scattering angle of 180° and the magnitude of the scattering coefficient then determines the value of β for particular scattering condition. Examples of the scattering phase function for an oceanic aerosol for 1.06 μm and 10.6 μm are shown in Figures 24 and 25. One can see that scattering at 1.06 μm for this type of aerosol is sharply peaked in the forward direction while it is more nearly angularly isotropic at 10.6 μm. Even though the magnitude of σ is much lower at

10.6 μm than at 1.06 μm for the oceanic aerosol the ratio of β/σ is actually larger at the longer wavelength.

Similar results to those tabulated in Table 5 and shown in Figures 24 and 25 were performed for the continental component in LOWTRAN 5. The angular scattering phase function results at 10.6 μm are quite similar to those shown in Figure 25 but the results for the continental component at 10.6 μm do not show the strong forward scattering peak.

Figure 26 is a plot of the LOWTRAN 5 continental component angular scattering phase function for 1.06 μm showing a more uniform, nearly angular isotropic behavior.

Calculations were also performed using the WGM model for 70% and 95% RH, for windspeeds between 0 and 10 m/s and for 0.55 μm, 3.8 μm and 10.6 μm wavelengths. The results of these calculations are shown in Table 6. Here we see that the ratio of scattering to extinction is even more constant between 0.55 μm and 3.8 μm wavelengths than for the LOWTRAN 5 oceanic component case. However we see that this ratio falls from a value near unity for 3.8 μm to about 0.4 to 0.6 at 10.6 μm, raising doubts about the validity of the assumptions required by the Klett inversion method at 10.6 μm.

Results of calculations of the backscatter coefficient β for the oceanic and rural components of LOWTRAN 5 for the two cases: a) 2 km visibility and 95% RH and b) 5 km visibility and 70% RH are plotted as a function of wavelength in Figure 27. Results of calculations using an advection fog model for 2 km and 5 km visibilities [22] are also shown in the figure.

When the results such as those shown in Table 5 and Figures 24-26 for continental and oceanic aerosol components

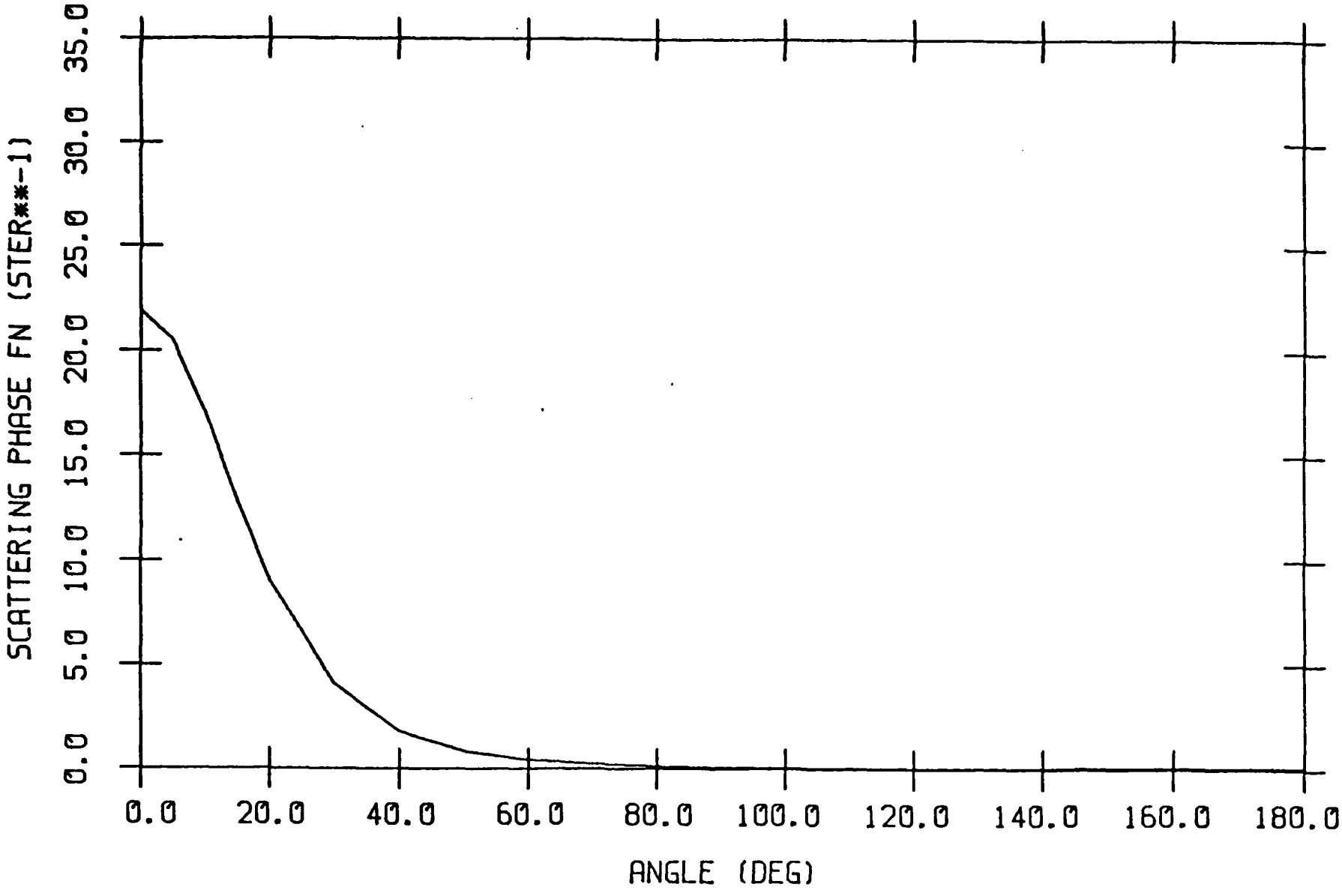

FIGURE 24. OCEANIC AEROSOL SCATTERING PHASE FUNCTION FOR 1.06 μm.

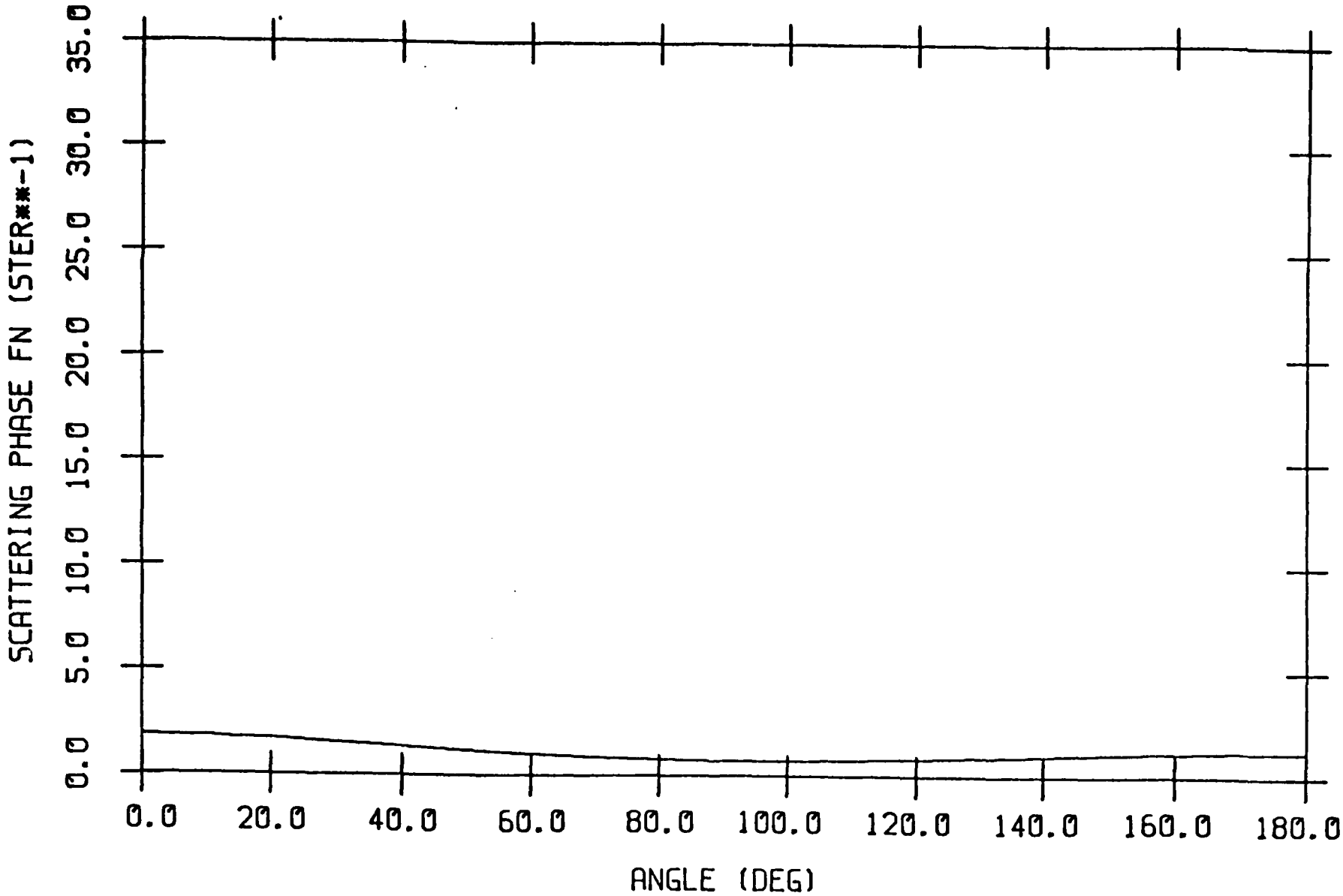

FIGURE 25. OCEANIC AEROSOL SCATTERING PHASE FUNCTION FOR 10.59 μm.

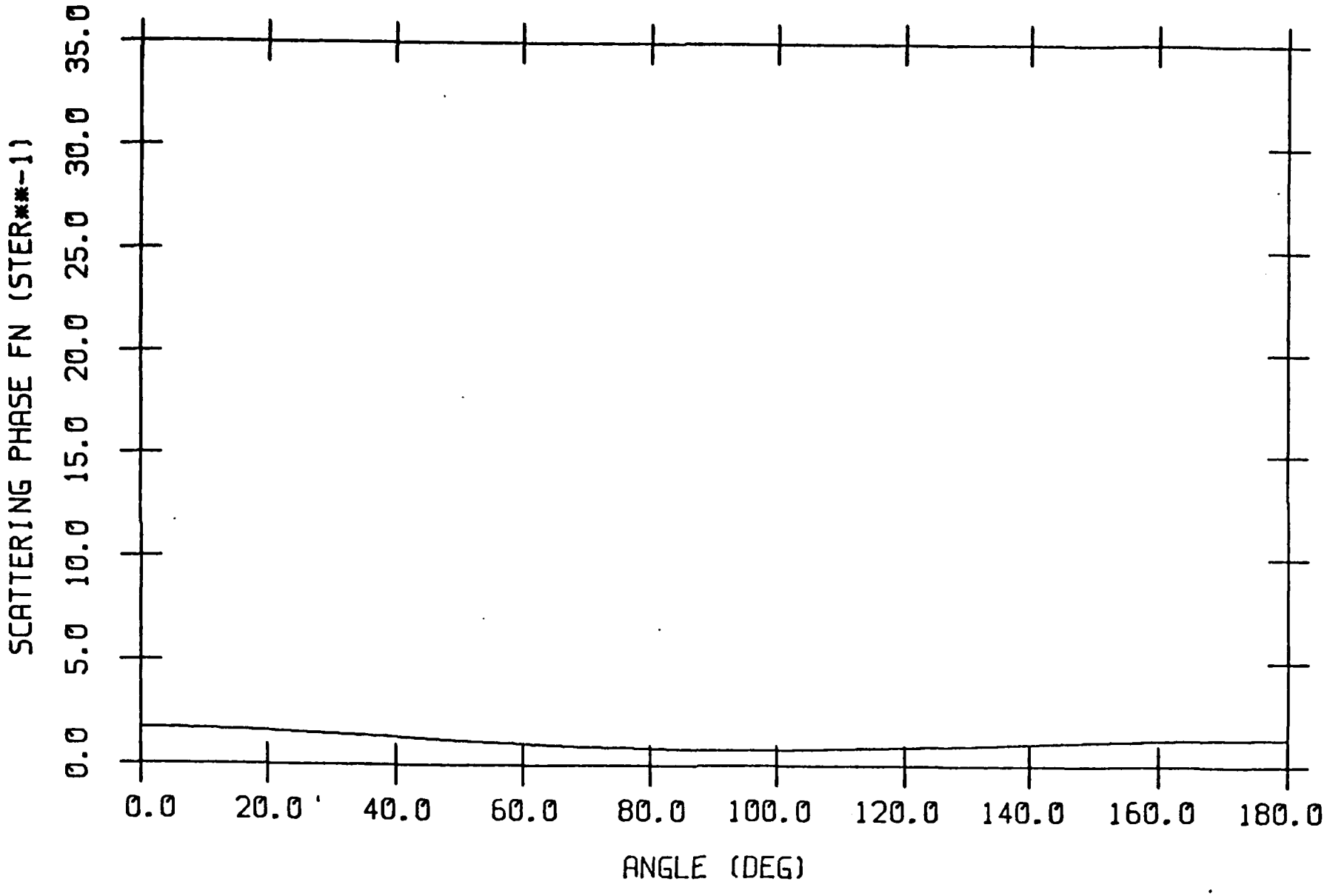

FIGURE 26. CONTINENTAL AEROSOL SCATTERING PHASE FUNCTION FOR 1.06 μm.

Table 6

Aerosol Extinction
Calculations Performed Using the

Wells, Gal, Munn Model

Wavelength - 0.55μm 2km Visibility

Wind Speed	70% Relative Humidity				95% Relative Humidity			
	Extinction	Absorption	Scattering	Scatt/Ext	Extinction	Absorption	Scattering	Scatt/Ext
0	1.955 +00	2.855 -03	1.952 +00	9.985 -01	1.955 +00	8.410 -04	1.954 +00	9.996 -01
5	1.955 +00	5.560 -03	1.949 +00	9.972 -01	1.955 +00	2.133 -03	1.953 +00	9.989 -01
10	1.955 +00	8.859 -03	1.946 +00	9.955 -01	1.955 +00	3.233 -03	1.952 +00	9.983 -01
				Wavelength = 3.8μm				
	70% Relative Humidity				95% Relative Humidity			
0	5.656 -01	1.623 -02	5.494 -01	9.713 -01	5.737 -01	1.727 -02	5.564 -01	9.699 -01
5	1.368 +00	2.672 -02	1.341 +00	9.805 -01	1.695 +00	4.621 -02	1.649 +00	9.727 -01
10	1.791 +00	4.047 -02	1.750 +00	9.774 -01	2.065 +00	7.249 -02	1.992 +00	9.649 -01
				Wavelength = 10.6μm				
	70% Relative Humidity				95% Relative Humidity			
0	1.425 -01	7.940 -02	6.310 -02	4.428 -01	1.626 -01	9.469 -02	6.795 -02	4.178 -01
5	2.870 -01	1.448 -01	1.421 -01	4.953 -01	4.894 -01	2.379 -01	2.516 -01	5.140 -01
10	4.771 -01	1.764 -01	3.008 -01	6.304 -01	7.910 -01	2.939 -01	4.971 -01	6.284 -01

wind speed in m/s

extinction, absorption and scattering coefficients in km^{-1}

Table 6 - Cont.

Wavelength = 0.55um 5km Visibility

Wind Speed	70% Relative Humidity				95% Relative Humidity			
	Extinction	Absorption	Scattering	Scatt/Ext	Extinction	Absorption	Scattering	Scatt/Ext
0	7.820 -01	1.142 -03	7.808 -01	.9985	7.820 -01	3.364 -04	7.816 -01	.9996
5	7.820 -01	2.224 -03	7.796 -03	.9972	7.820 -01	8.532 -04	7.808 -01	.9999
10	7.820 -01	3.544 -03	7.784 -01	.9955	7.820 -01	1.293 -03	7.808 -01	.9983
	Wavelength = 3.8μm							
	70% Relative Humidity				95% Relative Humidity			
0	2.262 -01	6.492 -03	2.198 -01	.9713	2.295 -01	6.908 -03	2.226 -01	.9699
5	5.472 -01	1.069 -02	5.364 -01	.9805	6.780 -01	1.848 -02	6.596 -01	.9727
10	7.164 -01	1.619 -02	7.000 -01	.9774	8.260 -01	2.900 -02	7.968 -01	.9649
	Wavelength = 10.6μm							
	70% Relative Humidity				95% Relative Humidity			
0	5.700 -02	3.176 -02	2.524 -02	.4428	6.504 -02	3.788 -02	2.718 -02	.4178
5	1.148 -01	5.792 -02	5.684 -02	.4953	1.958 -01	9.516 -02	1.006 -01	.5140
10	1.908 -01	7.056 -02	1.203 -01	.6304	3.164 -01	1.176 -01	1.988 -01	.6284

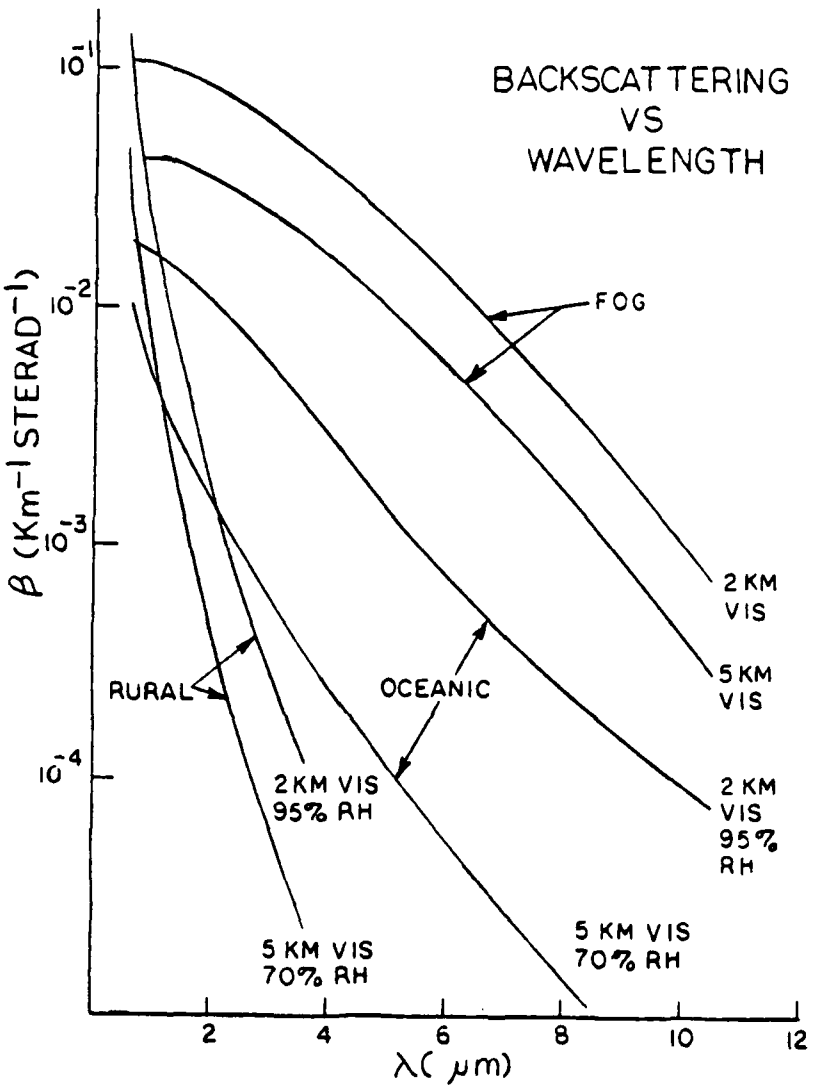

FIGURE 27. CALCULATED AEROSOL BACKSCATTER COEFFICIENTS VERSUS WAVELENGTH FOR DIFFERENT AEROSOL MODELS WITH DIFFERENT VISIBILITIES AND RELATIVE HUMIDITIES.

are combined compensating effects occur. An actual marine aerosol distribution will consist of certain proportions of one component to the other. The behavior of quantities like the scattering phase function (e.g. Figures 24 and 26) for different components when combined in a given ratio will produce results which are dependent upon the relative proportions of continental and marine components. That is, results of calculations of the ratio of β/σ as a function of wavelength will depend upon the relative proportions of the two components chosen. Figure 28 is an example of a plot of the ratio β/σ versus wavelength for LOWTRAN 5 using equal components of rural and oceanic aerosol distributions. The 5 km visibility case is shown. Results for the 5 km visibility fog model are shown also.

Using the results shown in Figure 28 we can perform estimates of backscattered signal levels given a particular LIDAR system configuration. The results of these calculations will represent a "nominal case" for operation in a maritime atmosphere. The information discussed in Sections 2.2 and 2.3 can then be used as a basis for interpreting the nominal case results and estimating the changes in system performance that might result from excursions in scattering and backscatter corresponding to the range of infrared and visible scattering variations documented earlier.

A brief review of LIDAR measurement techniques and approaches will be presented in Section 3 and some of the more important considerations involved in implementing a LIDAR measurement system on shipboard will be discussed in Section 4.

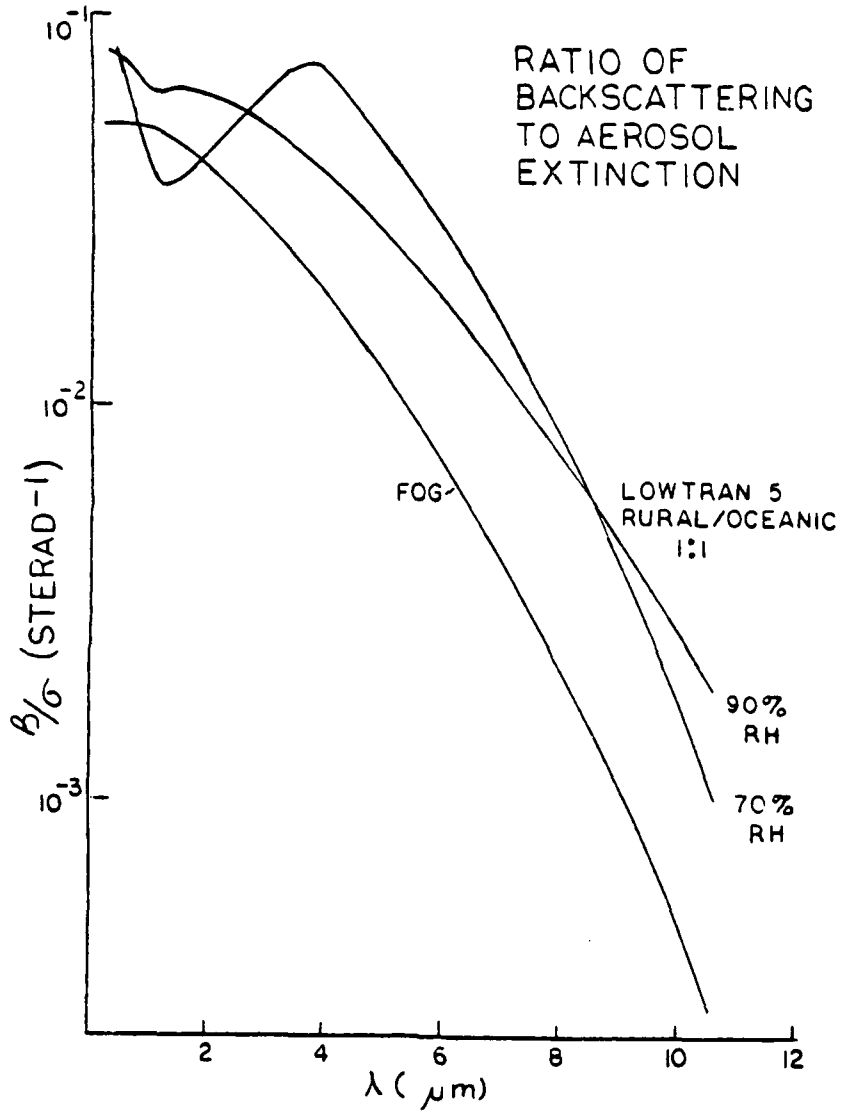

FIGURE 28. CALCULATED RATIO OF AEROSOL BACKSCATTER TO EXTINCTION COEFFICIENTS VERSUS WAVELENGTH FOR DIFFERENT AEROSOL MODELS WITH DIFFERENT VISIBILITIES AND RELATIVE HUMIDITIES.

3
LIDAR MEASUREMENT SYSTEM APPROACHES

3.1 TECHNIQUES USING CW LASERS

In an attempt to circumvent the problems associated with conventional pulsed LIDAR systems, several variations using CW lasers have been proposed and investigated [37-43]. Reduction of eye safety problems realized by the use of low power CW laser sources as opposed to high peak power pulsed lasers is an attractive feature of CW LIDARS. The costs and complexity associated with high-speed digital processing hardware can be reduced by using simplified analog data acquisition and processing of CW signals. The CW LIDAR techniques which have been investigated and are described in references 37-43 can be divided into three types of systems, namely a) those using a fixed frequency of modulation of the CW laser source (chopped CW source), b) systems where the CW laser modulation frequency is swept thru a range ("chirped" modulation of the CW source, analogous to a chirped radar system) and c) systems where range discrimination is accomplished by spatial analysis of an image formed by the backscattered return light. The beam-image-profile approach described in references 40-42 is an example of this type of system. Considerations involved in these types of CW LIDAR systems will now be briefly reviewed.

3.1.1 FIXED FREQUENCY MODULATED LIDARS (CHOPPED CW LASER SOURCES)

Stokes has reviewed the work of Kreid [37], Paulson [38], and Bufton and Iyer [39] in a recent report [40]. Kreid presented an engineering evaluation but did not experimentally verify his results. The other authors reported on the results of measurements using a CW LIDAR. The basic

approach in these systems is a comparison of the phase of the backscattered return signal to the phase of the source. This can be seen from the following analysis.

The LIDAR return at time t given by the LIDAR equation is:

$$P(t) = \int_0^\infty \beta(z)\, A_D \frac{f(z)}{z^2}\, P_o\left(\frac{t-2z}{c}\right) \exp\left(-\int_0^\infty 2\alpha(\xi)\,d\xi\right) dz \qquad (1)$$

where $\beta(z)$ is the backscatter coefficient, α is the extinction coefficient, z is range, P_o is the modulated laser power, c is the velocity of light, $P_o(t) = \bar{P}_o + \hat{P}_o \sin(\omega t)$, A_D is the collection optic area and $f(z)$ is the correction for actual receiver collection cone. For an exact result, the atmosphere must be homogeneous so that:

$$\alpha = \alpha(z), \quad \beta = \beta(z). \qquad (2)$$

If we also substitute the expression for $P_o(t)$ we obtain:

$$P(t) = A_D \beta\, \bar{P}_o \int_0^\infty \exp(-2\alpha z)\, \frac{f(z)\,dz}{z^2} \quad [\text{DC term}] +$$

$$A_D \beta\, \hat{P}_o \int_0^\infty \exp -2\alpha z\, \sin\omega(t-2z/c)\, \frac{f(z)}{z^2}\, dz \quad [\text{AC term}]. \qquad (3)$$

If we set the AC term equal to:

$$P(t) = A \sin\omega t - B \cos\omega t$$

$$= (A^2 + B^2)^{1/2} \sin(\omega t - \phi), \qquad (4)$$

then A & B may be evaluated:

$$A = A_D \beta \hat{P}_o \int_o^\infty \exp(-2\alpha z) \cos(2\omega z/c) \frac{f(z)dz}{z^2} \quad (5)$$

$$B = A_D \beta \hat{P}_o \int_o^\infty \exp(-2\alpha z) \sin(2\omega z/c) \frac{f(z)dz}{z^2} \quad (6)$$

The phase angle ϕ is then evaluated as:

$$\phi(\alpha,\omega) = \tan^{-1} (B/A) \quad (7)$$

and from this the extinction coefficient can be determined.

A CW LIDAR system was constructed and tested by Paulson who pointed out that a visibility measurement with such a system is most sensitive to atmospheric conditions near the convergence distance (point of crossover of the LIDAR transmitted beam and receiver field-of-view).

In order to investigate the CW LIDAR phase shift sensitivity as a function of crossover distance and atmospheric homogenity, a simulation of a CW LIDAR response was performed for several cases. Results of this simulation are shown in Figure 29 where the phase angle response of the system is plotted against visibility.

The response of the system to a uniform atmosphere of the indicated visibility is shown by the solid curves for values of the LIDAR crossover range, Zo = 10 m, 100 m and 200 m. These curves may be considered as calibration curves.

Response of the LIDAR to a non-uniform atmosphere is shown by the dashed curves for the same values of Zo. Here the LIDAR is located in a clear air region and a region of uniform aerosol is located a distance Z' away from the LIDAR. For the case of Zo >> Z' where the system crossover occurs

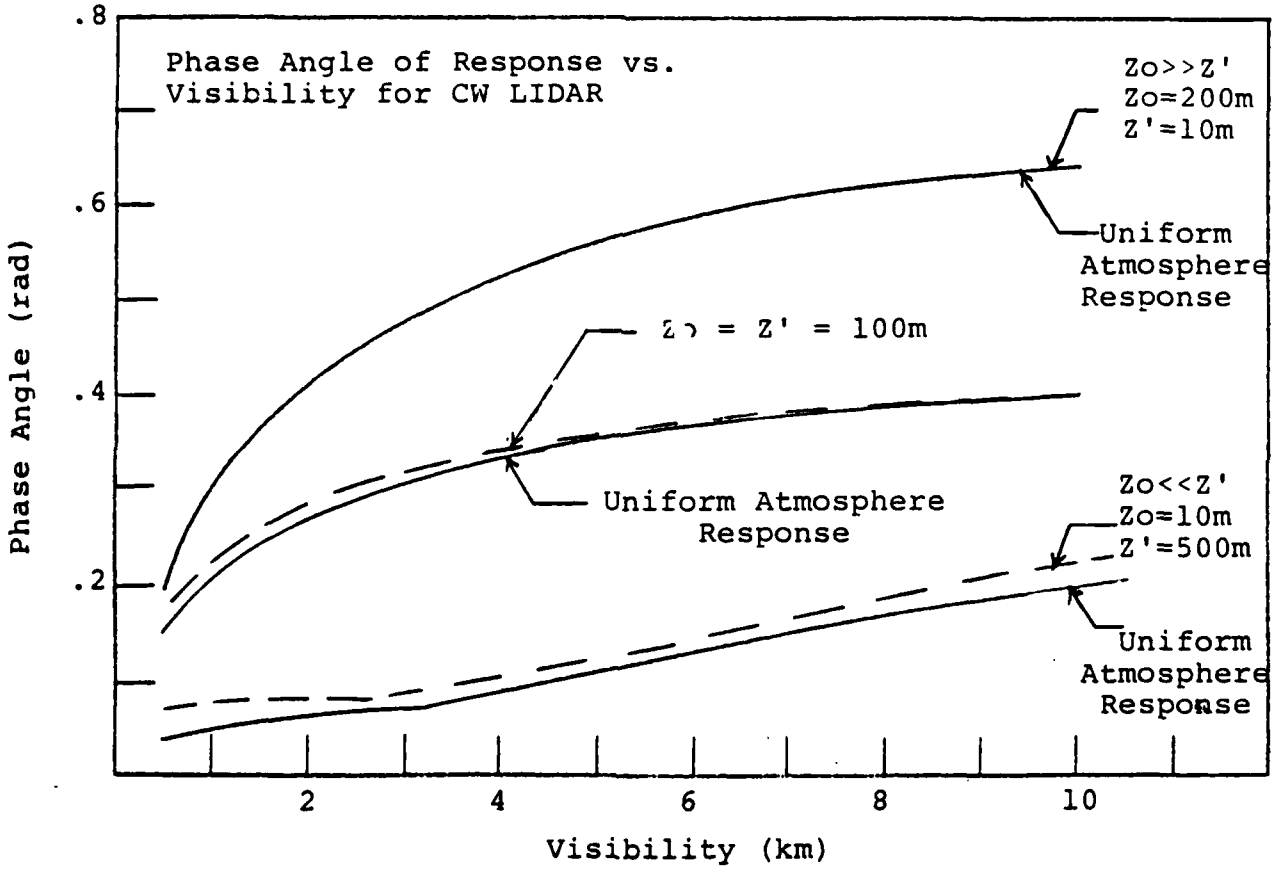

FIGURE 29. CALCULATED PHASE ANGLE OF CW LIDAR RESPONSE VERSUS VISIBILITY FOR UNIFORM AND NON-UNIFORM ATMOSPHERIC AEROSOL DISTRIBUTIONS.

well beyond the atmospheric discontinuity, the uniform atmosphere calibration response curve and the inhomogeneous atmosphere response curve essentially coincide showing that the system performs quite well.

The response curve(s) also shows that for Zo = 200 m the sensitivity of phase angle response to changes in visibility is good and is only starting to flatten out for $R_v \geq 10$ km, indicating that useful measurements can be obtained for this and higher visibilities. For cases where the crossover range lies near the boundary of the atmospheric inhomogenity (Zo = Z') or inside it (Zo << Z') the system response to the inhomogoneous atmosphere differs from that in a uniform atmosphere. The middle and lower curves in Figure 29 demonstrate these cases. With Zo and Z' each set equal to 100 m we see that reasonable results are still obtained although the visibility is slightly underestimated in a non-uniform atmosphere. The lower curves show that visibility estimates can be in error by 20% to 50% for the case where for the Zo << Z'. The use of return beam phase comparisons as a measure of visibility with a CW LIDAR system is seen to be sensitive to the relative locations of the system optical crossover and atmospheric inhomogeneities. The location of the optical crossover with such a system is very sensitive to system optical alignment. This fact can be inferred from Figure 29 by noting that the three "calibration-response" curves for a uniform atmosphere differ appreciably depending upon the location of the optical crossover. Paulson [38] and Bufton and Iyer [39] have also reported that optical alignment sensitivity is the principal source of error in the operation of such systems.

3.1.2 SWEPT FREQUENCY MODULATED LIDARS ("CHIRPED" CW LASER SOURCES)

A LIDAR based on frequency-swept-modulation of the source, analogous to a "chirped" radar, is described by Stokes [40]. The analysis and evaluation of this approach presented by Stokes shows that the system is primarily sensitive to nonuniformities and discontinuities in the atmosphere and is not a practical approach for measuring extinction due to uniformly distributed scatters. The FM technique has been demonstrated to provide range resolved information about inhomogeneities, but it does not respond to the average backscatter and hence is not useful for measuring visibility.

It is interesting to speculate on the possibility that an FM-CW LIDAR could also be operated as a fixed-frequency modulated system using phase discrimination. The complementary character of the information provided by the two types of systems would then provide all of the required information. The FM-CW LIDAR return could be used to provide the map of inhomogeneities required to properly interpret the CW LIDAR return.

3.1.3 BEAM IMAGE PROFILING (BIP) LIDAR

The BIP LIDAR technique was developed at NOSC and is also described by Stokes [40]. This is a simplified CW LIDAR approach that uses geometry rather than time to separate the signal return from different ranges. The technique has been studied and under development for some time at NOSC [40-43]. The offset in the optical axes of the BIP LIDAR laser transmitter and receiver causes the backscattered return signal to form a line image in the receiver telescope at an oblique angle to the receiver telscope axis. In the BIP LIDAR the distance of a point in the line image

from the telescope axis is inversely proportional range. The mapping of the light backscattered from the transmitted beam along the length of the image goes inversely as the square of the range, building in an automatic compensation for the $1/r^2$ fall-off of a LIDAR return signal. Several discreet detectors and signal processing channels can be used to measure the image brightness at different locations along the image and thus measure the return signal from different ranges. Recent developments in commercially available linear Si diode array detectors containing as many as 1024 detectors and packaged in integrated circuit housings along with integral clocking electronics provide a detector module ideally suited to this application. Jensen [43] has summarized the results of tests and intercomparisons of a BIP LIDAR system with simultaneous measurements using other instruments at NOSC. The conclusions reached were that intercomparisons of the BIP LIDAR measurements with telephotometers, nephelometers and aerosol spectrometers generally showed agreement to within a factor of two. The critical nature of system optical alignment and the dependence of the system calibration upon the thermal stability of this alignment seem to be the major factors limiting the usefulness of the BIP system for use in routine visibility measurements. A three-dimensional computer search routine was required to determine the image vanishing point on the detector array before data could be calibrated in visibility.

3.1.4 SUMMARY OF ADVANTAGES AND DISADVANTAGES OF CW LIDAR APPROACHES

There are several potential advantages to the use of CW LIDAR techniques in designing a single-ended visibility measurement system which make the evaluation of such systems for this application worthwhile. The same arguments pro

and con generally apply to the three variations of CW systems previously described. Some important advantages of a CW system are:

- Eye safety problems are simplified due to the use of a CW laser.
- Low electro-magnetic-interference (EMI) generation.
- The assumed relationship between extinction and backscatter is not required (as in the application of the Klett method with a pulsed LIDAR).
- Some simplification in electronic signal processing complexity is possible since high-speed analog-to-digital converters are not required. The signal processing (e.g. phase comparison of transmitted and backscattered beams) can be readily implemented with analog electronics.
- Inherent optical-geometrical compensation for $1/r^2$ signal loss (BIP LIDAR only).

The findings presented in references 37-43 together with the analysis shown in Figure 29 suggest several limitations inherent in the CW LIDAR approach when these systems are considered for routine use in a visibility measurement application. Principal among these disadvantages are the following:

- Difficult optical alignment requirements limit the utility and measurement accuracy with all of the systems described in the literature. This is the overriding limitation of these systems.
- The phase comparison method using a fixed-frequency-modulated CW source can only work exactly for a uniform atmospheric path.
- The swept-frequency-modulated "chirped" system has been shown to respond only to discontinuities in backscatter and hence is not useful for visibility measurements in a homogeneous atmosphere.

- The BIP LIDAR system has an inherent non-linear range resolution due to the compression of the return signal from distant ranges near the image vanishing point.

3.2 APPLICATION OF PULSED LIDAR SYSTEMS TO VISIBILITY MEASUREMENTS

3.2.1 GENERAL CHARACTERISTICS OF A PULSED LIDAR SYSTEM

A LIDAR using a pulsed laser source is generally much simpler in optical design and construction than the CW LIDAR systems discussed earlier and described in references 36-42. For shipboard visibility (aerosol extinction) measurement applications a monostatic LIDAR system would be most practical. In this configuration the laser source and receiver are nearly co-located adjacent to one another or possibly coaxial and the projected beam and receiver field-of-view converge or overlap at a distance of several tens of meters away from the LIDAR. A relatively short laser pulse of about 10^{-8} sec duration is used in order to obtain good range resolution of the LIDAR backscatter profile.

Some means is required to record and store the rapidly varying time dependent backscatter signal so that the signal strength as a function of time, i.e., range may be determined. A transient recording capability or very high speed analog-to-digital converter is required to capture the high-speed transient LIDAR return signal. These considerations will be discussed in greater detail in Section 3.3.

3.2.2 SIGNAL PROCESSING METHODS

The LIDAR equation for the instantaneous received power P(r) can be written:

$$P(r) = P_o \frac{c\tau}{2} A_R \frac{\beta(r)}{r^2} \exp[-2\int_o^r \sigma(r')dr'] \quad (8)$$

where P_o is the transmitted power at time t_o, c is the velocity of light, τ is the pulse duration, A_R is the effective receiver area, r is the range, $\beta(r)$ is the volume backscatter coefficient and $\sigma(r)$ is the attenuation coefficient. The LIDAR equation can be re-written in terms of the $1/r^2$ compensated, logarithmic signal variable S(r):

$$S(r) = \ln(r^2 P(r)). \quad (9)$$

The LIDAR equation (8) then becomes:

$$S(r) - S(r_o) = \ln \beta/\beta_o - 2\int_{r_o}^r \sigma dr' \quad (10)$$

where β_o is evaluated at the reference range r_o.

3.2.2.1 Slope and Ratio Methods of Signal Inversion

The "slope" method requires that the atmosphere be homogeneous so that:

$$\frac{d\beta}{dr} = 0 \quad (11)$$

In this case, the volume extinction is simply:

$$\sigma = -\frac{1}{2}\frac{dS}{dr} \quad (12)$$

Since in reality S(r) is never exactly a linear function of r, i.e., σ is never exactly independent of range, a least-squares fitting procedure may be applied to evaluate $\frac{dS}{dr}$. In doing so, one hopes that path discontinuities will

simply average out. A variant of the "slope" method is to break up the return signal into short segments. In this way, the probability of encountering a scattering discontinuity within a given segment is decreased and the associated probability that $\frac{d\beta}{dr}$ is small or zero is increased. When summing over a path, it is hoped that one can identify discontinuities and correct them. This approach works best when changes in scattering occur at sharp boundaries so that their effect can be detected and ignored.

The "ratio" method is essentially identical to the previous method in assumptions and results. Its formulation, however, points out the fact that if two points in a LIDAR return share the same backscatter coefficients, the transmission along the path joining those points can be evaluated independent of the scattering behavior along the path. Thus, the ratio technique is useful for evaluating the transmission between two points which bound the region of inhomogeneity in an otherwise homogeneous atmosphere.

3.2.2.2 Klett Method of Signal Inversion

The most general inversion technique is a solution to the LIDAR equation assuming a power law relationship between volume extinction and backscatter:

$$\beta = \quad . \tag{13}$$

Then the LIDAR equation becomes:

$$\frac{dS}{dr} = \frac{k}{\sigma}\frac{d\sigma}{dr} - 2\sigma \tag{14}$$

whose solution can be written as:

$$\sigma(r) = \exp\left(\frac{S(r) - S(r_o)}{k}\right) \Big/ \sigma_o^{-1} - \frac{2}{k} \int_{r_o}^{r} \exp\left(\frac{S(r) - S(r_o)}{k}\right) dr' . \quad (15)$$

This solution allows arbitrary path structure so long as the power law relation between σ and β is valid. Generally, this equation has not been used due to its extreme sensitivity to noise and the initial determination of σ_o at range r_o (evaluated using the slope method). Klett [35,36] noted in his paper that the prime reason for this effect is the mathematical instability in the equation structure. Klett shows that the reason for this is that σ_o is typically evaluated near the LIDAR itself so that $\sigma(r)$ is always evaluated at ranges where the return signal and thus the S/N is diminished. It is the differencing of two rather large numbers to yield a small result in the denominator that cause the trouble. This situation is greatly reduced if σ_o is evaluated at a range r_m greater than those of interest. Then the LIDAR equation becomes:

$$\sigma(r) = \exp\left(\frac{S(r) - S(r_m)}{k}\right) \Big/ \sigma_m^{-1} + \frac{2}{k} \int_{r}^{r_m} \exp\left(\frac{S(r) - S(r_m)}{k}\right) dr' \quad (16)$$

and stability of the solution is greatly improved by this simple modification.

3.3 CHARACTERISTICS OF THE ANGVS/5 MODEL-1 VISIOCEILOMETER

The Army has been quite successful in developing a hand-held LIDAR which is suited to Army requirements. The development was initiated at the Night Vision and Electro-Optics Laboratory (NVEOL) [44] and is an on-going activity at the Atmospheric Sciences Laboratory (ASL) at the White Sands Missile Range (WSMR) [45].

AD-A123 701

NAVAL OCEAN SYSTEMS CENTER, SAN DIEGO, CA
SHIPBOARD VISIBILITY MEASUREMENT SYSTEM DEFINITION STUDY
BY: JA DOWLING, TJ ROGNE OPTIMETRICS, INC., LAS CRUCES, NM

2 OF 2
CR 13
JAN 1982

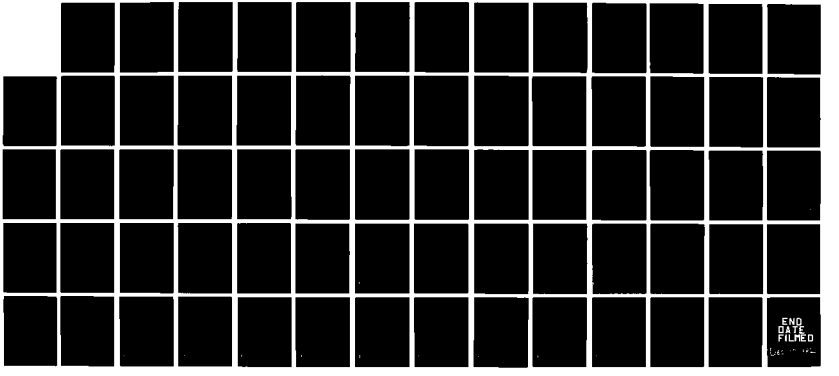

The LIDAR is a visioceilometer (ASL Model-1) based on the AN/GVS-5 portable laser rangefinder. This device is quite small -- occupying a volume less than one cubic foot. A second generation (Model-2) version will be designed for hand-held operation and will be battery powered using a belt pack. Each module of the Model-2 version is expected to weigh between 5 and 6 pounds. The ASL development program has strongly emphasized miniaturization since the design goal of portability by the foot soldier has been a major factor.

The ASL AN/GVS-5 based visioceilometer incorporates the following system design parameters:

laser wavelength:	1.06 μm
laser pulse length:	6 ns
laser pulse energy:	10 mJ
source diameter:	1.6 cm
source divergence:	1.0 mr
receiver diameter:	5.72 cm
receiver field-of-view:	3.0 mr

The ASL Model-1 represents one alternative approach and motivation in the development of a prototype shipboard LIDAR-based visibility measurement system. The emphasis in the development of this device has been on compactness and portability for use by the foot-soldier. The incorporation of MIL-SPEC ruggedized hardware components such as the ANGVS/5 laser range finder is attractive for field or shipboard use since these components are the result of extensive engineering investments and are designed to operate under a wide range of environmental conditions and treatment for which laboratory or research grade equipment is not suited.

The ASL Model-1 visioceilometer was recently used in conjunction with tests carried out at the NOSC remote sensing facility on Point Loma, San Diego, CA [46]. The limited comparisons of vertical aerosol extinction profiles measured with an aircraft-mounted aerosol spectrometer and vertical soundings with the Model-1 LIDAR show good agreement in one case and disagreement in another, attributable to possible differences in the aerosols along the paths sampled by the vertically spiraling aircraft and by the LIDAR. The position taken by the authors is that the cursory comparisons attempted thus far are inadequate to draw meaningful conclusions and that further tests will be needed to discern any systematic differences in comparisons of the two approaches to extinction measurements.

3.4 DATA PROCESSING OF PULSED LIDAR SIGNALS

3.4.1 CHARGE COUPLED DEVICE (CCD) - MICROPROCESSOR APPROACH IN THE ASL MODEL-L VISIOCEILOMETER

The signal processing used by the Model-1 visioceilometer involves several distinct parts. These serve to record the range dependent LIDAR return for either display or analysis. The two basic problems with recording a LIDAR return are the large dynamic range of the signal and its wide bandwidth. The first of these problems is addressed by a logarithmic gain compression scheme which compresses four decades of input to two decades of output. This compressed signal is then recorded in a rather special way. Because the visioceilometer is intended to be a hand-held, battery powered unit, its power consumption must be low. On the other hand, the bandwidth of the signal to be recorded must be very large since digital recording requires high sample rates (such as 20 MHz). Unfortunately, the analog to digital (A/D) conversion devices

which operate at the required speeds and accuracy consume rather large amounts of power and are not well suited for a battery powered, hand-held device. This apparently led to the use of a charge coupled device (CCD) as a high speed analog buffer. Analog samples of the compressed detector video are placed into the CCD buffer at a 20 MHz rate. The CCD accomplishes this with very low power consumption. After the signal is recorded in this manner, it can be read out of the CCD at a slower rate (44 KHz in the visioceilometer case) such that a low power A/D converter may be used. Once the digital version of the recorded signal is obtained, it is post-processed by a minicomputer for display or analysis. Such things as the $1/r^2$ dependence of the backscattered signal are removed at this point.

While use of the CCD is critical to the hand-held unit, it does add some complications. A major one is a time dependent decay of the signal held in the CCD buffer. Each element of the signal is held in the buffer for a different length of time. Thus, this decay appears as a range dependent variation which must be removed in post processing. Unfortunately, this decay is temperature dependent such that its accurate removal is not trivial.

For application to a shipboard system, however, we are not faced with the same stringent power requirements. Thus, direct digitization of the compressed detector video is a possibility. This would eliminate the temperature dependent decay problems associated with the CCD. Additionally, other signal processing techniques could be useful. As an example, the $1/r^2$ characteristic of the signal could be removed in real time prior to the logarithmic compression and digitization. This would greatly simplify the required post processing of the LIDAR return.

3.4.2 HIGH SPEED ANALOG-TO-DIGITAL CONVERSION (ADC) - MINICOMPUTER APPROACH

The design philosophy which has been emphasized in the ASL visioceilometer data acquisition subsystem design described in the previous section has emphasized low power consumption and miniaturization. The use of a CCD for transient analog sampling of the LIDAR return, followed by slower analog-to-digital conversion (ADC) is well suited to the configuration of that system apart from the thermal stability problems mentioned. In a shipboard LIDAR system design the constraints of space and power consumption, while important, are nowhere as severe as in a unit designed for hand-held operation as in the visioceilometer.

High-performance, compact ADC modules are currently available which exceed the 20 MHz sampling rate used in the visioceilometer.

A modularized multi-channel analyzer system offered by Le Croy Research Systems Corporation (model 3500) includes a programmable 8085 A microprocessor, display, data storage, and CAMAC-based modular data acquisition features. Small, plug-in transient digitizer modules compatible with this system are currently available with true 8-bit dynamic range at 50 MHz sampling rates. This is over twice the sampling rate currently used in the ASL Model-1 visioceilometer. A very high-speed ADC module for this system will be available by summer 1982 offering a 200 MHz sampling rate with true 8-bit analog to digital conversion [47].

The large variations seen in the data presented in Section 2.2 and the lack of any clear choice of model to represent these variations argue for continued collection of LIDAR measurements in maritime conditions and evaluation of these data. To the extent that the LIDAR returns are

processed on-line with pre-selected algorithms using pre-programmed microprocessors, the value of the data for establishing the suitability of various signal inversion methods (e.g. the Klett inversion method) is reduced. Currently the ASL Model-1 visioceilometer data are reduced off-line using a minicomputer system [46] but eventually on-line microprocessor reduction of the LIDAR returns is envisioned. The latter approach will be required in a shipboard system designed for routine aerosol extinction measurement. Based on the current state of understanding of experimental data and model development, it seems appropriate to exercise a shipboard LIDAR system at one, or preferably two infrared wavelengths, and to test the validity of various signal inversion approaches.

4
LIDAR APPLICATION TO A SHIPBOARD MEASUREMENT ENVIRONMENT

4.1 EYE SAFETY

Eye safety concerns and potential problems are an important aspect of the design and operation of a pulsed laser system especially when it is intended for use in an outdoor environment. A shipboard measurement system based on the LIDAR approach would necessarily have to be operated in close proximity to ship's crew members routinely performing a wide variety of tasks taking place at many locations throughout the ship. To the extent that it is possible to design an eye-safe LIDAR system and retain adequate system measurement sensitivity, a significant advantage can be realized. Approval for fleet utilization can be greatly facilitated or impeded by the eye safety issue. The apparent reduction in sensitivity arising from reduced system aerosol backscatter efficiency for wavelengths longer than 1.4 μm can be more than offset by the increase in maximum permissible exposure (MPE) (for direct intrabeam viewing) of ∿ 2,000 with respect to the Nd-YAG laser wavelength of 1.06 μm.

Instrument optical alignment procedures and adjustments which involve working at close quarters with a 1.06 μm laser source and consequently include the possibility of direct specular reflection of a small diameter beam into the eye are especially potentially hazardous. For visible sources with wavelengths below 0.7 μm the operator's eye can sense and help in avoidance of direct viewing of the beam. However coherent laser radiations at wavelengths between 0.7 μm and 1.4 μm do not cause a visual sensation in spite of being directly transmitted by the lens of the

eye and imaged as a potentially damaging intense spot on the retina, requiring that particular caution must be exercised while working with such sources. Evaluation of alternatives to the use of readily available and reliable Nd-YAG laser sources should be given careful consideration from the eye safety viewpoint alone, apart from the many other issues to be considered in the development of a shipboard measurement system.

4.1.1 ESTIMATE OF EYE EXPOSURE HAZARD FROM THE ASL MODEL-1 VISIOCEILOMETER

The maximum permissible exposure (MPE) for intrabeam viewing of a 1.06 μm pulsed laser (single pulse between 10^{-9} and 5×10^{-5} sec) is 5×10^{-6} J/cm^2 according to guidance published by the American National Standards Institute [48]. If the pulse repetition frequency (PRF) is increased to 10 pps then the MPE value decreases to 1.7×10^{-6} J/cm^2 per pulse. Assuming a PRF of 1 pps for the AN/GVS-5 specifications given in Section 3.3 then a safe eye exposure distance (SEED) may be calculated. The beam divergence is specified as 1.0 mr which is about 6 times the diffraction limit of a Gaussian mode diffracting from the 0.8 cm aperture. The SEED value S can be found from the relation:

$$\frac{E_p}{\pi(\frac{S\theta}{2})^2} \leq \text{MPE} \qquad (17)$$

where E_p is the laser pulse energy in joules and θ is the beam divergence angle in radians. Using the ASL Model-1 values we find:

$$\frac{4 \times 10^{-2}}{\pi(S \times 10^{-3})^2} \leq 5 \times 10^{-6} \text{ J/cm}^2 \qquad (18)$$

or $S \geq .505 \times 10^5$ cm = 505 m. If the PRF is increased to 10 pps the SEED value increases to about 1.6 km. The ANSI requirement [48] states that direct intrabeam viewing of the launched laser pulse must be prevented until the beam has traveled at least 505 m for the 1 pps case and 1.6 km for the 10 pps case. An alternate approach to this potential eye safety problem can be evaluated by considering what increase in transmitter aperture size would be needed to reduce the SEED value to zero for a pulse energy of 10^{-2} J. That is, how large must the launched beam cross sectional area (A_B) be before it is eye-safe as it leaves the transmitting aperture? In this case:

$$\frac{10^{-2} \text{ joules}}{A_B} \leq 5 \times 10^{-6} \text{ J/cm}^2 \qquad (19)$$

or $A_B \geq 2 \times 10^3$ cm^2. This requires a transmitter mirror diameter of about 50 cm (20") diameter which is clearly out of the question for the Army application but could be considered for a shipboard measurement, keeping in mind the close quarters that such a unit would be used in aboard ship.

4.1.2 WAVELENGTH CONTROL FOR EYE SAFETY

If an operating wavelength longer than 1.4 μm can be used, the MPE value increases dramatically from 5×10^{-6} J/cm^2 to 10^{-2} J/cm^2 for 1 pps repetition rates. For wavelengths of 1.4 μm and longer the lens of the human eye is no longer transparent and focusing of an exceedingly small and intense spot of coherent light on the retina of the eye no longer occurs. Possible eye hazard considerations then concern exposure of the sensitive surface of the eye to the laser radiation and depend upon the actual energy density in the beam at the surface of the eye, not in a tiny focal

spot formed on the retina. Consequently an increase of about 2000 in the MPE values applies.

It can be seen from Equation 19 that a transmitter aperture area only slightly larger than 1 cm^2 would correspond to an intra-beam energy density meeting the MPE requirement for wavelengths longer than 1.4 μm at 1 pps and that a transmitted beam area of about 1.6 cm^2 would be eye safe for 10 pps repetition rates.

4.1.2.1 Stimulated Raman Scattering as a Wavelength Shifting Mechanism

We have seen from the discussion and MPE values presented in the previous section that a significant reduction in potential eye safety hazards results if laser wavelengths longer than 1.4 μm can be used with a LIDAR system. Several examples of highly developed, MIL-SPEC laser hardware operating at the Nd-YAG wavelength of 1.06 μm are currently being widely used in military laser designators and rangefinders. These devices have resulted from extensive development programs designed to produce extremely rugged and reliable components which will operate satisfactorily under very adverse circumstances and extremes of environmental conditions. The ASL Model-1 visioceilometer is based on the use of the AN/GVS-5 laser rangefinder source and receiver modules which are MIL-SPEC components. Additional MIL-SPEC systems will be discussed in the following section.

It would be highly advantageous in the development of a shipboard LIDAR to capitalize on the extensive hardware development which has occurred in the design and production of reliable MIL-SPEC laser sources. Nearly all of these systems operate at 1.06 μm, so that an efficient and reliable means of shifting the 1.06 μm wavelength to 1.4 μm or longer is needed in order to utilize exsisting MIL-SPEC

hardware and to simultaneously obtain an "eye safe" output for use as a LIDAR source.

Recent developments in laser frequency conversion using Stimulated Raman Scattering (SRS) have shown that energy conversion efficiencies to the first-Stokes output wavelengths for high pressure gaseous D_2 and CH_4 exceed 40% [49]. Design considerations and test results for a multiple-pass, optical-resonator Raman cell have been presented recently by Trutna and Byer [50]. Application of these techniques to the design and testing of a compact, efficient SRS cell used to shift 1.06 μm laser radiation to 1.54 μm using a methane filled cell and to 1.9 μm using hydrogen has been carried out by Hughes Research Laboratories [51]. The SRS first-Stokes-shifted wavelength for CH_4 pumped with the output of a Nd-YAG laser is 1.543 μm (6480.68 cm^{-1}). If a deuterium cell were used the output wavelength would be approximately 1.561 μm (6407.88 cm^{-1}). The SRS wavelength shifts are fixed by the vibrational energies of the scattering molecules (2914.2 cm^{-1} for CH_4 and 2987 cm^{-1} for D_2). Slight tuning adjustments of the SRS output frequency can be made to avoid possible overlap with interfering atmospheric absorption lines by use of an etalon and/or temperature tuning the 1.064 μm Nd-YAG output wavelength over a few tenths of a wavenumber.

Figures 30 and 31 show the calculated atmospheric transmission of a 5 km sea level path for a mid-latitude summer atmosphere (14.25 torr partial pressure of H_2O) in the spectral region near 1.54 μm. The interval between 6460 cm^{-1} and 6500 cm^{-1} is shown in Figure 30; Figure 31 is a higher dispersion plot of the interval between 6473 cm^{-1} and 6483 cm^{-1} showing the location of the 1.543 μm first-Stokes SRS line for CH_4. From an examination of Figure 31 it can be seen that a prominent atmospheric absorption feature

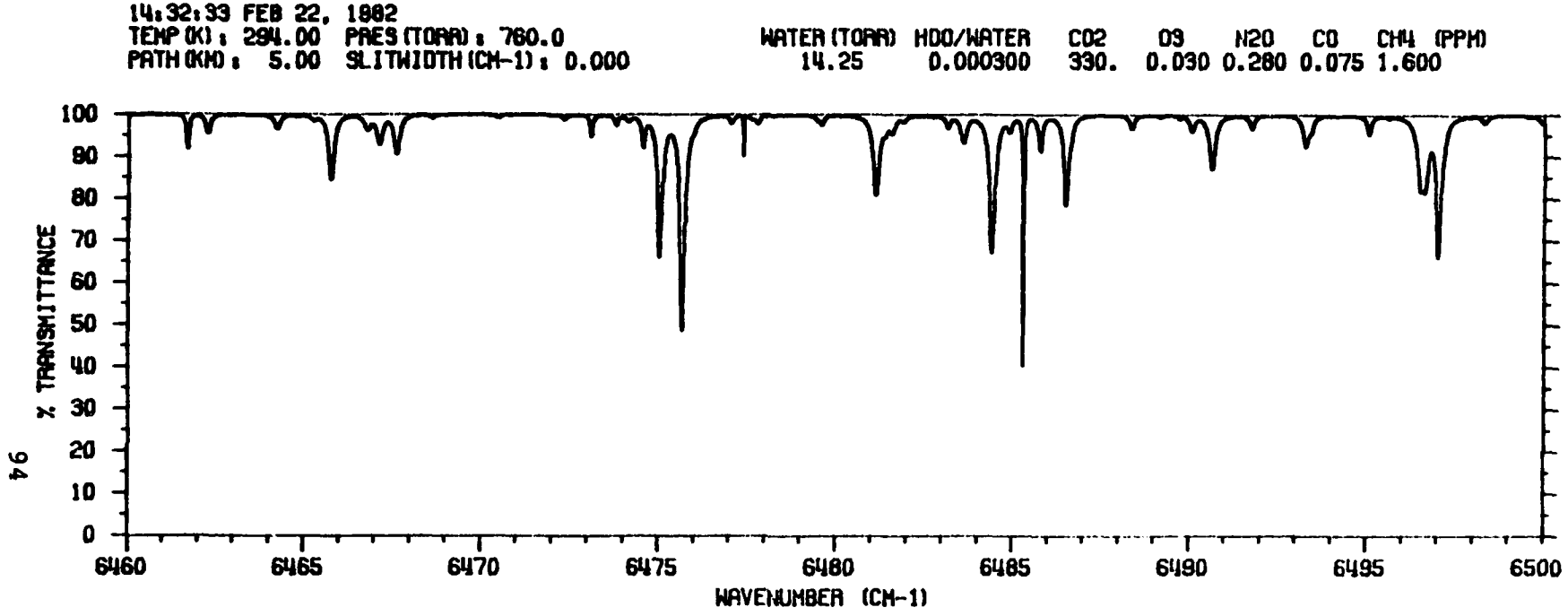

FIGURE 30. CALCULATED TRANSMISSION OF A 5km SEA-LEVEL ATMOSPHERIC PATH BETWEEN 6460 cm^{-1} AND 6500 cm^{-1}.

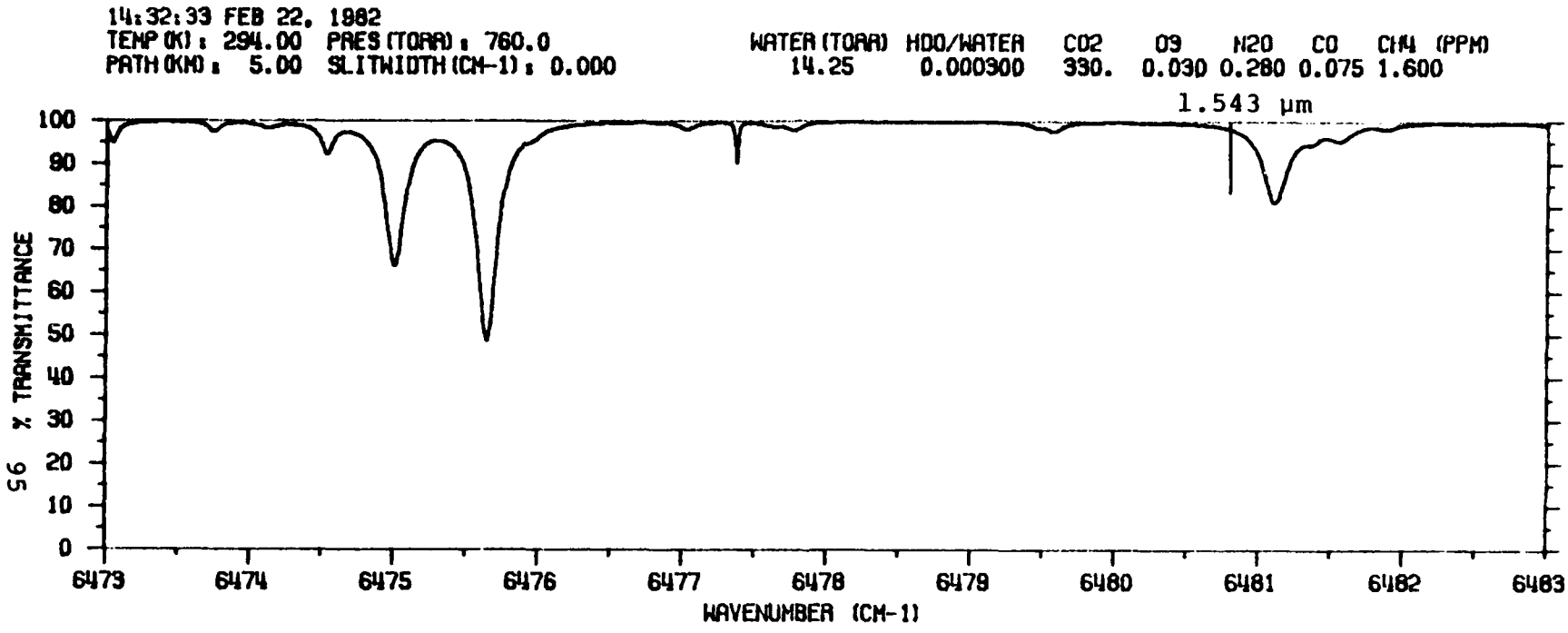

FIGURE 31. CALCULATED TRANSMISSION OF A 5km SEA-LEVEL ATMOSPHERIC PATH BETWEEN 6473 cm^{-1} AND 6483 cm^{-1}. LOCATION OF THE SRS LINE OF METHANE AT 1.543 µm IS INDICATED.

occurs near the 1.543 μm SRS line. The major contribution to this absorption feature is an H_2O line located at 6481.1110 cm^{-1}; minor contributions are due to weaker CO_2 and H_2O lines located at 6481.366 cm^{-1} and 6481.564 cm^{-1} respectively [52]. By tuning the Nd-YAG/CH_4 SRS output line by 0.2 cm^{-1} to 0.4 cm^{-1}, this near-coincidence of the CH_4 SRS line and the atmospheric water vapor line could be used as the basis of a differential absorption LIDAR (DIAL) scheme, expanding the usefulness of the shipboard LIDAR to include a capability for remote, long-path measurements of water vapor density in addition to the primary measurement function of aerosol extinction. It should be feasible (e.g. by means of an oscillating etalon) to shift the SRS line on and off of the atmospheric H_2O line on alternate pulses thereby providing two distinct LIDAR returns which can be ratioed to give the water vapor attenuation profile. Whether or not this particular aspect of the 1.543 μm SRS line of the Nd-YAG/CH_4 system is exploited, the SRS technique shows a great deal of promise in providing a relatively straightforward means to generate "eye safe" laser radiation using a relatively passive Raman cell together with proven, highly developed, MIL-SPEC 1.06 μm laser hardware.

4.2 SUITABILITY OF EXSISTING MIL-SPEC AND OTHER RUGGEDIZED E-O HARDWARE

4.2.1 MIL-SPEC 1.06 μm SYSTEMS

The AN/GVS-5 laser rangefinder system which has been incorporated into the Army ASL Model-1 visioceilometer is an example of the use of MIL-SPEC components for a LIDAR system. The characteristics of the AN/GVS-5 were listed in Section 3.3. Other, higher energy 1.06 μm MIL-SPEC sources have been developed for military laser designator applications and could be utilized in the development of a shipboard LIDAR. One such device is the AN/TVQ-2 Army

Ground Laser Locator Designator (GLLD). The GLLD output energy is about a factor of ten larger than that of the AN/GVS-5 and the device characteristics include reasonably good beam quality. The combined weight of the laser designator-rangefinder module of the GLLD is 12.7 kg (28 lbs.) and the battery supply module providing completely self-contained operation weighs 3.2 kg (7 lbs.). While this device is substantially larger than the AN/GVS-5, its' size and weight are quite compatible with use in a shipboard operation. The most probable configuration for using it as part of a shipboard LIDAR would involve interfacing the GLLD laser source with moderately large ($\sim$ 30 cm) aperture transmit/receive telescope optics. A more detailed discussion of such a configuration together with performance estimates are presented in Section 4.3. Use of an SRS cell together with the GLLD source to provide output pulse energeries in the range of tens of millijoules at 1.54 μm offers several attractive advantages. Cooling for the GLLD laser is provided by pressurized N_2 gas circulated through a N_2-air heat exchanger through which filtered external air is circulated by means of a blower. This technique offers the advantage that no cooling liquids are needed. The entire laser optical train and N_2 circulation path are hermetically sealed against the intrusion of contamination which could rapidly render the laser system inoperative. Thus, these features of the device are ideally suited to a shipboard installation where high humidity and salt-laden condensates can prove very detrimental to the delicate and critical optical components comprising the laser optical cavity.

Another MIL-SPEC 1.06 μm laser designator system incorporating similar design features to the GLLD but with about twice as large an output pulse energy is used in the Navy A-6 aircraft TRAM system. The N_2-air heat exchanger feature is used in the TRAM designator as well.

Both the GLLD system and the TRAM system are fully developed and currently in or near production. Availability of engineering development units from either program for evaluation as to their potential for use in a shipboard LIDAR development program should be pursued.

Several other liquid-cooled MIL-SPEC 1.06 μm sources are in production or advanced development and warrant further investigation. At this time the absence of a liquid coolant and the compactness and ruggedness of the GLLD and TRAM designator system designs appear to offer the most desireable characteristics for use in a shipboard LIDAR.

4.2.2 SYSTEMS OPERATING AT 10.6 μm

An alternative to operation at 1.06 μm or at the SRS shifted wavelength of 1.54 μm is the use of a CO_2 laser operating at 10.6 μm. This wavelength is well into the eye safe region but the anticipated LIDAR backscatter return signal is expected to be substantially smaller in most cases than the return signal at 1.06 μm or 1.54 μm (see Section 2.4, Figures 27 and 28). Cryogenically cooled detectors will be required with a 10.6 μm system and heterodyne detector techniques can be employed to gain a few orders of magnitude in system sensitivity to offset the low levels of aerosol backscatter at 10.6 μm.

Laser pulse energies greater than 10^{-1} joule are desireable for operation in moderate visibility conditions out to a few kilometers. At the present time development of MIL-SPEC CO_2 laser sources has lagged substantially behind that of 1.06 μm sources for US military systems. A promising, albeit rather low energy, ruggedized CO_2, transverse-electrical-atmospheric pressure (TEA) system is manufactured in the UK. This laser is used in the Marconi Avionics and Ferranti model 307 CO_2 laser rangefinders

manufactured for the military. The laser is of a ruggedized design, well suited for field use. The output pulse energy, however is specified at about 13 x 10^{-3}J with a peak power of 220 kw and pulse duration of 60 ns, making its use as a source for 10.6 μm aerosol backscatter measurements marginal for all but low visibility fog-type conditions where scattering at 10.6 μm is more nearly comparable to that at 1.06 μm.

Several developmental, compact CO_2 TEA lasers are being used in LIDAR type research instruments. These sources typically operate at higher pulse energy than the UK source described above but are not as well suited for routine use in the field. The most promising approach at the present time for obtaining a 10.6 μm source suitable for use in a shipboard LIDAR would seem to involve the upgrade and environmental protection of a compact, energetic TEA laser system operating in 10^{-1} to 1.0 J/pulse energy range.

4.3 SHIPBOARD LIDAR SYSTEM PERFORMANCE ESTIMATES

4.3.1 ASL MODEL-1 VISIOCEILOMETER SYSTEM

Using the results of calculations discussed earlier in Section 2.4 and shown in Figure 32 together with the ASL Model-1 visioceilometer characteristics discussed in Section 3.3, performance estimates of this system were carried out. The results of these estimates are shown in Figure 32 for ranges between 200 m and 1.0 km. Calculated peak power of the LIDAR return signal in watts is shown as a function of range for four model maritime aerosol distributions with 2 km, 5 km and 10 km visibilities and 70% relative humidity. Also shown by the dashed curve is the energy density in the transmitted beam E' as a function of range. One can see that E' is substantially larger than the 1.06 μm MPE value of 5 x 10^{-6} J/cm^2 (single pulse) or

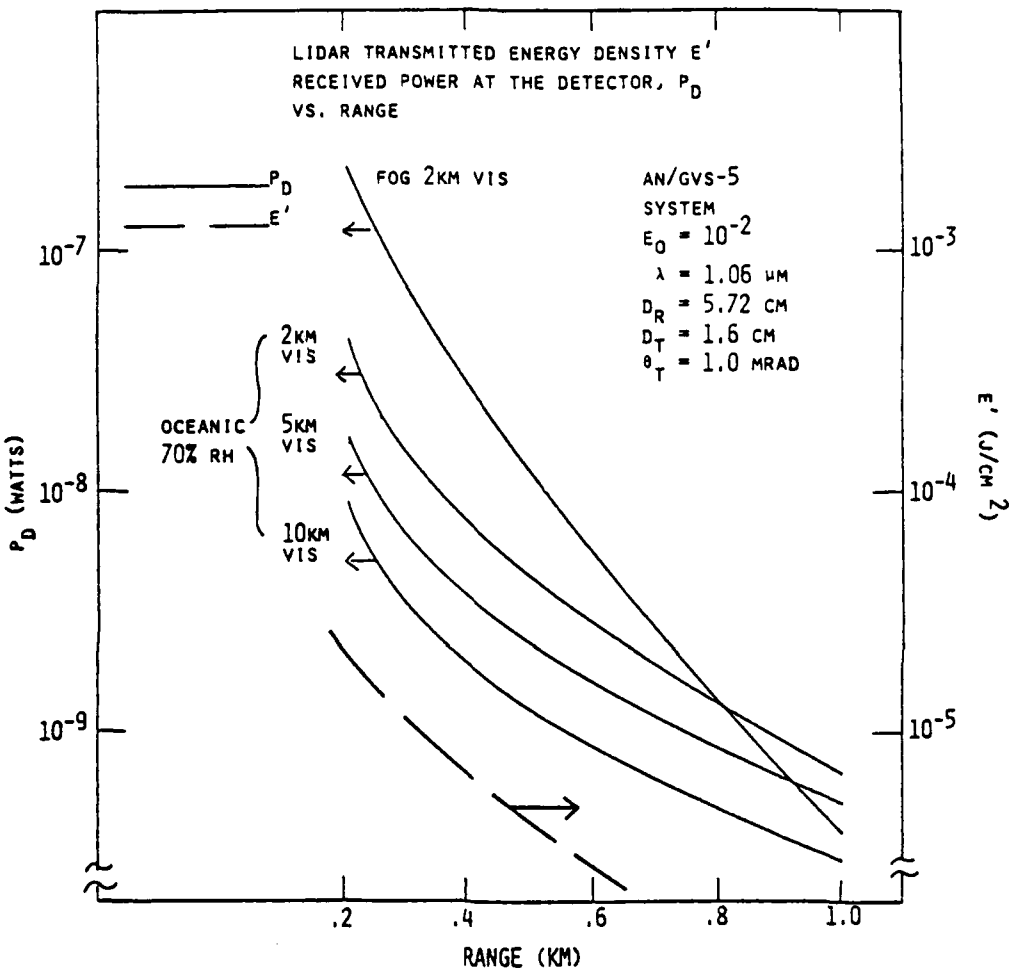

FIGURE 32. LIDAR TRANSMITTED ENERGY DENSITY E' AND RECEIVED PEAK POWER P_D VERSUS RANGE FOR THE ASL MODEL-1 (AN/GVS-5) VISIOCEILOMETER SYSTEM FOR VARIOUS TYPES OF MARINE AEROSOLS.

1.6×10^{-6} J/cm^2 at 10 pps for ranges shorter than about 500m. The safe eye exposure distance (SEED) for this device was calculated in Section 4.1.1 and found to be 505 m for 1 pps and 1.6 km for 10 pps. The return signal peak powers are seen to vary between 10^{-7} watts at $\sim$ 200 m to less than 10^{-9} watts for ranges in excess of 1 km, indicating that system performance will be marginal for greater ranges in intermediate backscatter situations.

4.3.2 UPGRADED 1.06 μm SYSTEM

The same type of analysis as shown in Figure 32 for the ASL Model-1 system was carried out for a hypothetical upgraded system with the following characteristics: pulse energy, $E_o = 10^{-1}$ J/pulse and transmitter and receiver diameter of 30.5 cm and a beam divergence of 1.0 mrad, the same as the ASL Model-1 system. The results of these calculations are shown in Figure 33. The larger transmitter aperture more than offsets the factor of ten pulse energy increase to give a lower energy density at the device output aperture, however it is still not below the eye safe limit of 5×10^{-6} J/cm^2. As can be seen in Figure 33 the energy density in the beam for this system is still determined primarily by the beam divergence and remains above the eye safe level over the ranges (0.2 km to 1.0 km) shown in the figure. If the sytem operating wavelength were longer than 1.4 μm the MPE would be 10^{-2} J/cm^2 and there would be no eye hazard even at the device aperture. The LIDAR return signal levels for the upgraded configuration shown in Figure 33 are approximately 2 orders of magnitude greater than those for the baseline ASL Model-1 device indicating that substantially improved performance can be expected for ranges longer than 1 km when compared to the ASL Model-1 system.

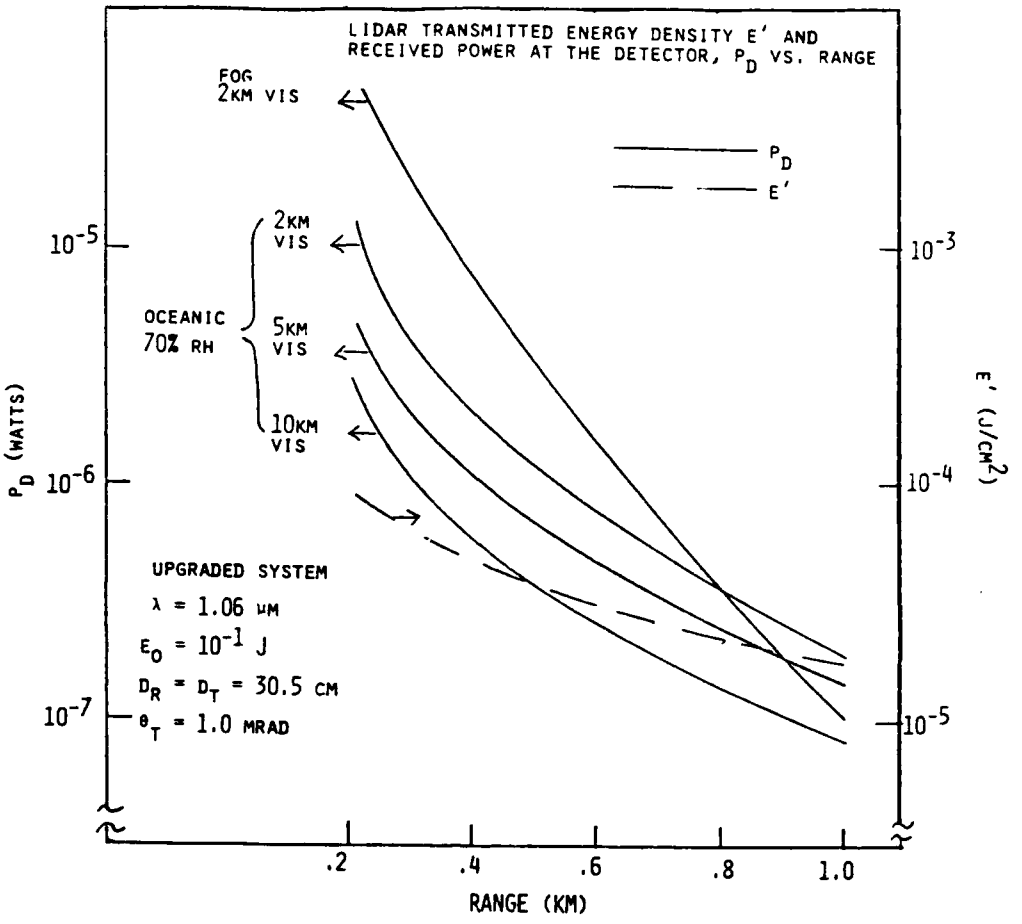

FIGURE 33. LIDAR TRANSMITTED ENERGY DENSITY E' AND RECEIVED PEAK POWER P_D VERSUS RANGE FOR AN UPGRADED LIDAR SYSTEM WITH THE CHARACTERISTICS SHOWN IN THE FIGURE.

Figure 34 shows a performance comparison of the two systems for fog and 2 km visibility oceanic aerosol conditions for ranges between 500 m and 5 km. The upgraded system is seen to generate useful return signal levels out to 5 km for the oceanic aerosol while the AN/GVS-5 based system (ASL Model-1 visioceilometer) is seen to generate marginally useful return signal levels for ranges greater than about 1.5 km.

4.3.3 COMPARISON OF SYSTEMS OPERATING IN THE 1.06 μm, 3-5 μm, and 8-12 μm REGIONS

Using the upgraded system characteristics and the calculated backscatter coefficients for a 2 km visibility oceanic aerosol a system performance comparison for 3 different wavelengths was generated. The results of this comparison are shown in Figure 35 for ranges between 200 m and 1.0 km. The rapid decrease of return signal peak power with increasing wavelength shows that higher output pulse energies and increased detector sensitivity e.g. a heterodyne configuration will be required for systems operating at 10.6 μm.

4.3.4 DEPENDENCE OF LIDAR SYSTEM PERFORMANCE ESTIMATES UPON AEROSOL EXTINCTION DATA AND MODEL VARIABILITY

When the variability in the infrared aerosol extinction data described in Section 2.2 is taken into account, adjustments to the nominal case backscatter calculations shown in Figure 27 can be made. Based on the range of values for σ_{IR} seen in the experimental aerosol extinction data one could anticipate worst case corrections to the calculated data shown in Figure 27 of about 0.1 at a wavelength of 0.55 μm, 0.08 at 1.06 μm and 0.25 at 3.8 μm. Lacking a sufficient body of 10.6 μm maritime optical transmission data and considering the uncertainties associated with the

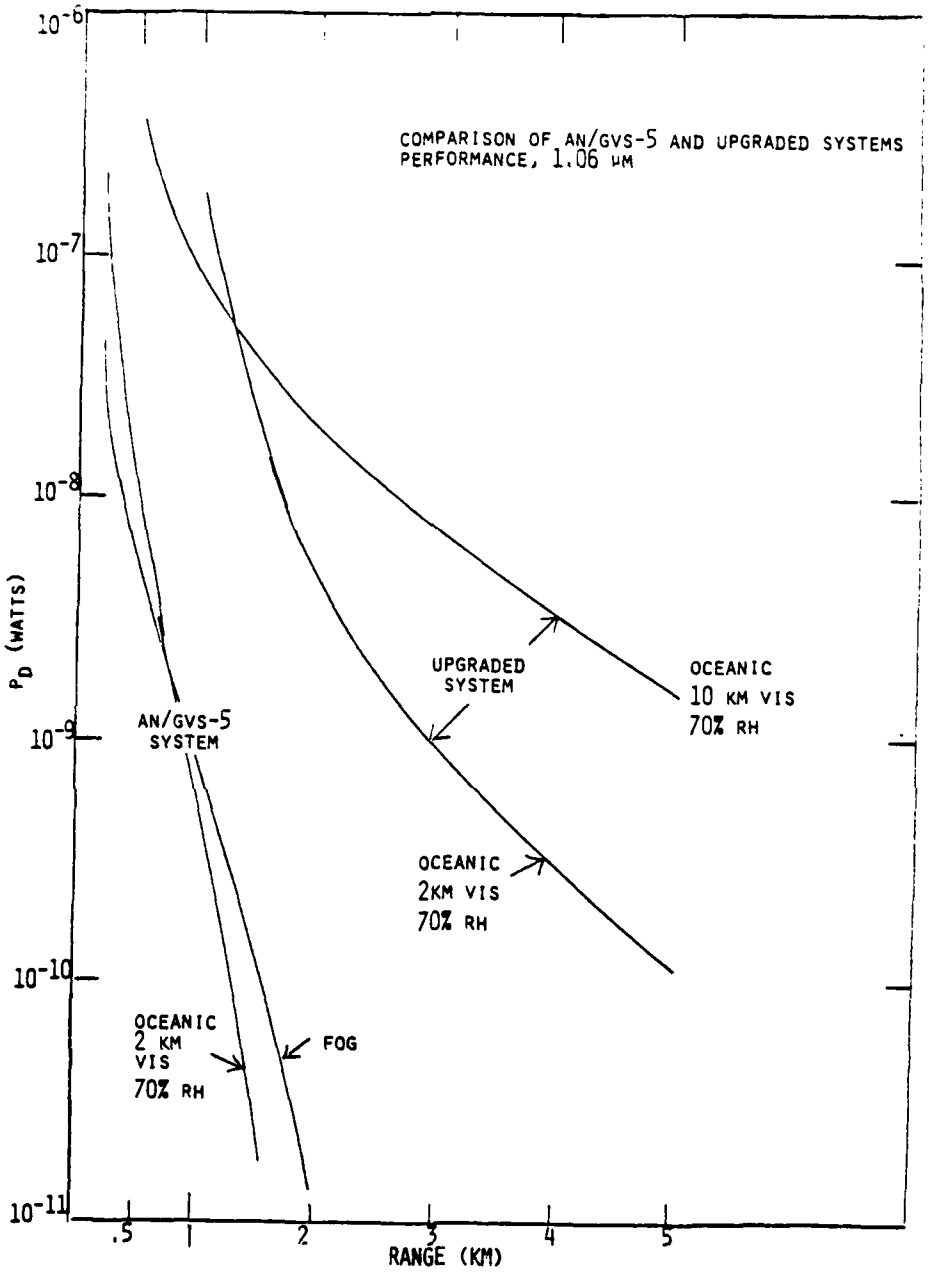

FIGURE 34. COMPARISON OF RECEIVED PEAK POWER P_D FOR THE AN/GVS-5 BASED AND UPGRADED SYSTEMS VERSUS RANGE.

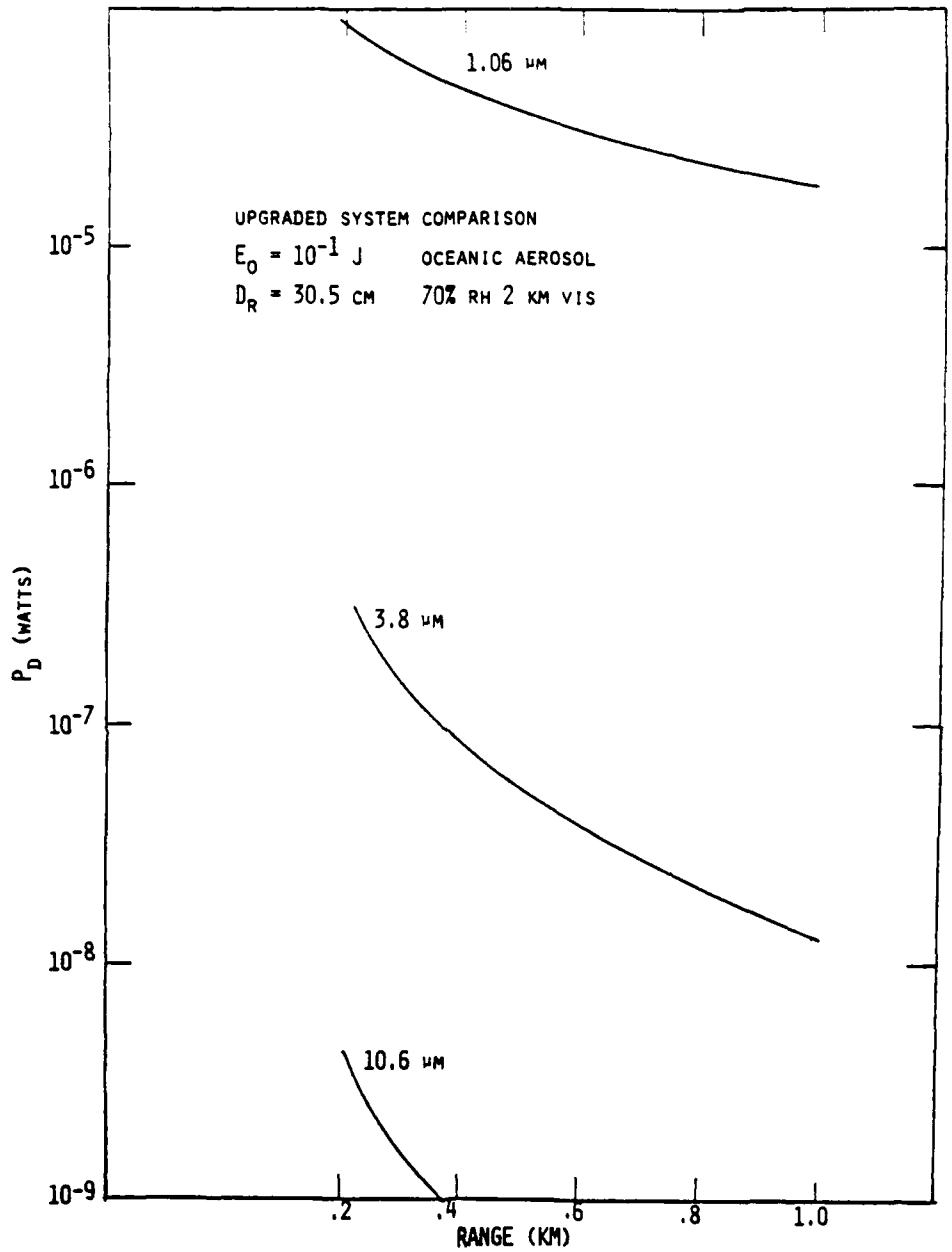

FIGURE 35. COMPARISON OF RECEIVED PEAK POWER LEVELS; P_D VERSUS RANGE FOR THREE SYSTEMS OPERATING AT PULSE ENERGIES OF 10^{-1} J/PULSE WITH 30.5 cm DIAMETER COLLECTING OPTICS AND 1.06 μm, 3.8 μm AND 10.6 μm WAVELENGTHS.

modeling of the water vapor continuum absorption in the 8-12 μm spectral region [23], the 0.25 correction factor appropriate for 3.8 μm may be applied to system performance estimates for 10.6 μm as well.

Model predictions for σ_{IR}/σ_{VIS} have been seen to vary by about a factor of two with changes in relative humidity and by about a factor of four with changes in windspeed. Considering the observed variations in experimental data and the variations exhibited by the computed model values for σ_{IR} over the range of windspeeds and relative humidities of greatest interest, the performance predictions shown in Figures 32-35 should reliable at the specified levels or somewhat lower but by no more than a factor of ten.

4.3.5 SIGNAL TO NOISE RATIO ESTIMATES

Using the estimates of collected signal power for various system configurations and ranges presented in Figures 32-35 together with detector noise equivalent power(NEP) estimates, the signal to noise ratio achievable with a prototype LIDAR system can be estimated. Table 7 summarizes signal to noise ratio calculations for several of the shipboard LIDAR configurations previously discussed. Column one of the table lists the system configuration. The ASL-1 system is the visioceilometer device based on the AN/GVS-5 laser rangefinder which is described in section 3.3. The upgraded system configuration listed in column one is based on a transmitter pulse energy of 10^{-1} joule and a receiver collector diameter of 30.5 cm. Signal to noise ratio estimates for several system configurations including upgraded 1.06 μm, 1.54 μm, 3.8 μm and 10.6 μm direct and heterodyne detection systems are shown in the table. Column two lists the operating wavelength. Column three lists the

TABLE 7
SIGNAL TO NOISE RATIO ESTIMATES

							2 km VIS 70% RH†					
							200m			1 km		5 km	
SYSTEM	λ (μm)	DETECTOR	TEMP (K)	D* (cm.Hz$^{\frac{1}{2}}$W^{-1})	BW (MHz)	NEP (w)	S (w)	S/N	S (w)	S/N	S (w)	S/N
ASL-1	1.06	Si	295	10^{12}	50	7.1E-10	4.6E-8	65	6.3E-10	0.90	1.4E-11	2.0E-2
Upgraded	1.06	Si	295	10^{12}	100	1.0E-9	9.3E-6	9.3E3	1.8E-7	1.8E2	1.1E-10	0.11
Upgraded	1.54	Ge	295	$5x10^{10}$††	100	2.0E-8	9.3E-6	4.7E2	1.8E-7	9.0	1.1E-10	5.5E-3
Upgraded	3.8	InSb	77	$2x10^{11}$	100	5.0E-9	3.1E-7	62	1.2E-8	2.4	4.5E-10	9.0E-2
Upgraded	10.6	HgCdTe	77	$3x10^{10}$	100	5.0E-8	4.3E-9	8.6E-2	1.7E-10	3.4E-3	6.1E-12	1.2E-4
Heterodyne	10.6	HgCdTe	77	---	100	3.7E-12†††	4.3E-9	1.2E3	1.7E-10	46	6.1E-12	1.7

† S and S/N values may be 2-3 times smaller considering competing effects due to higher RH and variability of σ and β/σ as discussed in section 4.3.4.

†† Probably a conservative estimate.

††† Theoretically possible but probably not fully realizable in practice.

appropriate detector and its operating temperature is listed in column four. The detector D*, operating bandwidth and noise equivalent power are listed in the next three columns. Calculated signal levels and signal to noise ratios are listed in the next three sections of the table for three ranges: 200m, 1 km and 5 km.

All of the calculations are appropriate for a measurement bandwidth of 100 MHz except for the ASL model-1 which employs a 50 MHz bandwidth. One can see from an inspection of the table that the detector detectivity (D*) is a factor limiting performance at the eye safe wavelength of 1.54 μm. It should be noted that rapid development of detectors for use at this wavelength is currently taking place accellerated by requirements for fiber optical communication applications (most optical fibers exhibit very low loss at this wavelength) and therefore that the D* value contained in Table 6 for the Ge photodiode detector will very likely be exceeded in the near future by some of the newer InGaAs photodiodes being optimized for use at this wavelength.

One can see from an inspection of the table that all of the system configurations provide useable signal to noise ratios for a 1 km range with the exception of the 10.6 μm direct detection configuration. For a range of 5 km most of the systems generate marginally useful return signal levels and consequently exhibit small signal to noise ratios. The best performance is seen in the upgraded 1.06 μm system and the heterodyne 10.6 μm system. In order to increase signal to noise ratios co-addition of multiple LIDAR signal returns can be implemented. The signal to noise ratio (S/N) is expected to improve as $n^{1/2}$ so that S/N ratios of 10^{-1} should be considered useful since for n=100, multiple laser pulse returns can be easily coadded using a 1 pps or 10 pps repetition rate. However when 10^4 or more pulses must be coadded to achieve

an improved S/N of ∿1.0 and the maximum pulse repetition rates for the 10^{-1} J/pulse lasers being considered are about 10 pps, the required co-addition times become prohibitively long. Accordingly, the upgraded 1.06 μm and 3.8 μm configurations appear to be useful for 5 km ranges. The ASL model - 1 system will probably not be routinely useable at this range nor will the 1.54 μm upgraded system and the 10.6 μm direct detection system unless appreciably higher D* detectors for these wavelengths can be obtained. The advantages of heterodyne detection become obvious when one examines the last row of the table. Although the backscattered return signals at 10.6 μm are 2 or 3 orders of magnitude smaller than those for the shorter wavelengths, the gain in detector effective noise-equivalent-power (NEP) more than offsets this loss and the result is useable S/N ratios out to 5 km for the conditions indicated in Table 6. The obvious conclusions that can be drawn from the values listed in the table are that improved detectors at 1.54 μm (with respect to the D* value listed) and heteorodyne detection at 10.6 μm will be very crucial to the successful implementation of LIDAR systems operating in the 10^{-1} J/pulse range at these wavelengths.

4.3.5.1 Techniques for Signal to Noise Ratio Improvement

The development of improved detectors for 1.54 μm should be accellerated by the rapid growth of the fiber optics industry. Improved Ge PIN photodiodes and/or InGaAs photodiodes with quantum efficiencies around 60% are being developed and becoming available for use in this wavelength region, therefore it should be possible to substantially improve S/N ratios for the 1.54 μm upgraded system configuration shown in Table 6. An improvement of a factor of ten in detector D* will be needed for useful performance of this system at a range of 5 km, increasing the estimated single pulse S/N to about 5×10^{-2}. LIDAR return S/N ratio can be further improved to a useful level for measurement by the co-addition of multiple pulses. Assuming a 10 pps repetition rate, co-addition of return signals for an interval of 40 seconds (i.e. 400 return pulses) would provide a S/N ratio improvement of 20, resulting in a final S/N ratio of unity.

There are very large potential advantages to be gained by the use of heterodyne detection techniques as shown by the entries listed in the last row of Table 6 (NEP $\sim 10^{-12}$ w in a 10^8 Hz bandwidth). Using the heterodyne approach the backscattered return signal from the transmitted pulse is mixed with the output of a local oscillator laser offset in frequency by 10 GHz or more. The LIDAR return signal is then detected as the beat frequency difference signal. Very high speed photodetectors and amplifiers are required in this configuration. Use of a rare isotope CO_2 laser and selection of the respective laser transitions such that the transmitter and local oscillator frequencies are offset by about 10 GHz should be relatively straightforward. Most of the rare isotope CO_2 laser lines have been measured with sufficient accuracy [53] so that choice of appropriate pairs of operating lines should not be a problem.

The effects of laser speckle patterns superimposed on the spatial distribution of backscattered radiation will tend to deteriorate its coherence and consequently will partially ameliorate the potential advantages offered by heterodyne detection. Atmospheric turbulence effects will also cause some loss of phase coherence and therefore impact heterodyne receiver performance. The turbulence effects should tend, however, to contribute to some randomizing or averaging of speckle patterns. Since the two phenomena should be uncorrellated or possibly anti-correllated, the resultant S/N decrease due to a noise like contribution by laser speckle, n_{sp} and that due to atmospheric turbulence, n_{tb} would be expected to be proportional to the root sum square addition of the two contributions, i.e. $n \approx (n_{sp}^2 + n_{tb}^2)^{\frac{1}{2}}$. Some, if not the full theoretical improvement over a direct detection system should be possible.

The MPE for $\lambda > 1.4$ μm is 10^{-2} J/cm^2 for 1 pps. For a system with a transmitter aperture diameter of 30.5 cm the transmitted beam cross sectional area is about 730 cm^2, therefore the laser pulse energy E_o could be as large as 7.3 joules (for a uniformly illuminated aperture) and the system would remain eye safe. Clearly an increase in E_o to the 1-5 J range would be permissible. The limitations in useable source energy are seen to be determined more by available source technology than by eye safety considerations. A stable oscillator-TEA laser amplifier configuration appears to be the most promising approach for obtaining the required 10.6 μm pulse energy at the present time. Research LIDAR systems incorporating these features are currently being fielded, however a significant amount of development and packaging will be needed before such a system can begin to approach the reliability of the MIL-SPEC Nd-YAG systems previously discussed.

4.4 SHIPBOARD IMPLEMENTATION

Several of the considerations impacting the implementation of a shipboard LIDAR system have been discussed previously in sections 4.1 and 4.2. A summary of that information will be incorporated here by describing the characteristics of a prototype shipboard LIDAR system, the development of which appears to be both feasible and highly useful at the present time.

Based on the earlier discussions concerning eye safety and recognizing the ambiguities present in scaling short wavelength data to the 8-12 μm region, a system simultaneously operating at 1.54 μm and 10.6 μm appears most worthwhile. Such a system can be made relatively compact although the extreme miniturization emphasized in the development of the ASL model - 1 system is not required. A system employing a common 30 cm (12 inch) diameter reflecting telescope both as transmitter and receiver for both wavelengths appears reasonable. The optics and source module for a prototype shipboard system would be contained in a cylinder less than or equal to 40 cm (16 inches) in diameter and about 1.2 m in length. A weight allowance of 50 to 75 lbs. should be sufficient for this assembly. The self-contained data acquisition and processing equipment might occupy about eight cubic feet and weigh about 150 lbs. This sub-system could be remotely located from the LIDAR optical head containing optics, laser sources, detectors and analog-to-digital converter, if desirable. In this configuration non-weatherized electronic modules could be housed in a sheltered area permitting system operation during a wider range of weather conditions than would be possible if the electronics sub-system were mounted adjacent to the LIDAR optical head. Initially shipboard testing of the LIDAR system might best be accomplished using a single physical

installation with the data sub-system adjacent to the optical head to permit simplified operation of the system. Once an adequate level of familiarity with system operation was gained and required changes in design and/or operational procedures had been determined, a more-permanent, all-weather installation could be planned.

It is anticipated that the optical head of the LIDAR system could be mounted on an existing or easily installed deck-mounted pedestal such as used to support shipboard signaling lights. Utilization of an existing, manually aimed pedestal should simplify shipboard installation and should be accompanied by some reduction in cost.

Operation of the shipboard LIDAR could be eventually performed by one person, probably the ship's meteorological officer. A team of one or two scientists working in conjunction with the ship's officer would be required to initially operate, test and evaluate the system's performance and suitability for shipboard use. Eventually the system would be operated by the ship's meteorological officer and used to collect data on operational cruises, thereby generating the necessary data base of marine aerosol extinction collected simultaneously in the infrared wavelength bands of interest for E-O systems operation.

An optimally useable format for the LIDAR data should be determined so that it may be readily used in a PREOS-type FLIR performance prediction. Some provision should be made during the shipboard LIDAR testing and evaluation program to operate the system along with a FLIR performance prediction scheme such as PREOS and simultaneously with actual FLIR measurements performed under well documented test conditions. In this way the correspondence of the LIDAR-PREOS measurement/prediction approach may be directly evaluated against the performance of a FLIR system.

5
RECOMMENDATIONS

In light of the large indeterminacy associated with existing aerosol models, an important requirement exists to develop a reliable shipboard LIDAR system to be used to collect a near-, mid- and long-wavelength infrared marine aerosol extinction data base to be used for model verification, and to provide a real-time measure of infrared aerosol extinction for use in E-O systems performance assessments at sea. Accordingly, it is recommended that a twofold program be undertaken to design, develop and operate a dual-wavelength shipboard LIDAR system operating in the "eye-safe" near- and far infrared wavelength bands. This system would be used on several cruises to collect a marine aerosol extinction data base and to develop a prototype instrument for widespread shipboard deployment. The latter will be used to provide routine, in-situ measurements of marine aerosol effects on Navy E-O/IR systems.

The specific approach recommended in carrying out the shipboard LIDAR development program involves the design and development of an eye safe, 1.54 μm shipboard LIDAR utilizing proven MIL-SPEC modules together with a stimulated Raman scattering module to produce 1.54 μm radiation.

Development of the 1.54 μm source would be based upon a prior evaluation of candidate MIL-SPEC 1.06 μm sources. The two most promising candidates identified at this time are the AN/TVQ-2 GLLD system and the A-6 TRAM system as discussed in section 4.2. These units (presumably engineering demonstration units) would be evaluated regarding

their availability for the shipboard LIDAR program. Acquisition cost and time constraints would be part of the evaluation. A stimulated Raman scattering (SRS) cell would be developed and interfaced with the 1.06 μm MIL-SPEC source to produce an eye safe 1.54 μm operating wavelength.

A second phase of instrumentation development is concerned with producing a reliable and suitably energetic source of 10.6 μm radiation. An evaluation of the Marconi/Ferranti system described in section 4.2 together with ruggedized and environmentally conditioned hybrid-TEA CO_2 lasers using an oscillator-amplifier configuration should be performed. The potential advantages of heterodyne detection for operation at CO_2 wavelengths should be explored as previously discussed in section 4.3.5.

At the same time that first-generation LIDAR system prototype hardware development is being performed, system performance estimates and measurement planning to evaluate and refine marine aerosol models should be undertaken. Implementation of such a plan would, in general terms, involve the collection, reduction and analysis of at-sea, marine aerosol extinction data gathered during several cruises spanning at least a two-year period.

A parallel evaluation and preliminary design effort concerned with possible differential-absorption LIDAR (DIAL) and laser-Doppler-velocimeter (LDV) variations of the basic shipboard LIDAR should be undertaken. Using these additional alternative features, the shipboard LIDAR could be used for humidity and wind profile measurements as well.

Based on the results and experience gained during the first-generation, prototype system development and deployment, during which the aerosol-model-validation data base is collected, the design, construction and testing of a second-generation, ruggedized LIDAR system for eventual widespread shipboard deployment should be undertaken.

REFERENCES

1. Snyder, F.P., "PROCAL-PREOS: A Fast Running Airborne FLIR System Performance Model", Naval Ocean Systems Center Technical Note TN 810, February, 1980.

2. Dowling, J.A. and Rogne, T.G., "Interim Progress Report Number 1; Shipboard Visibility Measurement System Definition Study" OptiMetrics interim report on Naval Ocean Systems Center Contract N6601-81-C-0127, 15 September, 1981.

3. Dowling, J.A., "Definition of a Remote Sensing System for the Measurement of Marine Aerosol Extinction: A Shipboard Visibility Meter" talk presented at the 1981 National OSA meeting, Orlando, Florida, October, 1981.

4. Richter, Juergen H. and Hughes, Herbert G., "Electro-Optical Atmospheric Transmission Effort in the Marine Environment", Naval Ocean Systems Center Technical Report 696, May, 1981.

5. Katz, B.S., "Impact of Aerosol Modeling on Performance Calculations of Electro-Optic (E-O) Systems Operating in Marine Environments", SPIE Proceedings 305, 1981.

6. Barnhardt, E.A. and Streete, J.C., "A Method For Predicting Atmospheric Aerosol Scattering Coefficients in the Infrared", Appl. Optics, 9, 1337 (1970).

7. Selby, J.E.A., Shettle, E.P. and McClatchey, R.A., "Atmospheric Transmittance from 0.28 to 28.5 μm: Supplement LOWTRAN 3B", AFGL TR-76-0258, 1976.

8. Kneizys, F.Y. et al, "Atmospheric Transmittance/Radiance: Computer Code LOWTRAN 5", AFGL TR-80-0067, 1980.

9. Wells, W.C., Gal, G. and Munn, M.W., "Aerosol Distributions in Maritime Air and Predicted Scattering Coefficients in the Infrared", Appl. Opt. 16, 654, 1977.

10. Noonkester, V.R., "Offshore Aerosol Spectra and Humidity Relations Near Southern California", Amer. Meteor. Soc. 113, 1980.

11. Fitzgerald, J.W., "Approximate Formulas for the Equilibrium Size of an Aerosol Particle as a Function of its Dry Size and Composition and the Ambient Relative Humidity", J. Appl. Meteor. 14, 1044 (1975).

12. Davis, J.S. et al, "Marine Electro-Optical Micro-Meteorological Data Base and Statistical Analysis", Science Applications Inc., Report SAI 164-087-249, December, 1978.

13. Katz, B.S., Hepfer, K. and McMeekin, N.A., "Electro-Optical Meteorological Sensitivity Study", Naval Surface Weapons Center Report, NSWC TR-79-67, 1979.

14. Katz, B.S. and Goroch, A.K., "A Climatology of North Atlantic Effects on Forward Looking Infrared (FLIR) Systems" Naval Environmental Prediction Research Facility Report, NAVENVPREDRSCHFAC TR-81-02, July, 1981.

15. DeJong, A.N., "Long Range Transmission Measurements over Sea-Water", TNO Technical Report PHL 1978-08 (1978).

16. Cutten, D.R., Infrared Physics 19, 81 (1979).

17. Cutten, D.R., "Preliminary Assessment of Infrared Transmission Data Measured Over Ocean Type Waters in a Temperate Environment" Technical Memo, ERL 0063 TM (1979).

18. Cutten, D.R., Infrared Physics 19, 663 (1979).

19. Matthews, G.B., Ackerman, A., Williams, B.E., de Violini, R. and Rosenthal, J., "Atmospheric Transmission and Supporting Meteorology in the Marine Environment at San Nicolas Island", PMTC Technical Publication TP-79-19 (1979).

20. Dowling, J.A., "A Review of Recent Atmospheric Infrared Transmission Measurements in Maritime Locations", appearing in Atmospheric Water Vapor, Academic Press, Inc., pg. 113, (1980).

21. Fenn, R.W. "OPAQUE-A Measurement Program on Optical Atmospheric Quantities in Europe; Volume 1 - The NATO OPAQUE Program", Air Force Geophysics Laboratory Report AFGL TR-78-0011, January, 1978.

22. Turner, R.E. et al, "Model Development for E-O SAEL; Natural Aerosol Contrast, Laser Transmission and Turbulence" Science Applications Inc. Report SAI-78-008-AA (VII) (1978).

23. Dowling, J.A., "Analysis of 1977 Cape Canaveral Air Force Station Laser and High-Resolution Atmospheric Transmission Data Base", NRL report to be published (1982).

24. Dowling, J.A., et al, "Results of Laser-Calibrated High Resolution Transmission Measurements and Comparisons with Broadband Transmission Data: San Nicolas Island, CA, May 1979", NRL report to be published (1982).

25. Private communication in the form of meteorological data supplied by A.N. DeJong to one of the authors (JAD) at the Naval Research Laboratory, Washington, D.C.

26. Matthews, G.B. and Williams, B.E. et al, "Atmospheric Transmission and Supporting Meteorology in the Marine Environment at San Nicolas Island", semiannual report - Pacific Missile Test Center Report, TP-79-19 (1978).

27. Katz, B.S. and DeBold, F.C., "A Statistical Evaluation of Optical Propagation Codes Using 1978 San Nicolas Island Transmissometer Measurements", Proceedings of the 29th National IRIS Symposium, Orlando, Florida, 19-21 May, 1981.

28. Dowling, J.A., "Laser Transmissometer Calibration of Long-Path Atmospheric Transmission Measurements", SPIE Proceedings 308, 135 (1981).

29. Dowling, J.A., Hanley, S.T., Curcio, J.A., Gott, C.O. and Woytko, M.A., "Laser Extinction and High-Resolution Atmospheric Transmission Measurements Conducted at White Sands Missile Range, NM, March 1979" NRL Report 8446, November, 1980.

30. Guttman, A. Editor, Cosden, T.H. et al "Data Compendium for Atmospheric Laser Propagation Studies Conducted at Cape Canaveral, Florida, February-May 1977" NRL Memorandum Report 3611, September 1977.

31. Dowling, J.A., et al "Atmospheric Extinction Measurements at Nd-YAG and DF Laser Wavelengths performed in conjuntion with the JAN Propagation Tests, June-September 1975" NRL Report 8058, February 10, 1978.

32. Cosden, T.H. et al,"Atmospheric Transmission Measurements Program Report for 1 July through 30 September, 1976 (TQ 1976)", NRL Report 8104, September 1, 1977.

33. Trusty, G.L. and Cosden, T.H., "Optical Extinction Predictions from Measurements Aboard a British Weather Ship", NRL Report 8497, August, 1981.

34. Private communication in the form of unpublished data supplied to one of the authors (JAD) by G.L. Trusty, Naval Research Laboratory. These data are currently available in reference 32.

35. Klett, J.D., "On the Analytical Inversion of LIDAR Returns from an Inhomogeneous Atmosphere" Atmospheric Sciences Laboratory Report ASL-CR-0008-3, April 1980.

36. Klett, J.D., "Stable Analytical Inversion Solution for Processing LIDAR Returns", Appl. Optics 20, 211 (1981).

37. Kreid, D.K., "Atmospheric Visibility Measurement by a Modulated CW LIDAR", Appl. Opt. 15, 1823 (1976).

38. Paulson, M.R., "An Evaluation of a Modulated CW Laser Backscattering System for Determining Atmospheric Visibility" Naval Ocean Systems Center, Technical Note TN 260 (1977).

39. Bufton, J.L. and Iyer, I.S., "Continuous Wave LIDAR Measurement of Atmospheric Visibility", Appl. Opt. 17, 265 (1978).

40. Stokes, R.B., "Evaluation of CW LIDAR Techniques for Measuring Visibility", Naval Ocean Systems Center, Technical Note TN 598, 15 January, 1979.

41. Stokes, R.B., "Beam Image Profiling (BIP) LIDAR: Design and Preliminary Evaluation", Naval Ocean Systems Center, Technical Note TN 782, 28 September, 1979.

42. Stokes, R.B., "Beam Image Profiling (BIP) LIDAR: User's Manual and Continued Evaluation", Naval Ocean Systems Center Technical Note TN 811, 11 January, 1980.

43. Jensen, D.R., "Atmospheric Visibility Measurements Using a Beam Image Profiling LIDAR: A Final Evaluation", Naval Ocean Systems Center, Technical Note TN 953, 15 January, 1981.

44. Saphow, H. et al, "Design Approach for the Visioceilometer AN/GMQ-( ) (XE-1)" Night Vision and Electro-Optics Laboratory Report DELNV-TR-79-4, September 1979.

45. Bonner, R.S. and Lentz, W.J., "The Visioceilometer: A Portable Cloud Height and Visibility Indicator" Atmospheric Sciences Laboratory Report ASL-TR-0042, October, 1979.

46. Hughes, H.G., Jensen, D.R., Stephens, D.H. and Lentz, J., "A Modified Gama Aerosol Model Beneath Maritime Stratus Based on LIDAR Returns", Naval Ocean Systems Center, Technical Note NOSC TN 1079, November, 1981.

47. Private communication, Mr. Andrew Keyser, Le Croy Research Systems, Palo Alto, CA to J.A. Dowling.

48. "American National Standard for the Safe Use of Lasers-ANSI Z136.1 - 1976", American National Standards Institute, 1430 Broadway, NY, NY, March 1976.

49. Byer, Robert L. "Frequency Conversion Via Stimulated Raman Scattering", Electro-Optical Systems Design, February 1980.

50. Trutna, W.R. and R.L. Byer "Multiple-Pass Raman Gain Cell", Appl. Opt. 19, 301, 1980.

51. David Rockwell, Hughes Research Laboratories, private communication.

52. Rothman, L.S. "AFGL Atmospheric Absorption Line Parameters Compilation: 1980 Version", Appl. Opt. 20, 791 (1981).

53. Freed, C., Ross, A.H.M., and O'Donnell, R.G. "Determination of Laser Line Frequencies and Vibrational-Rotational Constants of the $^{12}C^{18}O_2$, $^{13}C^{16}O_2$, and $^{13}C^{18}O_2$ Isotopes from Measurements of CW Beat Frequencies with Fast HgCdTe Photodiodes and Microwave Frequency Counters", J. Mol. Spectros. 49, 439 (1974).

APPENDIX

PRESENTATION PRESENTED AT THE 1981 OPTICAL SOCIETY OF AMERICA CONFERENCE, ORLANDO, FLORIDA, OCTOBER, 1981.

DEFINITION OF A REMOTE SENSING SYSTEM FOR THE MEASUREMENT OF MARINE AEROSOL EXTINCTION: A SHIPBOARD VISIBILITY METER[+]

PRESENTED BY

JAMES A. DOWLING

1981 OSA NATIONAL MEETING
ORLANDO, FLORIDA

OPTIMETRICS, INC.

First National Bank Tower
Suite 200
Las Cruces, New Mexico 88001

[+]WORK SPONSORED BY THE NAVAL OCEAN SYSTEMS CENTER SAN DIEGO, CALIFORNIA

OptiMetrics, Inc.

OUTLINE

1. CHARACTERIZATION OF AEROSOL EXTINCTION IN THE SHIPBOARD MARITIME ENVIRONMENT

2. DEPENDENCE OF SYSTEM SENSITIVITY AND MEASUREMENT ACCURACY UPON OPERATIONAL PARAMETERS

3. PRACTICAL CONSIDERATIONS IN THE IMPLEMENTATION OF A SHIPBOARD SYSTEM

4. SUMMARY AND CONCLUSIONS

1. CHARACTERIZATION OF AEROSOL EXTINCTION IN THE MARITIME ENVIRONMENT

- CURRENT MODELS
  - VARIATION WITH WINDSPEED, HUMIDITY, WAVELENGTH
- RECENT MEASUREMENTS
  - LONG PATH OPTICAL TRANSMISSION
  - MARINE AEROSOL DISTRIBUTION MEASUREMENTS
- COMPARISON OF MODELS AND MEASUREMENTS
  - ANTICIPATED RANGES OF σ AND β

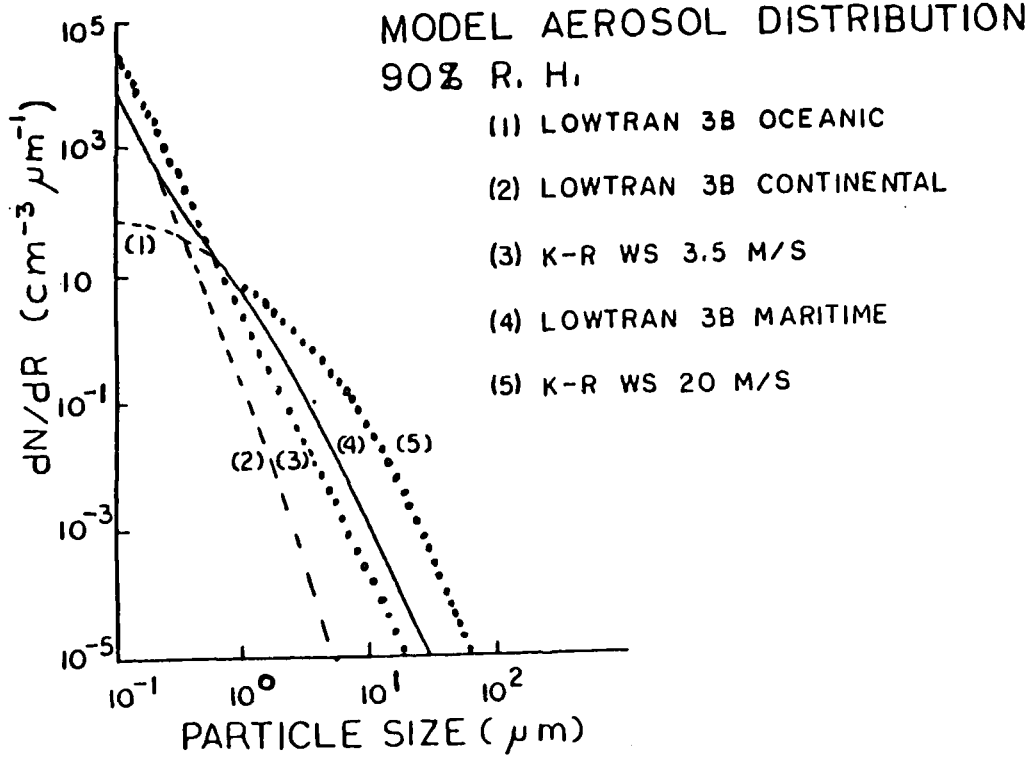
MODEL AEROSOL DISTRIBUTION
90% R. H.
(1) LOWTRAN 3B OCEANIC
(2) LOWTRAN 3B CONTINENTAL
(3) K-R WS 3.5 M/S
(4) LOWTRAN 3B MARITIME
(5) K-R WS 20 M/S
dN/dR (cm⁻³ μm⁻¹)
10⁵
10³
10
10⁻¹
10⁻³
10⁻⁵
10⁻¹
10⁰
10¹
10²
PARTICLE SIZE (μm)
(1)
(2)
(3)
(4)
(5)

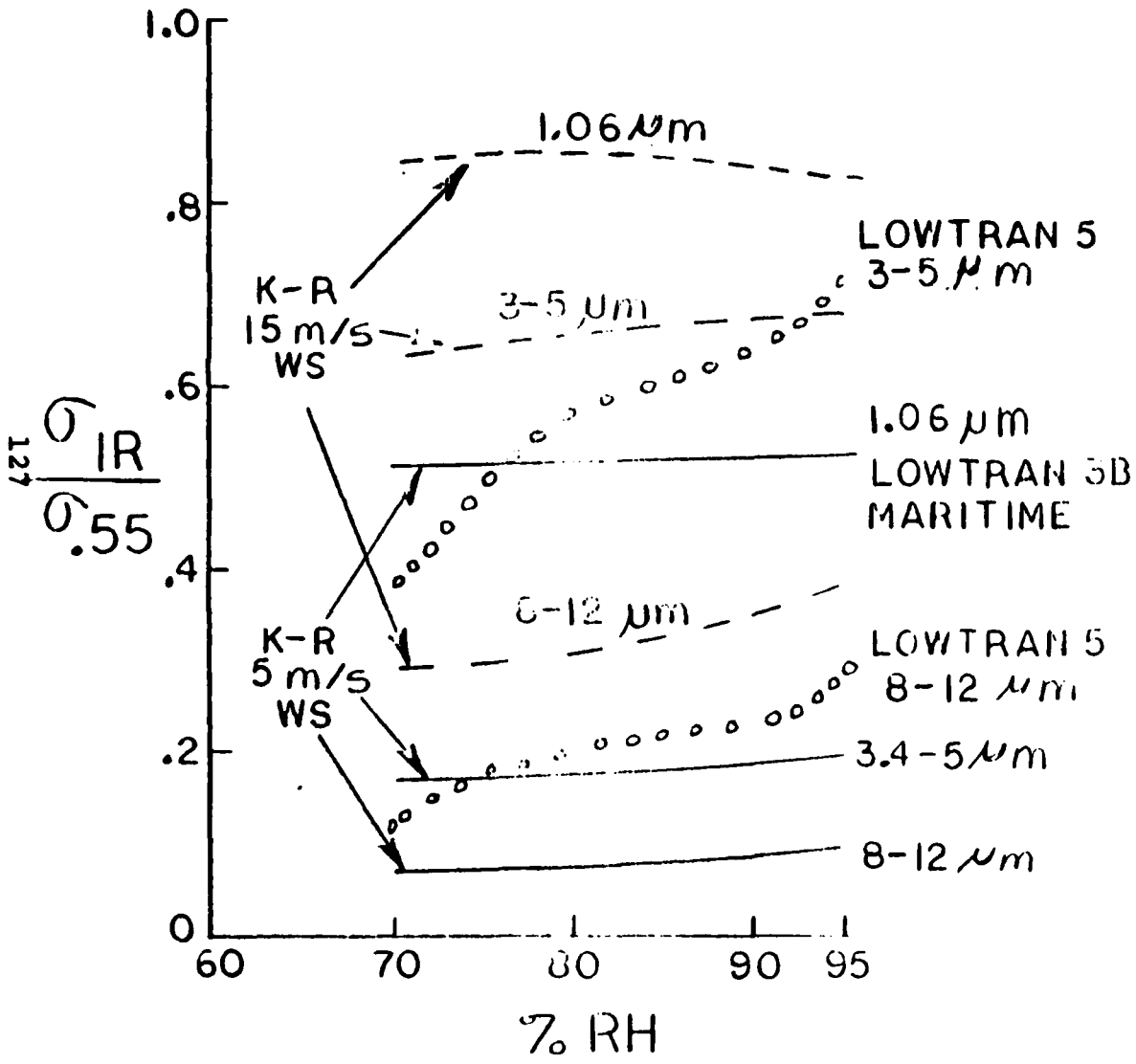

K-R AND LOWTRAN AEROSOL MODEL PREDICTIONS: RATIO OF IR/VIS EXTINCTION

OptiMetrics, Inc.

AEROSOL EXTINCTION CALCULATIONS WITH WELLS, GAL, MUNN MODEL FOR SEA SPRAY 2 KM VIS

WIND SPEED (M/S)	EXTINCTION (KM^{-1})	ABSORPTION (KM^{-1})	SCATTERING (KM^{-1})	SCATT/EXT	EXTINCTION	ABSORPTION	SCATTERING	SCATT/EXT
	70% RH .55 μM				95% RH .55 μM			
0	1.955	2.855E-3	1.952	.999	1.955	8.41E-4	1.954	.999
5	1.955	5.560E-3	1.949	.997	1.955	2.133E-3	1.953	.999
10	1.955	8.859E-3	1.946	.996	1.955	3.233E-3	1.952	.998
	70% RH 3.8 μM				95% RH 3.8 μM			
0	.565	1.623E-2	.549	.971	.573	1.727E-2	.556	.969
5	1.368	2.672E-2	1.341	.980	1.695	4.621E-2	1.649	.973
10	1.791	4.047E-2	1.750	.977	2.065	7.249E-2	1.992	.965
	70% RH 10.6 μM				95% RH 10.6 μM			
0	.143	7.940E-2	6.310E-2	.443	.163	9.47E-2	6.79E-2	.418
5	.287	.145	.142	.495	.489	.238	.252	.574
10	.477	.176	.301	.630	.791	.294	.497	.628

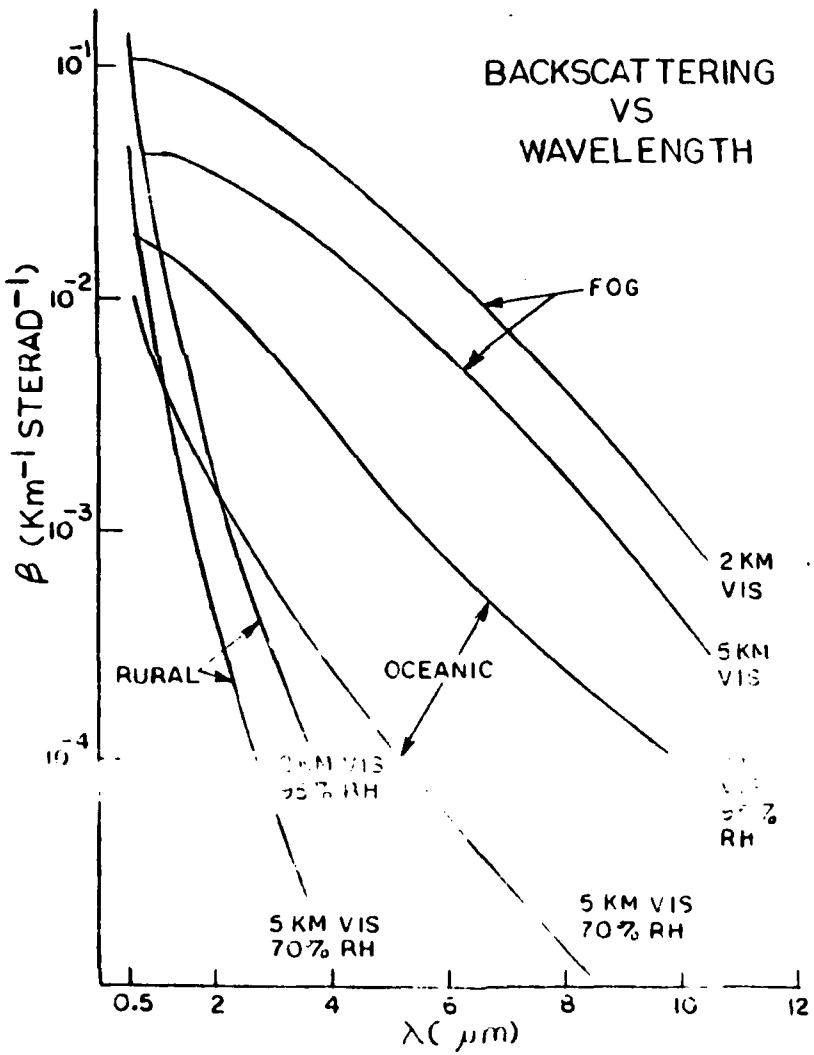
BACKSCATTERING
VS
WAVELENGTH
FOG
2 KM
VIS
5 KM
VIS
RURAL
OCEANIC
5 KM VIS
70% RH
5 KM VIS
70% RH
RH
10^{-1}
10^{-2}
10^{-3}
10^{-4}
β (Km^{-1} STERAD^{-1})
0.5
2
4
6
8
10
12
λ (μm)

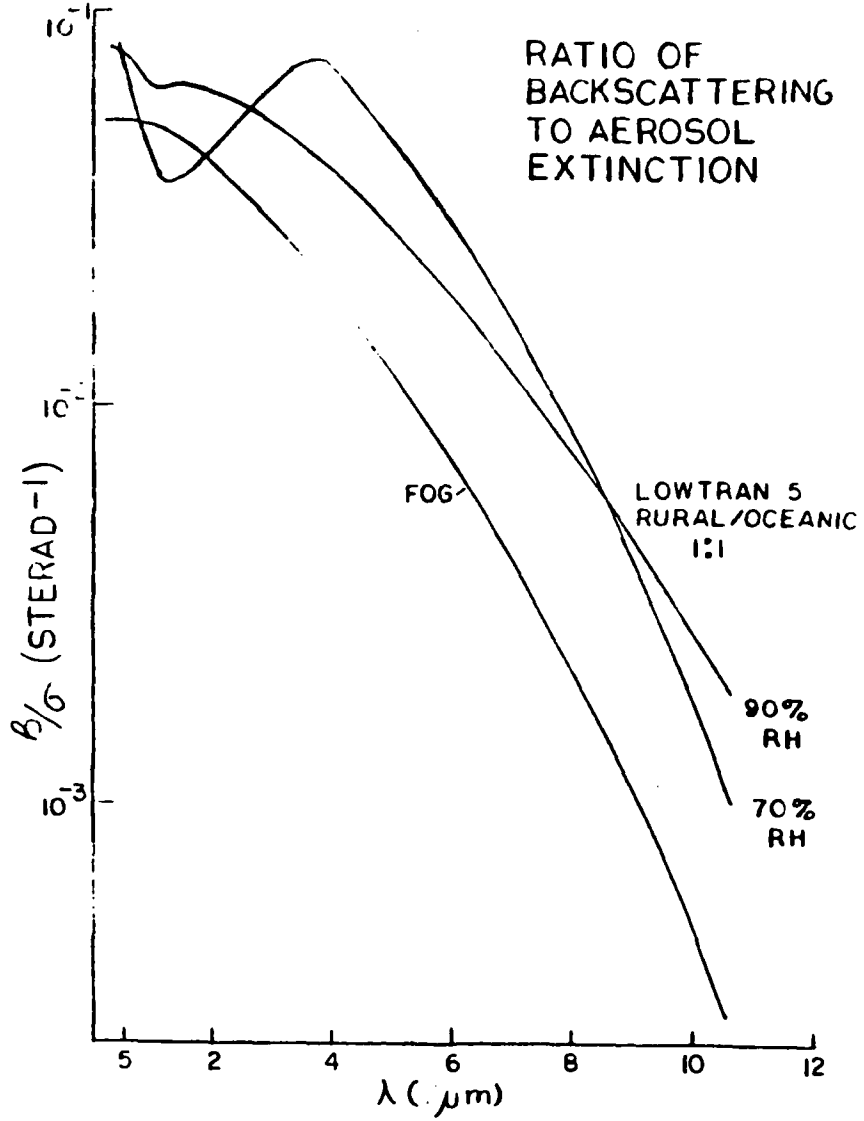
RATIO OF
BACKSCATTERING
TO AEROSOL
EXTINCTION
FOG
LOWTRAN 5
RURAL/OCEANIC
1:1
90%
RH
70%
RH
β/σ (STERAD-1)
λ (μm)
10⁻¹
10⁻²
10⁻³
5
2
4
6
8
10
12

OptiMetrics, Inc.

PLOT OF APPARENT AEROSOL EXTINCTION (AAE) COEFFICIENTS DERIVED FROM NRL LONG-PATH TRANSMISSION MEASUREMENTS AT CCAFS MINUS CALCULATED MOLECULAR ABSORPTION COEFFICIENTS FOR EACH DAY OF THE EXPERIMENT

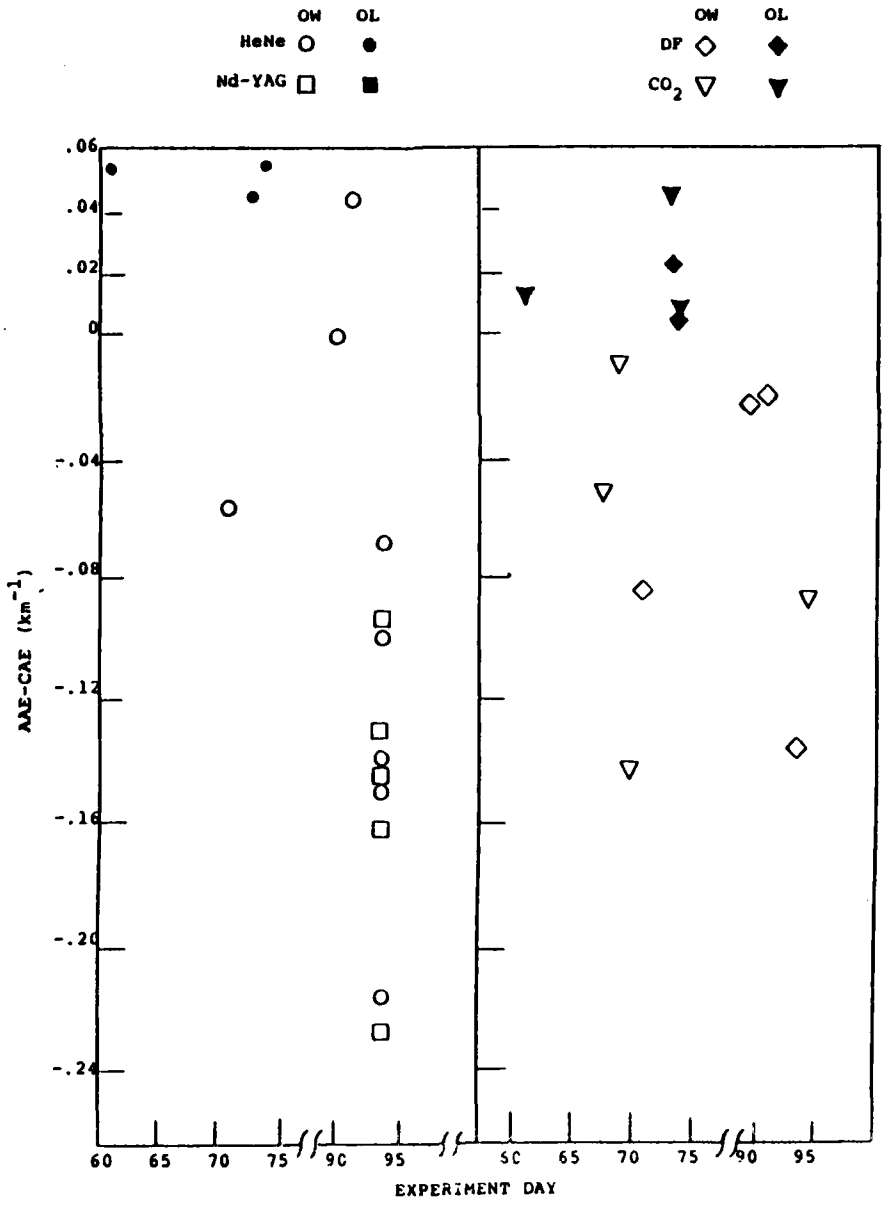

RATIO OF INFRARED TO VISIBLE AEROSOL EXTINCTION COEFFICIENTS VERSUS VISIBLE AEROSOL EXTINCTION COEFFICIENTS DERIVED FROM NRL NORTH ATLANTIC AEROSOL SPECTROMETER DATA.

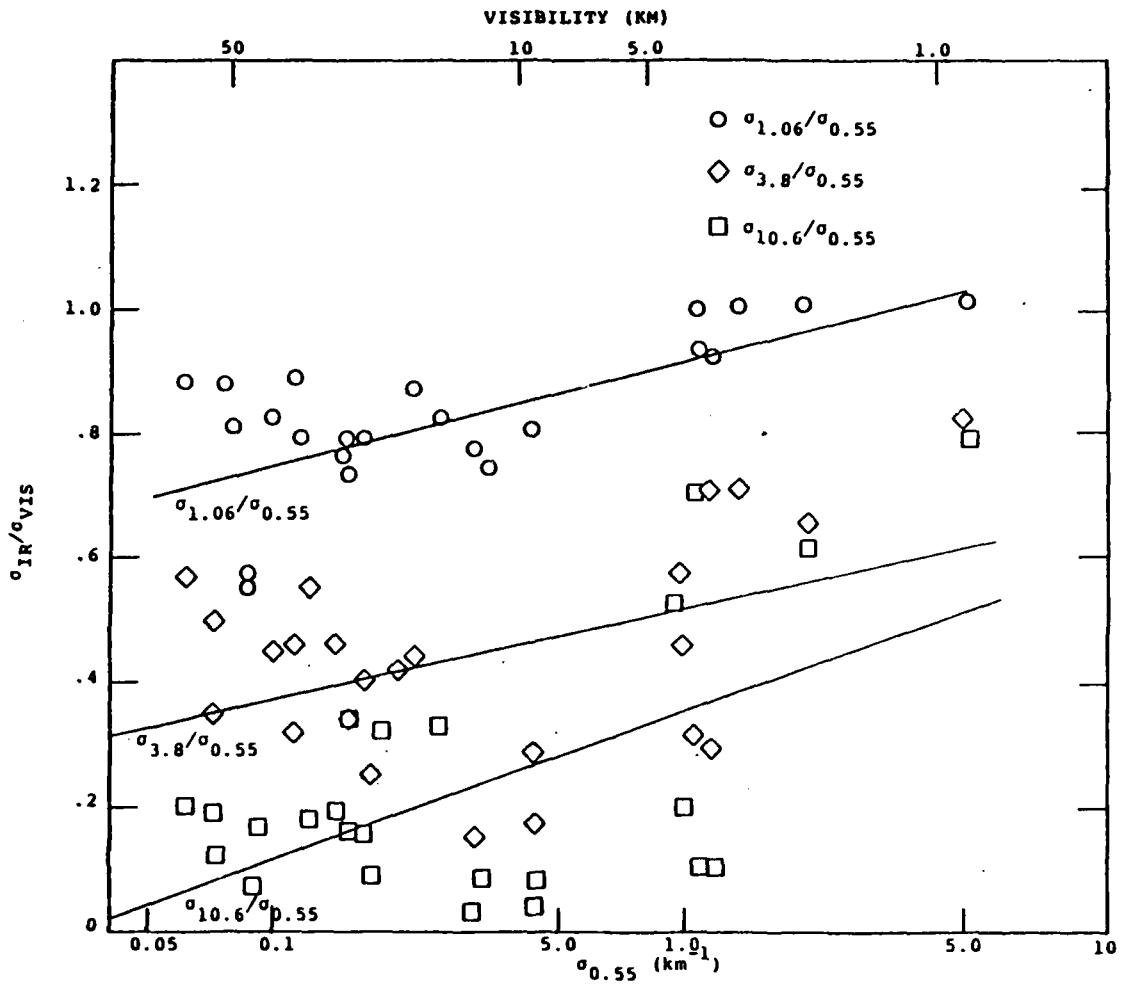

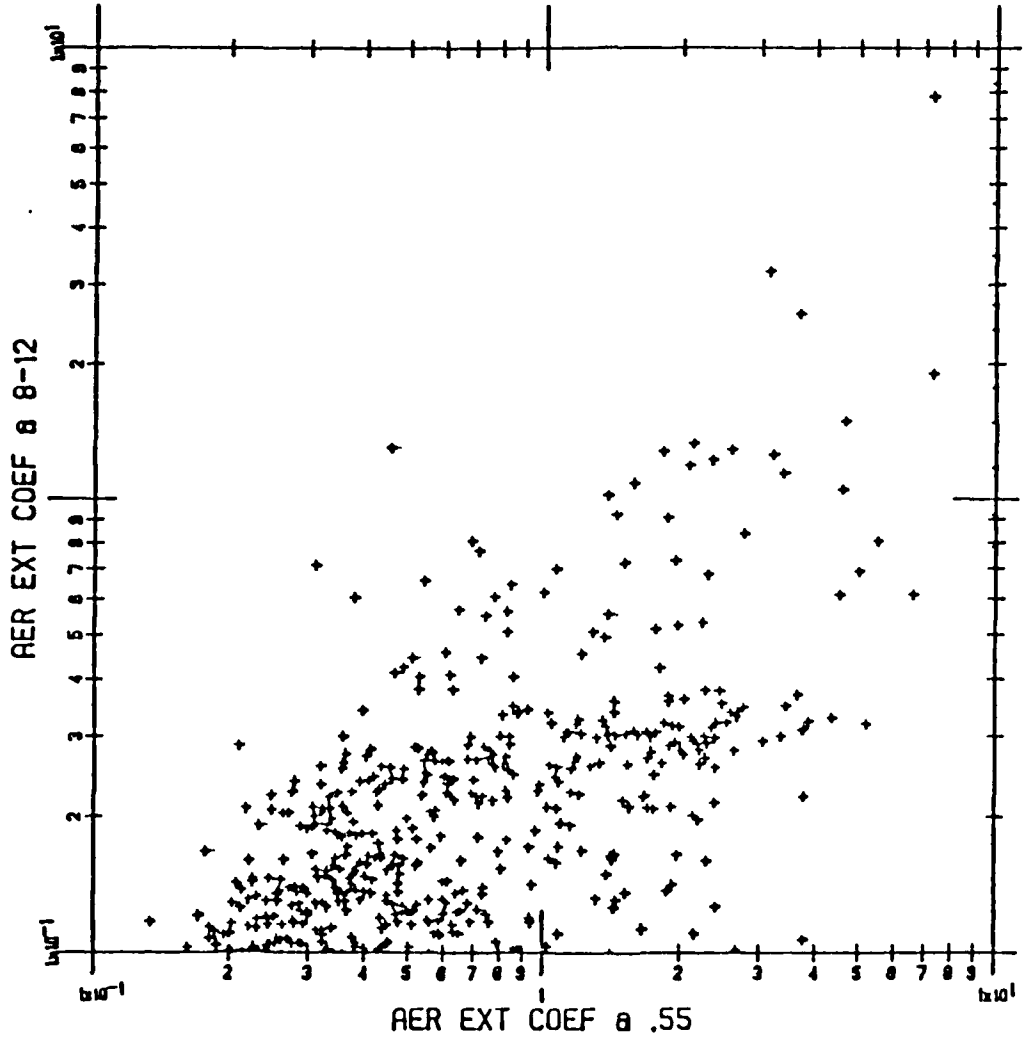

Aerosol Extinction Coefficient @ 0.55 μm Versus Aerosol Extinction Coefficient @ 8-12 μm. Derived from OPAQUE Netherlands 3/77-5/77 data.

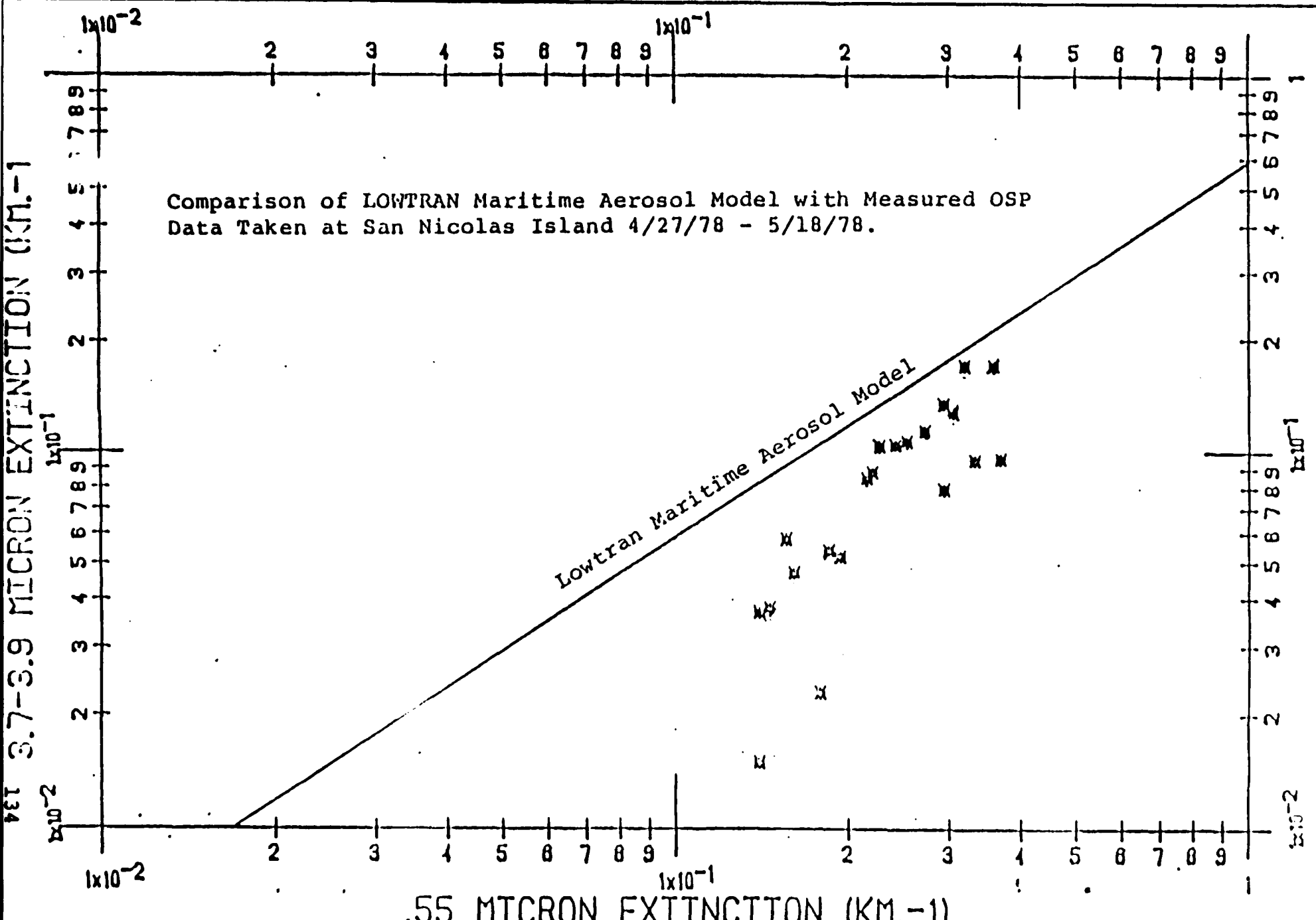
Comparison of LOWTRAN Maritime Aerosol Model with Measured OSP
Data Taken at San Nicolas Island 4/27/78 - 5/18/78.
Lowtran Maritime Aerosol Model
3.7-3.9 MICRON EXTINCTION (KM.-1)
.55 MICRON EXTINCTION (KM.-1)
1x10-2
1x10-1
1

2. DEPENDENCE OF SYSTEM SENSITIVITY AND MEASUREMENT ACCURACY ON:

- LASER POWER/ENERGY
- OPTICS SIZE
- OPERATING WAVELENGTH
- METHOD OF EXTINCTION COEFFICIENT EXTRACTION

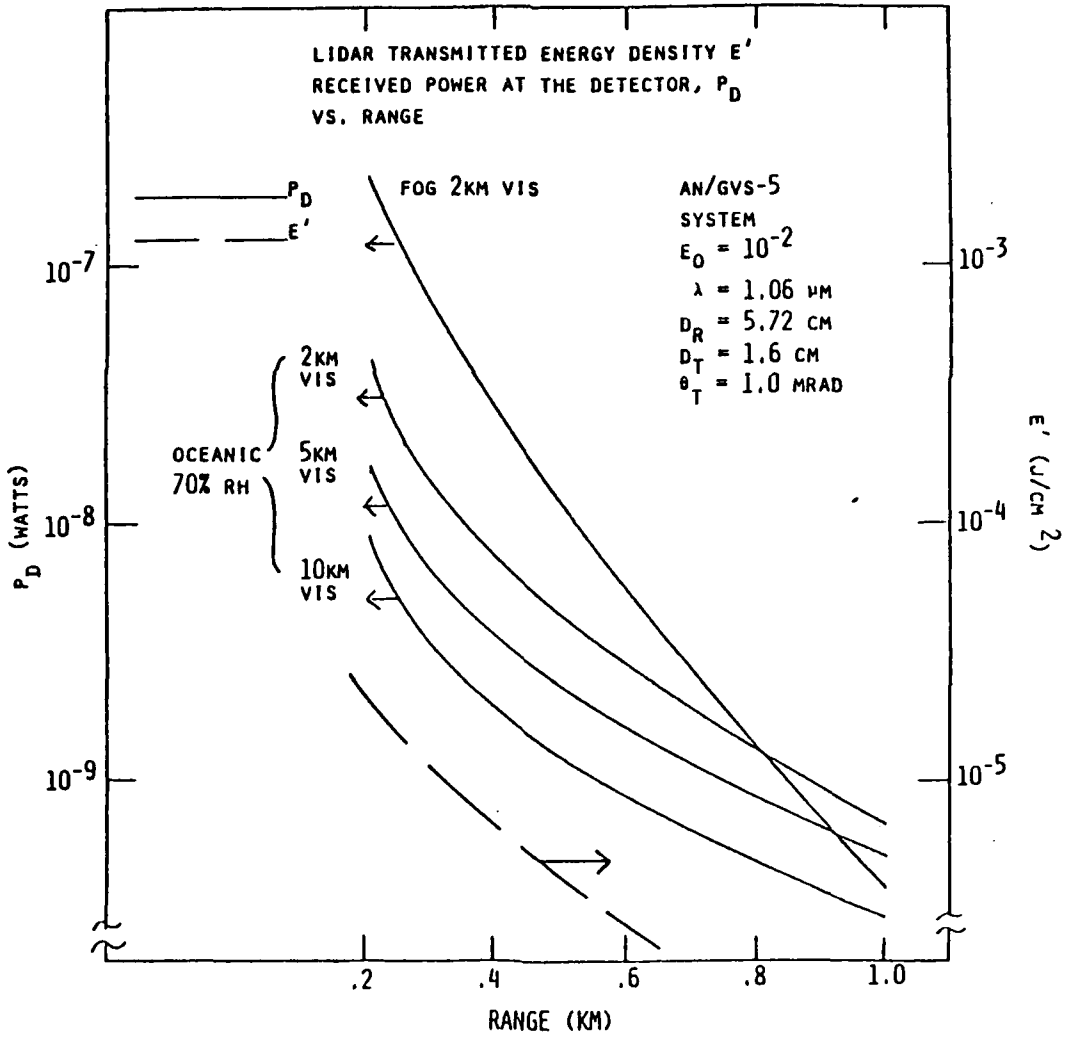
LIDAR TRANSMITTED ENERGY DENSITY E'
RECEIVED POWER AT THE DETECTOR, P_D
VS. RANGE
P_D
E'
FOG 2KM VIS
AN/GVS-5
SYSTEM
$E_O = 10^{-2}$
λ = 1.06 μM
D_R = 5.72 CM
D_T = 1.6 CM
θ_T = 1.0 MRAD
2KM VIS
OCEANIC
70% RH
5KM VIS
10KM VIS
10^{-7}
10^{-8}
10^{-9}
10^{-3}
10^{-4}
10^{-5}
P_D (WATTS)
E' (J/CM 2)
.2
.4
.6
.8
1.0
RANGE (KM)

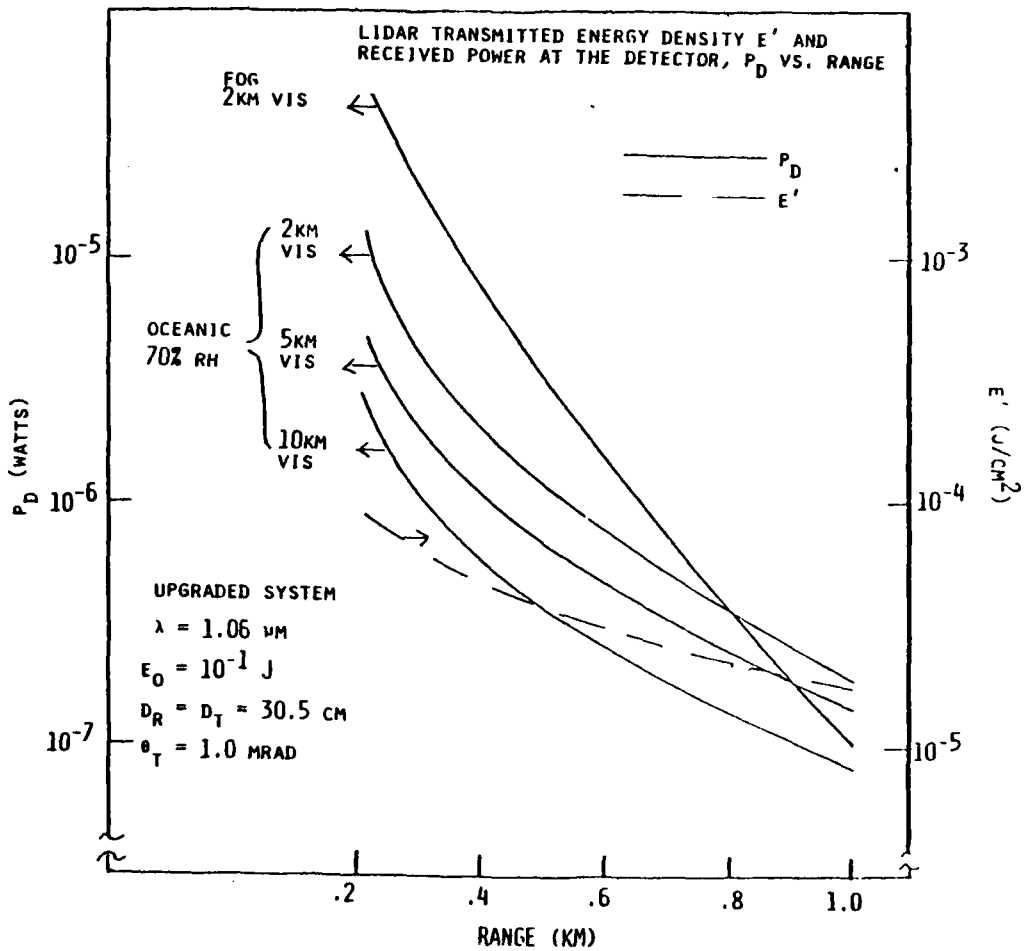
LIDAR TRANSMITTED ENERGY DENSITY E' AND
RECEIVED POWER AT THE DETECTOR, P_D VS. RANGE
FOG
2KM VIS
P_D
E'
2KM
VIS
OCEANIC
70% RH
5KM
VIS
10KM
VIS
10^{-5}
10^{-6}
10^{-7}
P_D (WATTS)
10^{-3}
10^{-4}
10^{-5}
E', (J/CM^2)
UPGRADED SYSTEM
λ = 1.06 μM
$E_O = 10^{-1}$ J
$D_R = D_T \approx 30.5$ CM
θ_T = 1.0 MRAD
.2
.4
.6
.8
1.0
RANGE (KM)

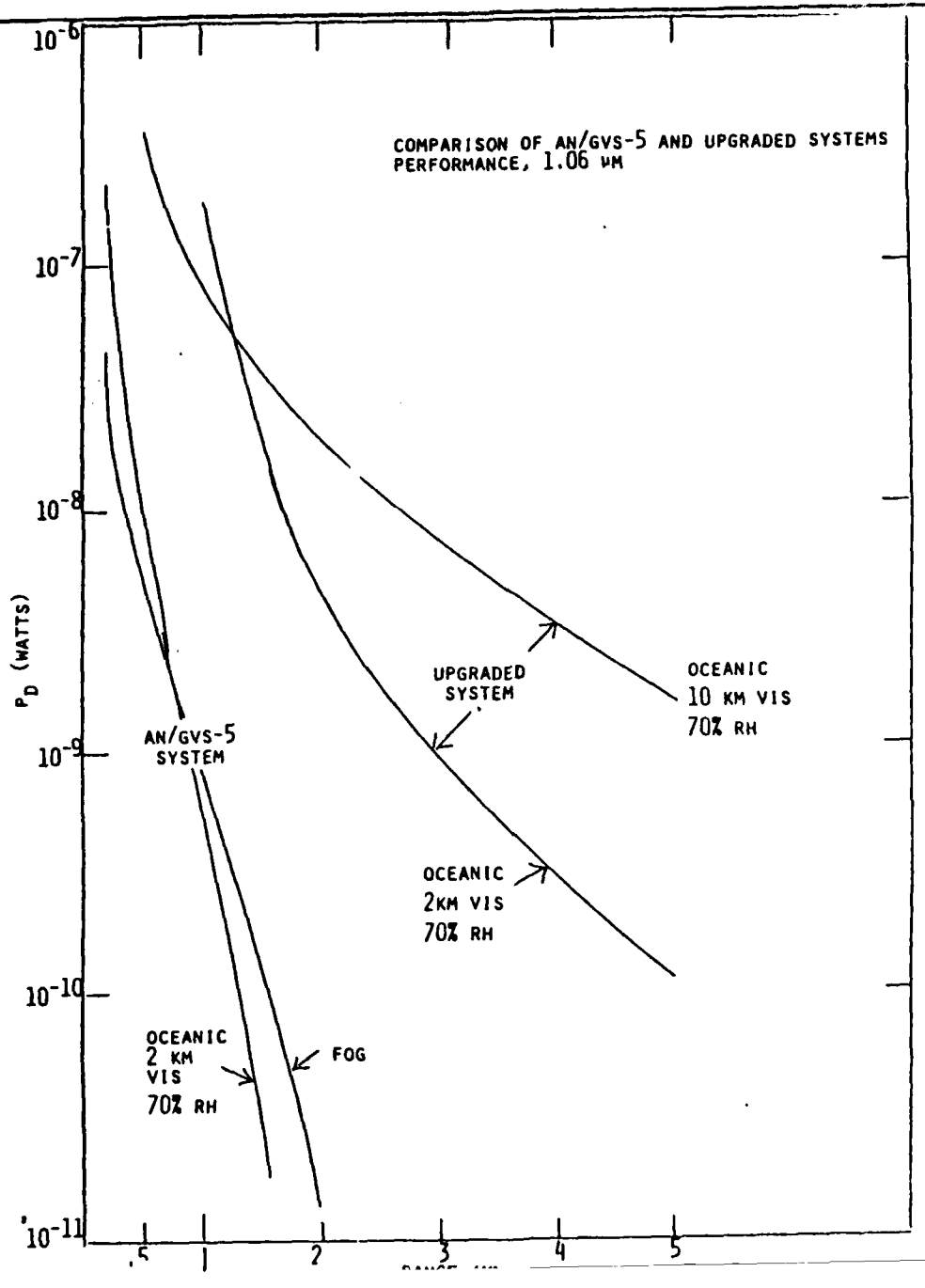
COMPARISON OF AN/GVS-5 AND UPGRADED SYSTEMS PERFORMANCE, 1.06 μM
10^{-6}
10^{-7}
10^{-8}
10^{-9}
10^{-10}
10^{-11}
P_D (WATTS)
AN/GVS-5 SYSTEM
UPGRADED SYSTEM
OCEANIC 10 KM VIS 70% RH
OCEANIC 2KM VIS 70% RH
OCEANIC 2 KM VIS 70% RH
FOG
.5
1
2
3
4
5

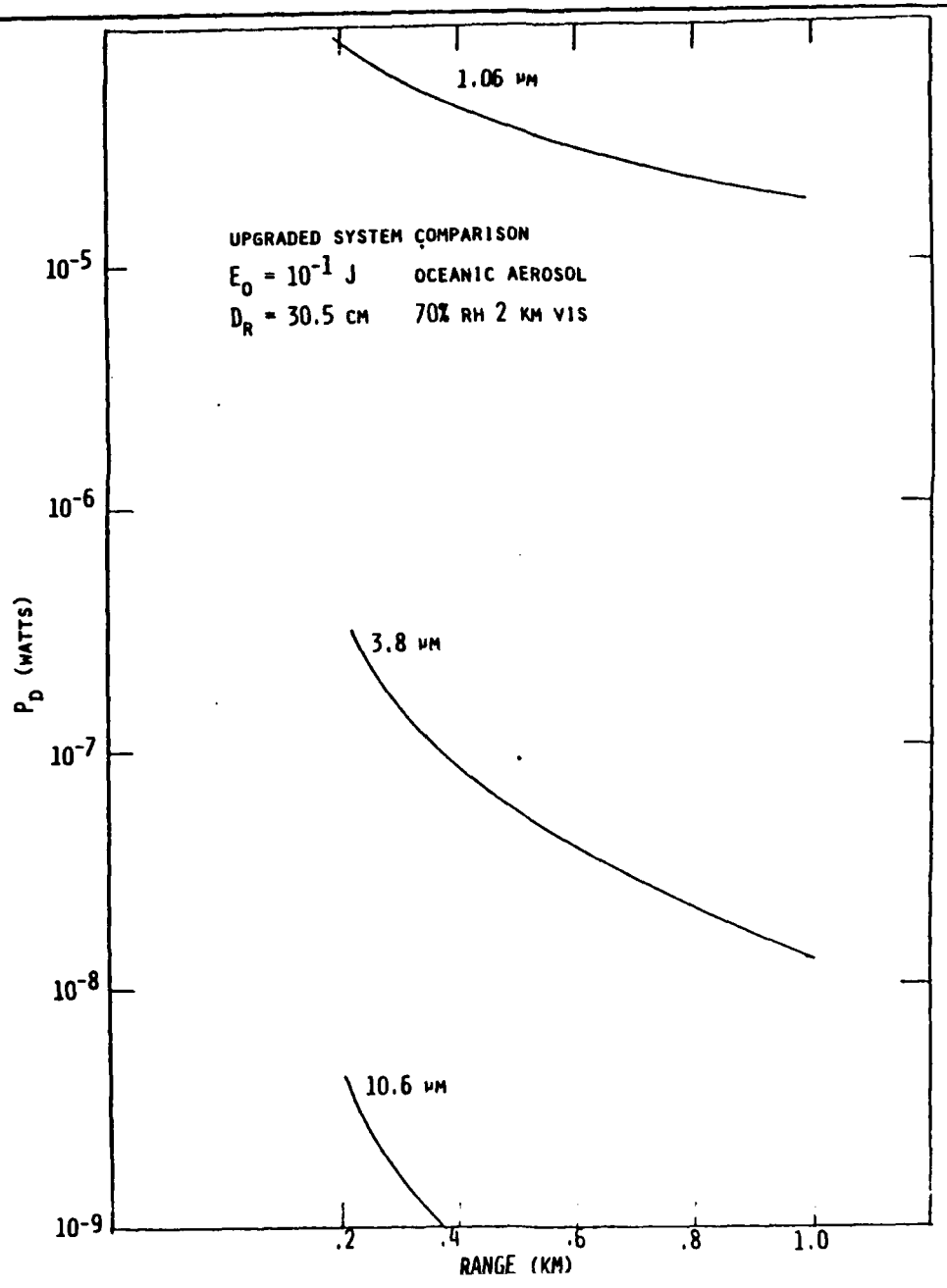
1.06 μM
UPGRADED SYSTEM COMPARISON
$E_0 = 10^{-1}$ J
D_R = 30.5 CM
OCEANIC AEROSOL
70% RH 2 KM VIS
10^{-5}
10^{-6}
10^{-7}
10^{-8}
10^{-9}
P_D (WATTS)
3.8 μM
10.6 μM
.2
.4
.6
.8
1.0
RANGE (KM)

METHODS FOR EXTRACTION OF THE EXTINCTION COEFFICIENT FROM LIDAR RETURNS

$$P_R(R) = C \frac{\beta(R)}{R^2} E^{-2 \int_{R_0}^{R} \sigma(R) DR}$$

DEFINE: $S(R) = \text{LN}\,(R^2 P_R(R))$

$$\frac{DS}{DR} = \frac{1}{\beta} \frac{D\beta}{DR} - 2\sigma$$

SLOPE METHOD:

ASSUME HOMOGENEOUS ATMOSPHERE:

$$\frac{D\beta}{DR} = 0 \; ; \quad \sigma = -\frac{1}{2} \frac{DS}{DR}$$

KLETT METHOD:

ASSUME $\beta = A\sigma^K$

THEN $\frac{DS}{DR} = \frac{K}{\sigma} \frac{D\sigma}{DR} - 2\sigma$

AND $$\sigma(R) = \frac{E\left(\frac{S(R) - S(R_M)}{K}\right)}{\sigma_M^{-1} + \frac{2}{K} \int_{R}^{R_M} E\left(\frac{S(R') - S(R_M)}{K}\right) DR'}$$

SOLUTION GENERATED FOR $R \leq R_M$

RATHER THAN FOR $R \geq R_0$

3. PRACTICAL CONSIDERATIONS IN THE IMPLEMENTATION OF A SHIPBOARD SYSTEM

- EYE SAFETY
- COMPATIBILITY WITH ONGOING SHIPBOARD OPERATIONS
- UTILIZATION OF EXISTING, RUGGEDIZED (MIL-SPEC) HARDWARE
- CHARACTERISTICS OF A PROTOTYPE SYSTEM

EYE SAFETY CONSIDERATIONS

- $\lambda > 1.4$ μM PROVIDES $\sim 10^3$ INCREASE IN MPE
  - WAVELENGTH SHIFTED 1.06 μM WITH RAMAN CELL TO 1.54 μM (CH_4) OR 1.9 μM (H_2)
  - HOLMIUM?
  - 3.5 μM OR 10.6 μM SOURCE

- LARGER APERTURE TRANSMITTER BEAM

  AN.GVS-5 SYSTEM: 5.72 CM DIAMETER

  UPGRADED SYSTEM: 30.5 CM DIAMETER

  - EXPOSURE REDUCED TO 3.5% OF SMALLER BEAM AT THE SAME RANGE

UTILIZATION OF EXISTING MIL-SPEC HARDWARE

1.06 μM

- AN/GVS-5 LASER RANGEFINDER
  - 10^{-2} J, 6 NS PULSE
  - VERY COMPACT, BATTERY POWERED, LIGHT WEIGHT
  - NOW USED IN ASL XE-2 VISIO-CEILOMETER

- AN/TVQ-2 GROUND LASER LOCATOR/DESIGNATOR (GLLD)
  - 10^{-1} J, ~ 20 NS PULSE
  - COMPACT, BATTERY POWERED, LIGHT WEIGHT (13 KG)
  - GOOD BEAM QUALITY
  - HIGH RELIABILITY

10.6 μM

- FERRANTI TYPE 307/MARCONI TEA CO_2 LASER RANGEFINDER
  - 1.3×10^{-2} J, 60 NS PULSE
  - MODERATELY COMPACT, BATTERY POWERED, LIGHT WEIGHT (10 KG)
  - GOOD BEAM QUALITY
  - RUGGED CONSTRUCTION

PROTOTYPE SHIPBOARD SYSTEM

- $E_0 \simeq 10^{-2}$ J
- $\lambda > 1.4$ μM
- $D_T = D_R \gtrsim 30$cm
- EXISTING MIL SPEC MODULES FOR LASER SOURCE, AUXILIARY OPTICS/MOUNTS AND POWER SUPPLY UTILIZED
- SELF-CONTAINED HYBRID RETURN SIGNAL PROCESSING AS IN NVEOL/ASL VISIO-CEILOMETER

SUMMARY AND CONCLUSIONS (PRELIMINARY)

AEROSOL MODELS

- WIDE RANGE OF EXTINCTION PREDICTIONS AS A FUNCTION OF RH, WS
  - K - R PREDICTS LOWER EXTINCTION THAN LOWTRAN 5 FOR $5_{M/S}$ WS; HIGHER FOR $15_{M/S}$ WS
  - LOWTRAN 5 RH DEPENDENCE STRONGER THAN K - R MODEL
- PREDICTED β AT 1 μM RANGES OVER A FACTOR OF $\sim$ 300 FOR 2 KM VIS FOG COMPARED WITH 5 KM VIS OCEANIC AEROSOL
- β/σ DECREASES BY A FACTOR OF 30 FOR 4 μM $< \lambda <$ 10 μM

AEROSOL DATA

- $\frac{\sigma\ IR}{\sigma.55}$ DATA SHOW LARGE AMOUNTS OF SCATTER; USUALLY FALL BELOW PREDICTED MODEL VALUES.

SUMMARY AND CONCLUSIONS (2)

SYSTEM PERFORMANCE EVALUATION

- AN/GVS-5 SYSTEM LIMITED TO OPERATION ≈ 1 KM
- UPGRADED SYSTEM ($E_0 = 10^{-1}$J, $D_R = 30.5$ CM) SHOWS GOOD PERFORMANCE FOR RANGES $\gtrsim$ 5 KM
- LARGER OPTICS, INCREASED PULSE ENERGY, HETERODYNE DETECTION REQUIRED FOR 10.6 μM SYSTEM DUE TO DECREASED β AND β/σ
- $\beta = A\sigma^K$ CONDITION REQUIRED FOR USE OF KLETT METHOD QUESTIONABLE AT 10.6 μM
- RELIABLE EXTIMATION OF σ FOR 8-12 μM FROM ANALYSIS OF 1.06 μM LIDAR RETURN NOT YET ESTABLISHED

SUMMARY AND CONCLUSIONS (3)

SHIPBOARD IMPLEMENTATION CONSIDERATIONS

- $\lambda > 1.4$ μM PROVIDES $\sim 10^3$ INCREASE IN MPE
- INCREASE OF D_T TO 30.5 CM REDUCES E' BY A FACTOR OF ~ 30
- AN/TVQ-2 (GLLD) SYSTEM IS A PROMISING CANDIDATE FOR LASER SOURCE SUBSYSTEM
- PROTOTYPE SYSTEM USING WAVELENGTH SHIFTED 1.06 μM SOURCE WITH $E_0 \simeq .05 - .1$ J AND $D_T = D_R \simeq 30$ CM SHOULD PROVIDE GOOD PERFORMANCE FOR $R \gtrsim 5$ KM WHILE REMAINING EYE SAFE

CONCLUSIONS (4)

- AEROSOL DATA SCATTER SHOWS:
  - NO CLEAR CHOICE OF MODEL
  - MODERATE CORRELATION OF VISIBLE WITH 1.06 μM - 3-5 μM SCATTERING
  - RELATIVE INDEPENDENCE OF VISIBLE/NEAR IR AND 10 μM SCATTERING

- SIMULTANEOUS NEAR IR (1.54 μM) AND 10 μM SHIPBOARD DATA REQUIRED (EMPIRICAL SHIPBOARD LIDAR DATA BASE)

- PROTOTYPE SHIPBOARD LIDAR CAN AND SHOULD BE DEVELOPED AND TESTED

RECOMMENDATIONS

1. EVALUATE TWO CANDIDATE MIL-SPEC 1.06 μM SOURCES:
   - A) GLLD - 10^{-1}J/PULSE
   - B) A - 6TRAM > 10^{-1}J/PULSE AND SELECT ONE FOR:
     - AVAILABILITY TO SHIPBOARD LIDAR DEVELOPMENT PROGRAM
       - (COST, TIME CONSTRAINTS)
     - COMPATIBILITY WITH LIDAR DESIGN AND SHIPBOARD INSTALLATION

2. DESIGN AND ENGINEER INTERFACE WITH CH_4 RAMAN CELL TO PRODUCE 1.54 μM OUTPUT

3. EVALUATE CANDIDATE 10.6 μM SOURCES:
   - A) MARCONI/FERRANTI (10^{-2}J/PULSE)
   - B) OTHER, MORE ENERGETIC CO_2 SOURCES

4. DESIGN PROTOTYPE SHIPBOARD LIDAR:
   - 1.54 μm — 0.05 - 0.2 J/PULSE (BASELINE)
   - 10.6 μm — 0.01 - ? J/PULSE (DESIREABLE)

     (HETERODYNE DETECTION PROBABLY REQUIRED FOR 10.6 μm OPERATION)
   - ~ 30 cm APERTURE
   - COMPACT DATA SYSTEM:
     - 25-200 MHz ADC
     - NEAR-REAL-TIME, SELF-CONTAINED INVERSION CAPABILITY (SLOPE, RATIO, KLETT)

5. CONSTRUCT AND OPERATE SHIPBOARD LIDAR TO:
   - TEST AND DEVELOP SHIPBOARD INSTRUMENT
   - COLLECT AT-SEA SLANT-PATH, NEAR IR (AND LWIR) AEROSOL EXTINCTION DATA BASE.

END
DATE
FILMED

DEC. 10, 1982